Title

Activating Events of the Unfolded Protein Response in *Saccharomyces cerevisiae*

Permalink

https://escholarship.org/uc/item/41d0j3x6

Author

Rubio, Claudia Ani Dabanian

Publication Date

2010

Peer reviewed|Thesis/dissertation

Activating Events of the Unfolded Protein Response in

Saccharomyces cerevisiae

by

Claudia Ani Dabanian Rubio

DISSERTATION

Submitted in partial satisfaction of the requirements for the degree of

DOCTOR OF PHILOSOPHY

in

Biochemistry and Molecular Biology

This thesis is dedicated to my parents,

Alyce and Guillermo Rubio, for their unconditional love and support and for

instilling in me the belief that I can do anything; and to my grandfather, Raffi, who

taught me the value of hard work and urged me to finish my PhD and get on with

my life.

Acknowledgements

First and foremost, I would like to thank Peter Walter for his unwavering optimism, his expansive approach to scientific research and his endless drive for discovery. Peter taught me to appreciate the playful side of science, reminded me to strive for excellence in my work and continuously pushed me to do the last experiment first. Thank you, Peter, for believing in me and for encouraging me to persevere through to the happy end.

I would also like to express my gratitude to members of the UCSF faculty who made important contributions to my success in graduate school. I thank my excellent thesis committee members, Christine Guthrie and David Morgan, for their wise counsel and support through difficult decisions and times of uncertainty; and Joe DeRisi for his spirited willingness to collaborate and for being an unofficial member of my advisory committee.

I am grateful to be a part of the large and eclectic Walter Lab family. Over the years the lab has been a constant source constructive criticism, unsolicited advice, helpful suggestions, and bizarre entertainment. I would like to thank Jason Brickner and Jess Leber for unknowingly wooing me to join the Walter lab with their practical jokes; Chris Patil for his wisdom and sound advice, his blatant honesty, his true friendship and for being the loudest; Alex Engel for his comraderie, his mad photography skills, exquisite musical taste and his love of backpacking; Niels Bradshaw for his endless scientific curiosity and eagerness to

open heart, her quirky, enchanting sense of humor and her phenomenal dance moves.

There are a few select people who were instrumental in making sure that all the important things happened during my time at UCSF. I am grateful to Teresa Donovan - without whom the Walter lab would fall apart at the seams - for her dedication to getting things done, for always knowing Peter's whereabouts and for all of the signatures; and to Sue Adams and Danny Dam for adeptly taking care of every administrative detail.

I am infinitely thankful for my inspiring group of friends in San Francisco, the likes of whom are too numerous to list, who reminded me to enjoy life and kept me from being overshadowed by the toils of graduate school; I am especially thankful for Marissa Berman and Alexa Frankenberg, my house mates and pseudo-sisters, who talked me through all of the hard times and celebrated my every success.

Last but certainly not least, I am thankful for my family: especially for my sister, Cristina, and her love, friendship and genuine interest in what I've been doing all these years; for my grandfather Raffi - who would have been relieved to witness my completion of graduate school - and his stories of our family history, his hard work and his commitment to our family; and to my parents, Alyce and Guillermo, for their undying support and love and for encouraging me to be my best self and to follow my dreams.

Abstract

In eukaryotic cells, the untoward accumulation of misfolded proteins inside the endoplasmic reticulum (ER) triggers a transcriptional program that restores cellular homeostasis. This program, called the unfolded protein response (UPR), is activated through a series of enzymatic steps that culminate in the production of a transcription factor that upregulates a set of target genes required for cell survival during ER stress. UPR activation occurs through an ER-resident sensor, Ire1, which is stimulated by misfolded proteins in the ER lumen. Activated Ire1 transmits a signal to its cytosolic portion, containing a kinase and an RNase, which *trans*-autophosphorylates and activates the RNase to cleave an mRNA encoding the Hac1 transcription factor. These cleavage products are ligated by tRNA ligase, Trl1, to produce a spliced form of *HAC1* mRNA that is translated into the transcription factor. Together, the coordinated activation of Ire1 and ligation by Trl1 to produce spliced *HAC1* mRNA comprise the central mechanism of UPR activation. This thesis describes my work toward understanding two key regulatory steps in UPR activation.

Several lines of evidence suggest that Ire1 kinase plays a role in the UPR that is autonomous from its role in RNase activation. First, RNase L, a close homolog of Ire1, is an RNase with a pseudokinase domain that has lost activity through evolution. Conservation of Ire1's kinase suggests that its activity is important for UPR fitness. Moreover, *in vitro* studies have shown that kinase-

inactive Ire1 retains RNase activity and, *in vivo*, kinase activity can be bypassed by ATP-competitive drugs. In an endeavor to understand the importance of Ire1 kinase we discovered that kinase activity contributes to the attenuation of Ire1 signaling and is imperative for homeostatic adaptation during ER stress.

The final chapters of this thesis describe my work to decipher how tRNA ligase achieves pathway specificity for the UPR. Trl1 splits its time between *HAC1* mRNA splicing and tRNA splicing. Our efforts to discern how Trl1 acts in *HAC1* mRNA splicing were unfruitful, however, this work enlightened our knowledge of Trl1 biology and set the stage for future work to elucidate Trl1's role in the UPR.

Table of Contents

List of Tables

List of Figures

Chapter 1

Introduction:

The Unfolded Protein Response in *Saccharomyces cerevisiae*

Introduction

Protein misfolding in the endoplasmic reticulum

Accurate folding and modification of proteins during their biogenesis is an essential to the proper function of all cells. Proteins can be broadly categorized into two classes: intracellular soluble proteins, which function within the cell, and transmembrane and secreted proteins, which are exposed to the extracellular milieiu. In eukaryotic cells, soluble proteins are generally folded within the cytoplasm of the cell whereas the majority of secreted and transmembrane proteins must enter the endoplasmic reticulum (ER) to be properly folded and modified. The ER provides an oxidative environment for the biogenesis of proteins, which must be prepared to function in the oxidizing environment outside the cell, and affords hydrophobic transmembrane proteins the chance to be inserted into membranes in their proper orientation. The unique folding and modification of these proteins is essential to their function and correct localization to their target membranes or to the extracellular space. The ER thereby serves as the quality control compartment of the secretory pathway.

Nascent proteins can enter the ER in one of two ways. Post-translational entry into the ER occurs after a protein has been fully synthesized in the cytoplasm. Alternatively, co-translational insertion into the ER occurs by a mechanism in which the translating ribosome feeds the nascent protein directly into the ER membrane.

A wide variety of modifications occur within the ER that are required for proteins to assume their correct structure and function (reviewed in (Patil and Walter 2001). The lumen of the ER is afforded the capacity to fold and modify client proteins by the presence of an assortment of ER-resident enzymes. Chaperones, such as Kar2, aid the folding of proteins into their proper, functional conformation (Schonberger et al. 1991). Disulfide-bond isomerases, such as Pdi1, promote the formation of disulfide linkages between cysteine residues (Tu et al. 2000). Oxidizing enzymes, such as Ero1, maintain the oxidative environment of the ER necessary for oxidative protein folding (Pollard et al. 1998). Carbohydrate modifications, such as glycosylation or myristylation, influence protein folding and likely contribute to proper localization (Dempski and Imperiali 2002). Thus, the cooperation of a multitude of enzymes inside the ER is required for the accurate processing and maturation of a given protein.

The ER is a dynamic organelle that is capable of changing in shape and volume according to fluctuating demands on the secretory pathway of the cell. When the influx of protein into the ER outweighs the capacity of the organelle, the ER expands to meet the increased need for protein folding. This expansion requires the cell to monitor changes in its secretory load and increase the production of ER components accordingly (Travers et al. 2000) and is mediated by the unfolded protein response.

The Unfolded Protein Response

The ability of the cell to monitor the protein folding status inside the ER and expand the organelle in response to need is a carefully controlled process that is mediated by an intracellular signaling pathway called the unfolded protein response (UPR). When the protein load in the ER outweighs its folding capacity, misfolded proteins accumulate inside the ER lumen and activate the UPR. Activation of this signaling pathway leads to the production of ER components required for the folding and modification of client proteins, for ER membrane expansion and for ER-associated degradation of proteins that cannot be properly folded (Travers et al. 2000). In this way the UPR affords the cell with the ability to maintain ER homeostasis.

The role of the UPR in maintaining ER homeostasis is integral for proper cell physiology. In higher organisms, many examples of UPR-related pathologies highlight the central role of this pathway in disease (Lin et al. 2008). Sustained activation of the UPR causes mammalian cells to undergo apoptosis (Lin et al. 2009) and can lead to diseases such as multiple myeloma (Lee et al. 2003). Likewise, faulty UPR signaling can lead to diabetes (Scheuner and Kaufman 2008). Moreover, the UPR is activated in a variety of cancer cells and is associated with neurodegenerative disease (Ma and Hendershot 2004; Matus et al. 2008; So et al. 2009).

Activation of the UPR is initiated by three known components. *IRE1* encodes an ER transmembrane kinase/RNase that monitors the folding state

inside the ER and relays the information to the cytosol (Cox et al. 1993; Mori et al. 1993). *TRL1*, encoding tRNA ligase, is required for completing the signal initiated by Ire1 (Sidrauski et al. 1996). *HAC1* encodes a bZip transcription factor that activates transcription of UPR target genes (Mori et al. 1996). When misfolded proteins accumulate in the ER lumen, Ire1 is activated and forms oligomers in the plane of the ER membrane. This oligomerization event brings the cytosolic portion of neighboring Ire1 molecules into proximity and drives activation of its kinase and RNase domains (Shamu and Walter 1996). *Trans-autophosphorylation* of Ire1 is coupled to activation of its site-specific RNase which initiates the non-canonical splicing of the mRNA encoding the Hac1 transcription factor. Ire1 oligomers recruit the unspliced form *HAC1* mRNA through a bipartite element in the 3' untranslated region of the mRNA and act as splicing centers within the cell (Aragon et al. 2009). Cleavage of *HAC1* mRNA by Ire1 liberates two exons that are subsequently ligated by Trl1. Ligation of *HAC1* exons produces a spliced form of *HAC1* mRNA that is translated to produce the Hac1 transcription factor (Cox and Walter 1996; Sidrauski et al. 1996). Hac1 protein is not made from the unspliced form of *HAC1* mRNA (Cox and Walter 1996) thus, activation of Ire1 provides the pivotal step in regulating Hac1 synthesis thereby activating transcription of UPR target genes (Fig. 1-1).

Ire1 is a complex signaling machine

Ire1 is a 127 kilo-Dalton (kD) single pass transmembrane protein with a domain residing in the ER lumen and two domains, a kinase and an RNase, in the cytoplasm (Fig.1-2). The lumenal domain of Ire1 (amino acids 1-526) acts as sensor of misfolded proteins and drives the oligomerization of Ire1 molecules. Competing theories on the mechanism by which Ire1 senses unfolded proteins have been proposed. In one model, the association of Ire1 with the ER-resident chaperone, Kar2 (also known as BiP), is proposed to prevent oligomerization of Ire1's lumenal domain. The accumulation of misfolded proteins compete with Ire1 for Kar2 binding such that increasing levels of misfolded proteins titrate Kar2 away from Ire1, allowing for its oligomerization and activation (Bertolotti et al. 2000; Okamura et al. 2000; Kimata et al. 2004). In a second model, the lumenal domain of Ire1 acts to sense protein misfolding by directly binding to unfolded regions in proteins via an MHC-like binding groove (Credle et al. 2005). In this model, the binding of unfolded peptide chains to the proposed peptide-binding groove of Ire1 provides the driving force for oligomerization and activation of the enzyme. A third hybrid model for Ire1 activation has been proposed in which Ire1 oligomerization is driven by dissociation of BiP while binding of misfolded proteins to Ire1 provide the activating signal (Kimata et al. 2007). However, *in vitro* evidence suggests that oligomerization of Ire1's cytosolic domains is sufficient to cause activation, suggesting that oligomerization and activation of Ire1 are coupled (Korennykh et

6

al. 2009). Recently, the binding of BiP to inactive Ire1 molecules has been shown to desensitize Ire1 to low levels of stress and promote deactivation upon resolution of ER stress. The authors propose that the interaction of BiP with Ire1 provides a buffer for activation and stabilizes the inactive state to aid in de-oligomerization (Pincus 2010). This model discounts the notion that BiP plays a swich-like regulatory role in Ire1 activation. Rather, it modulates the activity of Ire1 and contributes to the dynamic activation state and sensitivity of the UPR.

On the cytosolic side of the ER membrane, the transmembrane domain of Ire1 (amino acids 527-556) is separated from its kinase domain by a linker region (amino acids 557-672). This linker has not been assigned a function, though recent evidence suggests that it may play a role in recruiting *HAC1* mRNA (E. van Anken, unpublished data). Ire1 kinase is a CDK2-related serine-threonine kinase (amino acids 673-982) which *trans*-autophosphorylates neighboring Ire1 molecules upon activation. Phosphorylation by the kinase is coupled to activation of Ire1's RNase (amino acids 983-1115), which recognizes and cleaves specific sites in *HAC1* mRNA (Gonzalez et al. 1999). The activation of Ire1 thus proceeds through a series of complex enzymatic steps that culminate in the site-specific cleavage of *HAC1* mRNA to initiate the UPR signaling pathway.

Trl1 and its role in *HAC1* mRNA splicing

The role of Trl1[1] in the UPR was first revealed in a genetic screen for essential components of the UPR (Sidrauski et al. 1996). In this screen, an UPR-defective allele of Trl1, *trl1-100*, was discovered that abrogated growth of strains on UPR-inducing medium and failed to ligate *HAC1* mRNA exons liberated by Ire1 cleavage. The *trl1-100* mutation did not affect the catalytic function of the ligase since the mutant protein retained the ability to ligate tRNA halves, and did not alter Trl1 protein levels. Since the *trl1-100* mutation renders the ligase specifically defective for *HAC1* mRNA splicing, Trl1's function in the UPR is separable from its constitutive role in tRNA splicing. Splicing of *HAC1* mRNA proceeds through a mechanism analogous to that of tRNAs (Gonzalez et al. 1999). Indeed, cleavage by both Ire1 and tRNA endonuclease produces RNA molecules with chemically identical ends, thus the substrate for tRNA ligase in both cases is remarkably similar.

Trl1 is a trifunctional enzyme that catalyzes three chemical reactions at the cleaved ends of tRNA or *HAC1* mRNA exons to produce a ligated RNA molecule. The ends generated by Ire1 (or tRNA endonuclease) contain a 2',3'-cyclic phosphate on the 3' end of the 5' exon and a 5' hydroxyl group on the 3' exon (Gonzalez et al. 1999). Trl1 acts to catalyze ligation of these ends through the activity of three domains (Xu et al. 1990). First, the cyclic phosphate is hydrolyzed by its 2',3'-cyclic phosphodiesterase (CPD) activity, leaving 2'-

---

[1] *TRL1* was annotated as *RLG1* when its role in the UPR was discovered. The gene name has since changed to *TRL1* in the Saccharomyces Genome Database (www.yeastgenome.org), thus, tRNA ligase is referred to as Trl1 throughout this thesis.

phosphate and a 3'-hydroxyl. Next, Trl1 phosphorylates the 5'-hydroxyl present on the 3' exon through its nucleotide-dependent polynucleotide kinase activity. Finally, the resulting ends are sealed through the action of its ATP-dependent RNA ligase (Belford et al. 1993) (Fig1-3).

The work presented in this thesis provides new insights into our understanding of the enzymes involved in *HAC1* mRNA splicing. In Chapter 2 we describe the discovery that Ire1 kinase plays a role in disassembly of Ire1 signaling complexes and contributes to cell survival during the UPR. We describe a rationally designed variant of Ire1 in which Ire1 kinase activity is uncoupled from its RNase activity. We show that kinase-inactive *ire1* cells retain the ability to cleave *HAC1* mRNA, upregulate transcription of UPR target genes and restore homeostasis in the ER. However, these cells are unable to quell Ire1 signaling. We provide evidence that phosphorylation of Ire1 plays a role in disassembling Ire1 oligomers. In Chapter 3 we describe work carried out to elucidate the mechanism by which Trl1 achieves pathway specificity in the UPR. We show that Trl1 localizes diffusely to the cytoplasm and likely carries out *HAC1* mRNA ligation without forming stable interactions with other UPR components. In Chapter 4, we identify mutations in *TRL1* that are able to suppress the UPR-specific defect in *trl1-100* cells and describe a novel method for mapping extragenic suppressor mutations. We identify candidate mutations in *SKI2* that we propose will suppress the UPR-specific defect in *trl1-100* cells by stabilizing *HAC1* mRNA exons.

References

Aragon, T., E. van Anken, et al. (2009). "Messenger RNA targeting to endoplasmic reticulum stress signalling sites." <u>Nature</u> **457**(7230): 736-740.

Belford, H. G., S. K. Westaway, et al. (1993). "Multiple nucleotide cofactor use by yeast ligase in tRNA splicing. Evidence for independent ATP- and GTP-binding sites." <u>J Biol Chem</u> **268**(4): 2444-2450.

Bertolotti, A., Y. Zhang, et al. (2000). "Dynamic interaction of BiP and ER stress transducers in the unfolded-protein response." <u>Nat Cell Biol</u> **2**(6): 326-332.

Cox, J. S., C. E. Shamu, et al. (1993). "Transcriptional induction of genes encoding endoplasmic reticulum resident proteins requires a transmembrane protein kinase." <u>Cell</u> **73**(6): 1197-1206.

Cox, J. S. and P. Walter (1996). "A novel mechanism for regulating activity of a transcription factor that controls the unfolded protein response." <u>Cell</u> **87**(3): 391-404.

Credle, J. J., J. S. Finer-Moore, et al. (2005). "On the mechanism of sensing unfolded protein in the endoplasmic reticulum." <u>Proc Natl Acad Sci U S A</u> **102**(52): 18773-18784.

Dempski, R. E., Jr. and B. Imperiali (2002). "Oligosaccharyl transferase: gatekeeper to the secretory pathway." <u>Curr Opin Chem Biol</u> **6**(6): 844-850.

Gonzalez, T. N., C. Sidrauski, et al. (1999). "Mechanism of non-spliceosomal mRNA splicing in the unfolded protein response pathway." EMBO J **18**(11): 3119-3132.

Kimata, Y., Y. Ishiwata-Kimata, et al. (2007). "Two regulatory steps of ER-stress sensor Ire1 involving its cluster formation and interaction with unfolded proteins." J Cell Biol **179**(1): 75-86.

Kimata, Y., D. Oikawa, et al. (2004). "A role for BiP as an adjustor for the endoplasmic reticulum stress-sensing protein Ire1." J Cell Biol **167**(3): 445-456.

Korennykh, A. V., P. F. Egea, et al. (2009). "The unfolded protein response signals through high-order assembly of Ire1." Nature **457**(7230): 687-693.

Lee, A. H., N. N. Iwakoshi, et al. (2003). "Proteasome inhibitors disrupt the unfolded protein response in myeloma cells." Proc Natl Acad Sci U S A **100**(17): 9946-9951.

Lin, J. H., H. Li, et al. (2009). "Divergent effects of PERK and IRE1 signaling on cell viability." PLoS One **4**(1): e4170.

Lin, J. H., P. Walter, et al. (2008). "Endoplasmic reticulum stress in disease pathogenesis." Annu Rev Pathol **3**: 399-425.

Ma, Y. and L. M. Hendershot (2004). "The role of the unfolded protein response in tumour development: friend or foe?" Nat Rev Cancer **4**(12): 966-977.

Matus, S., F. Lisbona, et al. (2008). "The stress rheostat: an interplay between the unfolded protein response (UPR) and autophagy in neurodegeneration." Curr Mol Med **8**(3): 157-172.

Mori, K., T. Kawahara, et al. (1996). "Signalling from endoplasmic reticulum to nucleus: transcription factor with a basic-leucine zipper motif is required for the unfolded protein-response pathway." Genes Cells **1**(9): 803-817.

Mori, K., W. Ma, et al. (1993). "A transmembrane protein with a cdc2+/CDC28-related kinase activity is required for signaling from the ER to the nucleus." Cell **74**(4): 743-756.

Okamura, K., Y. Kimata, et al. (2000). "Dissociation of Kar2p/BiP from an ER sensory molecule, Ire1p, triggers the unfolded protein response in yeast." Biochem Biophys Res Commun **279**(2): 445-450.

Patil, C. and P. Walter (2001). "Intracellular signaling from the endoplasmic reticulum to the nucleus: the unfolded protein response in yeast and mammals." Curr Opin Cell Biol **13**(3): 349-355.

Pincus, D., Chevaleir, M., Aragon, T., van Anken, E., Vidal, S., El-Samad, H., Walter, P. (2010). "BiP binding to the ER-stress sensor Ire1 modulates the homeostatic regulation of the Unfolded Protein Response." PLoS Biol.

Pollard, M. G., K. J. Travers, et al. (1998). "Ero1p: a novel and ubiquitous protein with an essential role in oxidative protein folding in the endoplasmic reticulum." Mol Cell **1**(2): 171-182.

Scheuner, D. and R. J. Kaufman (2008). "The unfolded protein response: a
pathway that links insulin demand with beta-cell failure and diabetes."
Endocr Rev **29**(3): 317-333.

Schonberger, O., T. R. Hirst, et al. (1991). "Targeting and assembly of an
oligomeric bacterial enterotoxoid in the endoplasmic reticulum of
Saccharomyces cerevisiae." Mol Microbiol **5**(11): 2663-2671.

Shamu, C. E. and P. Walter (1996). "Oligomerization and phosphorylation of the
Ire1p kinase during intracellular signaling from the endoplasmic reticulum
to the nucleus." EMBO J **15**(12): 3028-3039.

Sidrauski, C., J. S. Cox, et al. (1996). "tRNA ligase is required for regulated
mRNA splicing in the unfolded protein response." Cell **87**(3): 405-413.

So, A. Y., E. de la Fuente, et al. (2009). "The unfolded protein response during
prostate cancer development." Cancer Metastasis Rev **28**(1-2): 219-223.

Travers, K. J., C. K. Patil, et al. (2000). "Functional and genomic analyses reveal
an essential coordination between the unfolded protein response and ER-
associated degradation." Cell **101**(3): 249-258.

Tu, B. P., S. C. Ho-Schleyer, et al. (2000). "Biochemical basis of oxidative protein
folding in the endoplasmic reticulum." Science **290**(5496): 1571-1574.

Xu, Q., D. Teplow, et al. (1990). "Domain structure in yeast tRNA ligase."
Biochemistry **29**(26): 6132-6138.

Figure 1-1   The Unfolded Protein Response in *Saccharomyces cerevisiae*

Ire1 resides in the ER membrane and is activated by the accumulation of

misfolded proteins in the ER lumen. Upon activation, Ire1 oligomerizes, bringing

the cytosolic portion of the protein into proximity. *Trans*-autophosphorylation of

neighboring Ire1 molecules is coupled to activation of its endonuclease domain,

which cleaves *HAC1* mRNA in the cytosol. The unspliced form of *HAC1* mRNA

is translationally repressed until Ire1 cleavage removes an inhibitory intron from

the message. The liberated exons are ligated by tRNA ligase to produce the

spliced form of *HAC1* mRNA that is translated to produce the Hac1 transcription

factor. Once synthesized, the Hac1 travels to the nucleus to activate

transcription of UPR target genes.

Figure 1-1

Nucleus

ER

Ire1

UPRE

P P

unspliced *HAC1* mRNA

tRNA
ligase

spliced *HAC1* mRNA

Hac1
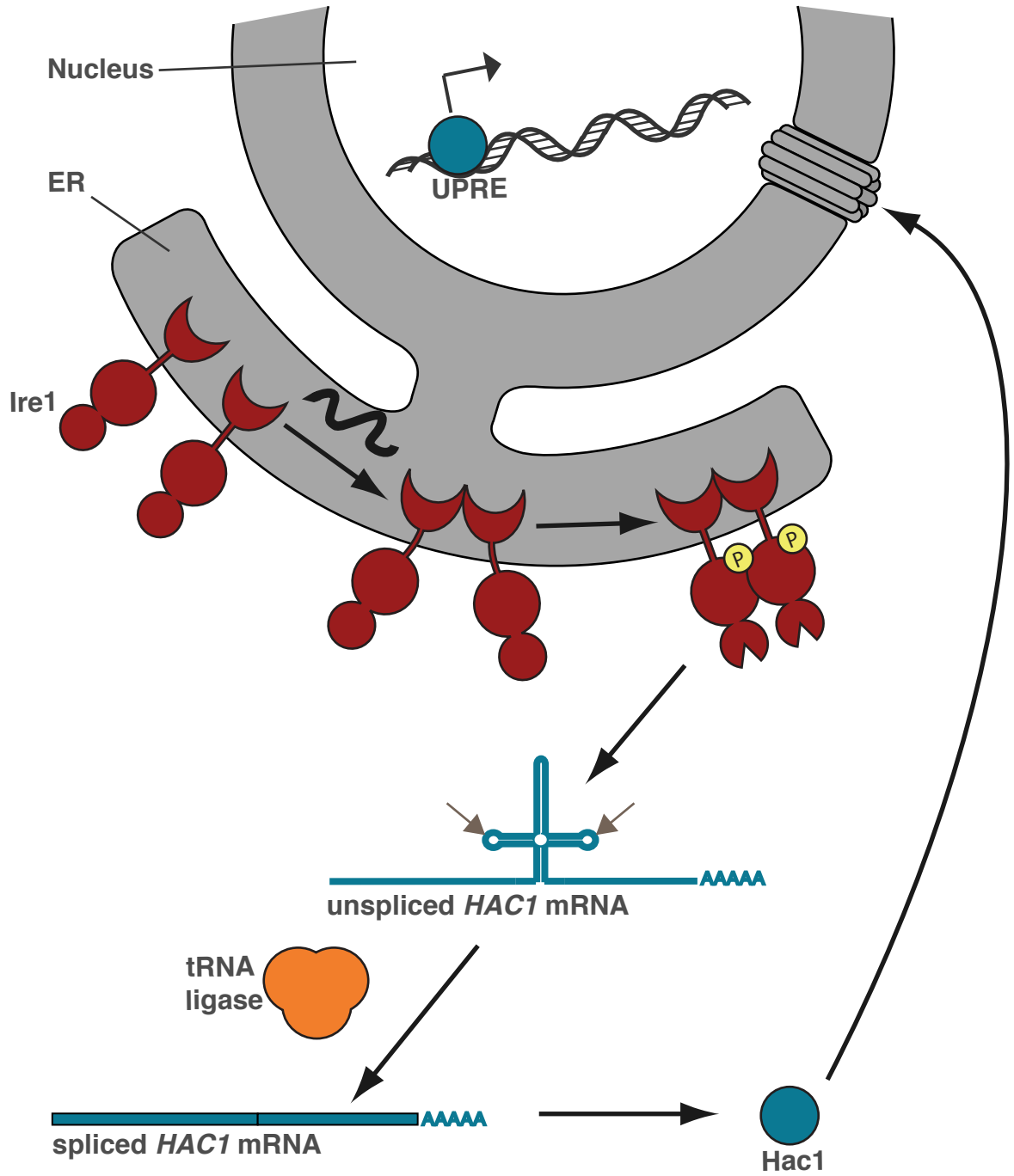
Figure 1-2   The domains of Ire1

Ire1 is a single-pass transmembrane protein with multiple domains. The lumenal

domain (1-526) senses misfolded proteins and drives oligomerization of Ire1

molecules. The lumenal domain is separated from the cytosolic portion of the

protein by a transmembrane domain (527-672) followed by a long cytosolic linker

(557-672).   The kinase domain (673-982) phosphorylates neighboring Ire1

molecules in the active oligomer and this phosphorylation event is coupled to

activation of the RNase (983-1115).

Figure 1-2

Lumenal Domain
(1-526)

TM
(527-556)

Linker
(557-672)

Kinase
(673-982)

RNase
(983-1115)

ER lumen

Cytoplasm
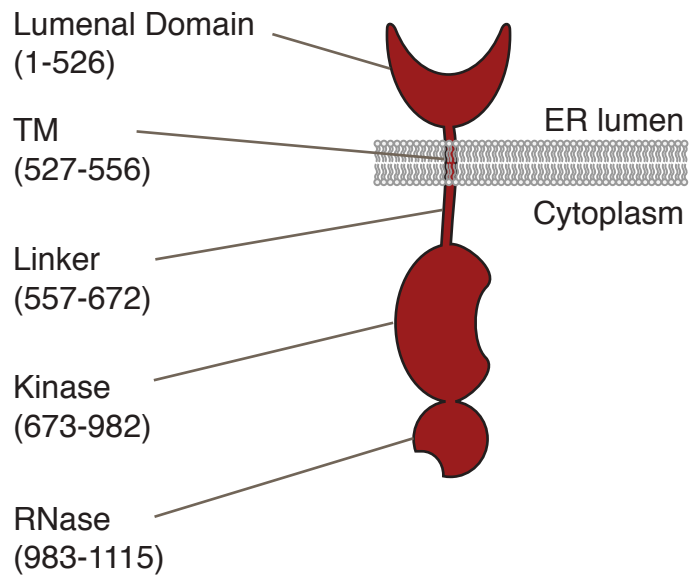
Figure 1-3   Trl1 ligates RNA in three catalytic steps

Cleavage by Ire1 produces a 3', 5'-cyclic phosphate and a 5'-hydroxyl. In order

to ligate these ends, Trl1 begins by opening the cyclic phosphate through the

activity of its cyclic phosphodiesterase (CPD). Next, the kinase of Trl1

phosphorylates the 5' end of the 3' exon using GTP or ATP as a substrate.

Finally, the adenylylate transferase of Trl1 adenylates the 5' phosphate using

ATP to produce a high-energy bond required for ligation. Ligation by Trl1 leaves

a 2'-phosphate on the ligated product that is removed by the essential enzyme,

Tpt1.

Figure 1-3
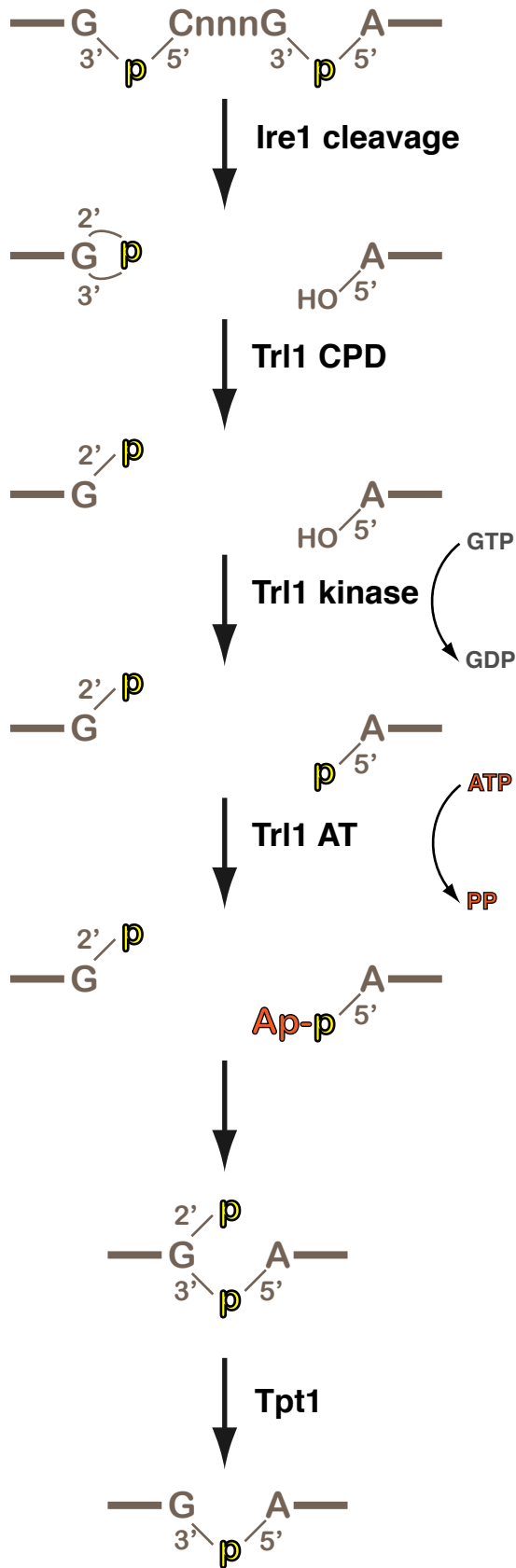
Chapter 2

Homeostatic adaptation to ER stress depends on Ire1 kinase activity

Homeostatic adaptation to ER stress depends on Ire1 kinase activity

Claudia Rubio[1,2], David Pincus[1,2], Alexei Korennykh[1,2], Sebastian Schuck[1,2],

Hana El-Samad[2], and Peter Walter[1,2,3]

[1]Howard Hughes Medical Institute, and

[2]Department of Biochemistry and Biophysics

University of California at San Francisco

San Francisco, CA 94158

Running title: Homeostatic adaptation to ER stress depends on Ire1 kinase

Keywords: Unfolded Protein Response, Ire1, kinase

Number of characters: 40,823

[3]To whom correspondence should be addressed: peter@walterlab.ucsf.edu

This chapter is a re-print of a manuscript submitted to JCB on July 14, 2010

Abstract

Accumulation of misfolded proteins in the lumen of the endoplasmic reticulum (ER) activates the unfolded protein response (UPR). Ire1, an ER-resident transmembrane kinase/RNase, senses the protein folding status inside the ER. When activated, Ire1 oligomerizes and *trans*-autophosphorylates, activating its RNase and initiating a non-conventional cytosolic mRNA splicing reaction. Splicing results in production of the transcription factor Hac1 that induces UPR target genes; expression of these genes restores homeostasis to the ER by increasing its protein folding capacity and allows abatement of UPR signaling. Here, we uncouple Ire1's RNase from its kinase activity by creating a catalytically inactive Ire1 kinase that retains the ability to bind nucleotide•Mg^{2+}. Cells expressing this mutant are able to regulate Ire1's RNase, splice *HAC1* mRNA, produce Hac1 protein, and induce UPR target genes. Unlike wild-type *IRE1*, kinase-inactive Ire1 cells displayed defects in Ire1 deactivation. Failure to properly inactivate Ire1 causes chronic ER stress and reduces cell survival under UPR-inducing conditions. We provide evidence that Ire1-catalyzed phosphoryl-transfer aids disassembly of oligomeric Ire1 signaling complexes. Thus, Ire1 kinase activity is a critical component of the UPR homeostatic feedback loop.

Introduction

In eukaryotic cells, all proteins that enter the secretory pathway must pass through the endoplasmic reticulum (ER) to be properly folded and modified. When the demand for protein folding in the ER exceeds the capacity of the compartment, misfolded proteins accumulate and activate the unfolded protein response (UPR). Activation of the UPR induces a broad transcriptional program, resulting in increased production of ER-resident protein folding machinery and ER-associated degradation components (Travers et al. 2000), and leading to ER expansion (Bernales et al. 2006; Schuck et al. 2009). As a consequence, the protein folding capacity of the ER is increased and protein folding stress is relieved. The UPR thus serves as a homeostatic feedback loop that monitors the state of the ER and alters gene expression to adjust protein folding capacity according to need, thereby restoring proper function to the ER.

In the yeast *Saccharomyces cerevisiae,* the UPR is initiated by an ER-resident transmembrane sensor, Ire1 (Cox et al. 1993; Mori et al. 1993). When activated by the accumulation of misfolded proteins, Ire1 removes a 252-nucleotide inhibitory intron from the mRNA encoding Hac1, a bZIP transcription factor that upregulates transcription of UPR target genes (Cox and Walter 1996; Mori et al. 1996; Travers et al. 2000). Removal of this intron and ligation of the severed exons by tRNA ligase produces a spliced form of *HAC1* mRNA that is efficiently translated into the Hac1 transcription factor (Cox and Walter 1996; Ruegsegger et al. 2001). Since unspliced *HAC1* mRNA is not translated prior to

the excision of this intron, Ire1 RNase activation provides the key switch in UPR signaling.

Ire1 is a single-pass transmembrane protein with one domain in the ER lumen and two domains, a kinase and an RNase, in the cytosol (Cox et al. 1993; Sidrauski and Walter 1997). The lumenal domain of Ire1 senses unfolded proteins and, once activated, drives Ire1 oligomerization (Shamu and Walter 1996; Credle et al. 2005). Ire1's lumenal domain resembles the peptide-binding domain of antigen-presenting major histocompatibility complex (MHC) proteins. We have proposed that direct binding of unfolded polypeptide chains to a presumed peptide binding groove in this domain provides the activating signal (Credle et al. 2005; Pincus 2010), although more indirect models of Ire1 activation have also been proposed (Bertolotti et al. 2000; Okamura et al. 2000; Kimata et al. 2004). Lateral oligomerization brings the cytosolic portion of neighboring Ire1 molecules into proximity, which promotes *trans*-autophosphorylation of Ire1 kinase and activation of the RNase (Shamu and Walter 1996).

Mutation of essential catalytic residues in the Ire1 kinase domain and phosphorylation sites in the kinase domain block *HAC1* mRNA splicing and prevent upregulation of UPR target genes (Cox et al. 1993; Mori et al. 1993; Shamu and Walter 1996) suggesting that phosphorylation by Ire1 kinase during activation is essential for RNase function. However, if the nucleotide-binding pocket of Ire1 kinase is mutated to specifically accomodate the ATP-competitive drug 1NM-PP1, Ire1 retains RNase activity in response to ER stress showing that

24

the requirement for phosphorylation can be entirely bypassed (Papa et al. 2003).

Occupation of the engineered 1NM-PP1 binding pocket is sufficient to cause the

conformational change in Ire1 that activates the RNase (Papa et al. 2003). Since

phosphorylation sites are necessary for RNase function but phosphorylation *per

se* appears dispensable, the functional significance of phosphoryl-transfer by Ire1

kinase has remained unclear.

Evidence from studies of Ire1-like enzymes supports the idea that

phosphoryl-transfer mediated by the kinase is indeed dispensable for nuclease

activation. RNase L, a close homolog of Ire1, is a cytosolic, ligand-activatable

RNase that has lost kinase activity but retained a catalytically inactive pseudo-

kinase domain (Dong et al. 2001). In contrast, the kinase activity of Ire1 has

been preserved in evolution, suggesting a functional role for Ire1-mediated

phosphoryl-transfer. Although previous findings with 1NM-PP1-sensitized Ire1

kinase are in apparent contradiction with this idea, those data show only that Ire1

kinase activity can be bypassed without consequence for RNase activation; they

do not rule out a possible role for the kinase in the broader scope of UPR

biology.

In this study, we explored the role of the Ire1 kinase function *in vitro* and *in

vivo* by rationally designed, conservative mutagenesis of central catalytic

residues in the Ire1 kinase active site. Mutations were designed to preserve

ATP•Mg^{2+} co-factor binding to Ire1 but to selectively disrupt catalytic

phosphotransfer. We show that these mutations yield a kinase-inactive Ire1 that

retains wild-type RNase activity in living cells. This variant of Ire1 is activated by

25

unfolded protein accumulation without a requirement for exogenous drugs, such as 1NM-PP1, thereby eliminating potential complications of off-target effects of the drug within the cell. These studies confirmed the view that Ire1's kinase domain regulates its RNase activity, but also revealed a critical role for phosphoryl-transfer in the homeostatic feedback of the UPR.

Results

Mutations in Ire1 kinase abolish phosphoryl-transfer but preserve RNase activity.

Based on sequence conservation between Ire1 and related CDK2-like kinases and on the recently solved crystal structures of the cytosolic portion of Ire1 (Lee et al. 2008; Korennykh et al. 2009), we designed an Ire1 variant with uncoupled kinase and RNase activities. To this end, we identified two catalytic residues, D797 and K799, in the nucleotide-binding pocket of Ire1 kinase. These residues are predicted to coordinate the terminal phosphate of ATP bound to Ire1 kinase (Fig. 1A), and by analogy to other kinases, are required to catalyze phosphotransfer (Lee et al. 2008). We reasoned that mutating these residues to aspargines would preserve overall steric packing, hydrophobicity and hydrogen bonding at the kinase active site but disable proton transfer and thereby abolish phosphorylation (Fig. S1A). Thus, we expected that the mutant Ire1(D797N,K799N) would be kinase-inactive but still able to activate its RNase via nucleotide binding. To complement these studies, we constructed a second kinase-inactive Ire1(D828A) variant. This mutation, which has been characterized previously (Mori et al. 1993; Huse and Kuriyan 2002; Papa et al. 2003), is predicted to disrupt coordination of the Mg^{2+} ion and block Ire1 kinase by preventing both electrophilic catalysis by Mg^{2+} (Bossemeyer et al. 1993; Huse and Kuriyan 2002) and critical Mg^{2+}-dependent conformational changes (see Discussion).

To carry out *in vitro* studies, we recombinantly expressed and purified the cytosolic portion of Ire1 wild-type (WT) and mutants. These constructs consisted of kinase and RNase domains preceded at the N-terminus by 32 amino acids derived from the linker region that tethers the kinase domain to the transmembrane region. We previously showed that this peptide extension is important, as it enhances Ire1's ability to active its RNase by up to four orders of magnitude (Korennykh et al. 2009). We term these constructs Ire1KR32 (WT) (Korennykh et al. 2009), Ire1KR32(D797N,K799N), and Ire1KR32(D828A).

MALDI mass spectrometry analyses have shown that WT Ire1KR32 is highly phosphorylated when purified from *E. coli*, likely as a result of autophosphorylation (Korennykh et al. 2009). Phosphorylation is evident in the mass-to-charge ratio (M/z) of WT Ire1KR32, which is significantly higher than expected based on its theoretical molecular weight. The shift of approximately 1.3 kD is consistent with the presence of approximately 17 phosphates and can be ameliorated by phosphatase treatment [13] (Fig. S1C). In contrast, purified Ire1KR32(D797N,K799N) and Ire1KR32(D828A) have M/z values that are precisely as expected based on their primary sequences, indicating that these proteins are entirely unphosphorylated (Supplemental Fig. S1B and Korennykh *et al.*, 2009, Supplemental Fig. S7). These data suggest that Ire1KR32(D797N,K799N) and Ire1KR32(D828A) are kinase-inactive.

To confirm that Ire1KR32(D797N,K799N) was indeed kinase-inactive, we measured *trans*-autophosphorylation of the recombinant proteins in an *in vitro* kinase assay. As expected, WT Ire1KR32 showed robust *trans*-

autophosphorylation (Fig. 1B, lanes 1-3) while Ire1KR32(D797N,K799N) and Ire1KR32(D828A) exhibited no detectable kinase activity (Fig. 1B, lanes 4-6 and 7-9, respectively). To show that the kinase-inactive Ire1 mutants are properly folded and competent substrates for phosphorylation, we mixed recombinant kinase-inactive Ire1 proteins with a shorter WT version, Ire1KR, lacking the 32-amino acid peptide extension (Korennykh et al. 2009). This enzyme retains WT kinase activity (Fig. 1B, lanes 10-12) and can be distinguished from the Ire1KR32 versions by its lower molecular weight. When we mixed Ire1KR *in vitro* with either Ire1KR32(D797N,K799N) or Ire1KR32(D828A), we detected robust phosphorylation of the mutant enzymes (Fig. 1B, lanes 13-15 and 16-18, respectively; upper bands). In these mixing reactions, the upper bands corresponding to kinase-inactive variants of Ire1 were more extensively labeled with radioactive phosphate than WT enzyme, likely due to the greater number of unphosphorylated residues in kinase-inactive Ire1 available for phosphorylation when introduced to kinase-active enzyme.

Based on the observation that occupation of the active site of Ire1 kinase by co-factor is sufficient to cause activation of the RNase, we expected that Ire1KR32(D797N,K799N) would retain RNase activity and that its activity would be stimulated by the presence of nucleotide. In contrast, Ire1KR32(D828A) should be non-responsive to the addition of co-factor. To test this prediction, we measured RNase activity in an *in vitro* cleavage assay using HP21, a previously characterized small substrate RNA containing a specific Ire1 cleavage site, in the presence or absence of ADP•Mg^{2+} co-factor. In previous experiments,

ADP•Mg^{2+} stimulates Ire1KR32's RNase activity by ~200-fold (Korennykh et al.

2009). Here, in the absence of co-factor, all three enzymes exhibited the same

basal RNase activity as Ire1KR32 (Fig. 1C, "apo"), consistent with previous

observations (Korennykh et al. 2009). Addition of ADP•Mg^{2+} increased the

RNase of Ire1KR32(D797N,K799N) 10-fold (versus ~100-fold for WT Ire1KR32)

and had no effect on the RNase activity of Ire1KR32(D828A) (Fig. 1C, "ADP").

Interestingly, the addition of APY29, a small molecule drug that activates Ire1

kinase without requiring Mg^{2+} [13], stimulated RNase activity of both

Ire1KR32(D797N,K799N) and Ire1KR32(D828A) (Fig. 1C). These data are

consistent with the idea that binding of co-factor stimulates the RNase activity of

Ire1 in the absence of phosphorylation (Papa et al. 2003). In *in vitro* assays

using the HP21 substrate, the RNase activity of Ire1KR32(D797N,K799N) was

10-fold lower than that of WT. However, when a larger 443-nt *Xbp1* mRNA-

derived RNA fragment was used as a substrate [13], Ire1KR32(D797N,K799N)

cleaved with a rate (k_{obs} = 0.19 s^{-1}) indistinguishable from that of WT Ire1KR32

(k_{obs} = 0.19 s^{-1}) (Fig. 1D). This longer substrate RNA more closely resembles

the endogenous *in vivo* substrate of Ire1 RNase, suggesting that kinase-inactive

Ire1(D797N,K799N) should retain RNase function in living cells.

Ire1 kinase activity is dispensable for *HAC1* mRNA splicing but enhances

cell survival under ER stress.

Since our *in vitro* results showed that we had successfully uncoupled the

kinase and RNase functions of Ire1, we used kinase-inactive Ire1(D797N,K799N)

to directly investigate the role of Ire1 kinase activity *in vivo*. This approach afforded the first opportunity to ask this question without requiring the addition of exogenous drug as past studies necessitated.

The *in vitro* studies predict that cells expressing Ire1(D797N,K799N) should splice *HAC1* mRNA upon UPR induction. To test this, we constructed strains that each carry a chromosomally integrated mutant *IRE1* allele as the sole copy of *IRE1* in the cell. We then induced the UPR and measured *HAC1* mRNA splicing by Northern blotting. We induced ER stress with DTT, which causes protein misfolding in the ER by disrupting disulfide bond formation. As predicted, spliced *HAC1* mRNA was produced upon DTT treatment in *ire1(D797N,K799N)* cells (Fig. 2A, lanes 7 & 8). In contrast, *HAC1* mRNA was not spliced in *ire1Δ* or *ire1(D828A)* cells. In these experiments, *ire1(D797N,K799N)* proved mildly hypomorphic, as the amount of spliced *HAC1* mRNA produced in the mutant cells was reduced compared to WT. The levels of this reduction varied between experiments and was frequently not detectable. Nevertheless, these data reinforce the notion that Ire1 kinase activity is not required for RNA splicing. Moreover, we can infer from these data that co-factor occupancy of the kinase active site is important *in vivo* and requires an intact Mg^{2+} binding site (which is destroyed in Ire1(D828A)). Thus, it is likely that nucleotide•Mg^{2+} binding to Ire1 kinase plays a key role in RNase activation *in vivo*.

We were surprised to discover that splicing of *HAC1* mRNA in *ire1(D797N,K799N)* cells failed to ensure cell survival under ER stress. When plated on UPR inducing medium, *ire1(D797N,K799N)* cells displayed a severe

31

growth defect (Fig. 2B). This resulted from loss of cell viability rather than growth

arrest: sustained ER stress, killed *ire1(D797N,K799N)* cells significantly earlier

than WT cells (Fig. 2C).

In search of an explanation for this growth defect, we tested whether

functional Hac1 protein was produced from spliced *HAC1* mRNA in

ire1(D797N,K799N) cells. To this end, we measured Hac1 protein production

and determined the scope of the transcriptional response by assessing global

mRNA expression after UPR induction.   WT *IRE1* or *ire1(D797N,K799N)* cells

expressing HA-tagged Hac1 were treated with DTT to induce the UPR and

probed for HA-Hac1 by Western blotting. *Ire1(D797N,K799N)* cells produced

Hac1 protein at nearly WT levels (Fig. 2D). Likewise, the microarray

transcriptional profile of UPR-induced *ire1(D797N,K799N)* cells revealed a profile

indistinguishable from that of WT cells (Supplemental Fig. S2A). Canonical UPR

target genes were upregulated with similar kinetics, and to a comparable extent,

in WT and *ire1(D797N,K799N)* cells. Specific UPR target genes are highlighted

in Figure 3A. Taken together, these data show that reduced *HAC1* mRNA

splicing in *ire1(D797N,K799N)* cells does not lead to impairment of canonical

UPR signaling.

One reason that a cell might die despite expression of target genes is that

mRNAs are not translated. To confirm that protein products corresponding to

UPR targets were also made, we determined Kar2 protein levels by Western

blotting and measured global translation rates during the ER stress. The

induction of Kar2 mirrored the microarray result for both WT and

ire1(D797N,K799N) mutant cells (Fig. 3B), confirming that expression of this canonical UPR target was intact in both strains. Furthermore, general translation rates were equivalent in both WT and *ire1(D797N,K799N)* cells (Supplemental Fig. S2), indicating that global mRNA translation was not impaired in mutant cells. No explanation for the enhanced loss of cell viability of *ire1(D797N,K799N)* mutant cells was evident in these data.

As a consequence of UPR activation, the ER expands to meet the increased need for protein folding capacity (Cox et al. 1997; Bernales et al. 2006; Schuck et al. 2009). To further ensure that UPR signaling downstream of Ire1 was unbroken, we measured ER expansion. Using a GFP-tagged version of the ER marker, Sec63 (Prinz et al. 2000), we quantified expansion of the cortical ER before and after UPR induction in WT and *ire1(D797N,K799N)* cells. In a confocal section of an unstressed cell, the cortical ER marked by Sec63-GFP is visible underneath the plasma membrane as a broken line. Upon ER stress, the cortical ER appears as a continuous line, indicating ER expansion. Consistent with microarray data showing normal induction of target genes, UPR-mediated ER expansion occurred normally in mutant cells (Fig. 3C & D). Taken together, the data presented thus far indicate that canonical UPR activation remains intact in *ire1(D797N,K799N)* cells.

Ire1(D797N,K799N) fails to adapt to sustained ER stress.

The negative feedback response that is mediated by the UPR is characterized by an activation phase in which Ire1 begins to signal and an

adaptive phase that occurs when cells adjust to ER stress and Ire1 is turned off (Pincus 2010). Since our findings indicate that Ire1 activation and induction of its downstream transcriptional targets are normal in *ire1(D797N,K799N)* cells, we set out to examine the dynamics of Ire1 activation and attenuation in *ire1(D797N,K799N)* cells. To this end, we took advantage of a splicing reporter, "SR", previously developed in our laboratory (Aragon et al. 2009). In SR, the *HAC1* open reading frame has been replaced by that of *GFP* (Fig. 4A), while the intron as well as the 5' and 3' UTRs of the *HAC1* mRNA are maintained so that translational inhibition of SR mimics that of the *HAC1* mRNA. Ire1-mediated splicing of this reporter produces a fluorescent GFP signal that can be quantitatively measured by flow cytometry.

In WT cells, SR fluorescence increased over time with increasing DTT concentration (Fig. 4B). At low DTT concentrations (below ~ 2 mM), Ire1 activity in WT cells reached a plateau after ~ 120 minutes. This plateau, a result of the long half-life of GFP, signifies Ire1 deactivation and is characteristic of an intact homeostatic response that restores the folding capacity of the ER and quells Ire1 signaling.

In *ire1(D797N,K799N)* cells, SR splicing in the first 60 to 120 minutes was identical to that observed in WT cells. However, Ire1 activity persisted throughout the time course and continued to rise even at doses of DTT to which WT cells adapted (Fig. 4C). This phenomenon was most evident when reporter activity was plotted as a function of DTT concentration (Fig. 4D and E). At the 60 minute time point, the dose-response curves for both WT and *ire1(D797N,K799N)* cells

overlapped, indicating that the activation phase for both WT and mutant enzymes was equivalent (Fig. 4D). In marked contrast, at 240 minutes, the curves deviated substantially (Fig. 4E), indicating that after prolonged ER stress Ire1(D797N,K799N) continued to signal at low and intermediate doses of DTT. Note that in these experiments both WT Ire1 and Ire1(D797N,K799N) displayed the same basal activity (Figs. 4D & 4E, [DTT] = 0.3 mM) and reached the same maximal activity ([DTT] = 3.3 mM), indicating that Ire1 activation *per se* was fully intact in the mutant cells (Supplemental Fig. S3).

As a second measure of Ire1 activity, we monitored Ire1 oligomer formation, which can be observed and quantified by fluorescent microscopy as foci in living cells. Oligomer formation closely correlates with *HAC1* mRNA splicing and therefore is a powerful tool for monitoring Ire1 activation *in vivo* (Aragon et al. 2009). As in our previous studies, we inserted GFP between the transmembrane linker and kinase domains of WT and mutant forms of Ire1, a location that does not interfere with Ire1 function (Aragon et al. 2009). We measured foci formation of functional WT and mutant Ire1-GFP under conditions at which the adaptation phase dose-response curves of Ire1(D797N,K799N) and WT are most divergent (Fig. 4E, [DTT] = 1 mM, dotted line). As shown in Figure 4F, Ire1(D797N,K799N)-GFP formed foci that persisted to the end of the 90 min time course of the experiment, whereas WT Ire1-GFP formed smaller, transient foci (Figs. 4F and G). This result is consistent with the observation that WT cells adapted to mild ER stress and shut down Ire1 signaling, while Ire1(D797N,K799N)-GFP activation was sustained in the mutant cells. These

data indicate that *ire1(D797N,K799N)* cells fail to adapt to sustained ER stress, suggesting that homeostatic feedback is impaired despite normal induction of UPR target genes.

When we monitored Ire1(D828A)-GFP foci, we observed that foci formed readily in 1 mM DTT and quickly became much larger than in either *ire1(D797N,K799N)-GFP* or WT *IRE1-GFP* cells (Fig. 4F). This phenotype would be consistent with a complete loss of homeostatic feedback: we reason that in the absence of *HAC1* mRNA splicing, homeostasis in the ER cannot be restored and futile Ire1 oligomerization, driven by the lumenal domain, continues without avail.

Ire1(D797N,K799N) cells are able to alleviate ER stress.

In principle, the impaired adaptation exhibited in *ire1(D797N,K799N)* cells could be due to a failure of the UPR to fix the problem in the ER or to an inability of Ire1 to deactivate once the stress has been relieved. To test the first possibility, we employed a reporter of ER redox potential. DTT induces the UPR by shifting the ER redox potential to become more reducing, causing accumulation of unfolded proteins; UPR induction, in turn, serves to re-oxidize the ER lumen. The level of ER stress can be assessed using an ER-targeted redox-sensitive green fluorescent protein (ero-GFP) reporter (Hanson et al. 2004; Merksamer et al. 2008).To test whether *ire1(D797N,K799N)* cells restore the oxidizing environment to the ER during sustained UPR insult, cells were treated with 0, 1, or 2 mM DTT (Figs. 5A-C) and the ratio of reduced/oxidized ero-GFP

("r/o ratio") was measured by flow cytometry. In WT cells, the ero-GFP r/o ratio increased upon DTT treatment and then gradually decreased as ero-GFP became re-oxidized over the course of the experiment (Fig. 5A).

In *ire1(D797N,K799N)* cells the basal r/o ratio of ero-GFP was elevated relative to that in WT cells (Fig. 5B, 0 mM DTT) and resulted in a relatively smaller fold increase. Despite the diminished dynamic range of the reporter, re-oxidation was evident in *ire1(D797N,K799N)* cells at both concentrations of DTT (Fig 5D), indicating that UPR induction restored the oxidative potential of the ER. By contrast, in *ire1(D828A)* cells, the ero-GFP r/o ratio showed normal baseline levels and plateaued after DTT addition, consistent with the requirement for UPR target gene induction to restore the oxidative environment of the ER (Fig. 5C and Fig 5D).

Deactivation of Ire1(D797N,K799N) is impaired.

An unexpected explanation for the elevated baseline of the ero-GFP r/o ratio in *ire1(D797N,K799N)* cells was provided by observing the intracellular localization of ero-GFP by fluorescent microscopy. In untreated WT cells, ero-GFP was localized to the ER as expected while in *ire1(D797N,K799N)* cells, ero-GFP was partially localized to the cytoplasm (Fig. 5E). The cytosolic ero-GFP likely accounts for the higher basal ero-GFP r/o ratio measured in Figure 5B, because the cytosol is a reducing environment.

The defect in translocation of ero-GFP into the ER seen in *ire1(D797N,K799N)* cells was puzzling since our preceding data revealed no

differences between wild type and *ire1(D797N,K799N)* cells in the absence of stress. Most relevantly, no translocation defect was observed for Sec63-GFP, which properly localized to the ER in *ire1(D797N,K799N)* cells (Fig. 3C). To confirm that translocation of endogenous ER-targeted proteins was normal, we analyzed the translocation of the ER chaperone Kar2. No difference in Kar2 translocation between untreated WT and *ire1(D797N,K799N)* cells was observed (data not shown). We therefore conclude that expression of the ero-GFP reporter is responsible for its own translocation defect in *ire1(D797N,K799N)* cells. We hypothesize that sustained expression of ER-targeted ero-GFP from a strong constitutive promoter causes chronic ER stress which, in *ire1(D797N,K799N)* cells, interferes with proper ero-GFP import into the ER.

To understand the nature of this ER translocation impairment, we turned to *ire1(D828A)* cells. These cells, which are unable to mount a productive UPR, properly localized ero-GFP to the ER (Fig. 5E). Notably, the ER in these cells was morphologically disfigured, an indication of the cell's defective UPR. The lack of cytosolic ero-GFP signal in *ire1(D828A)* cells demonstrates that loss of kinase activity alone is not sufficient to impair ER translocation. Rather, a productive UPR is additionally required to cause the defect observed in *ire1(D797N,K799N)* cells. One possibility is that *ire1(D797N,K799N)* cells fail to adapt to the chronic burden imposed on the ER by ero-GFP expression and do not properly deactivate Ire1. The resulting prolonged UPR signaling would create an overload of ER-targeted proteins, which might overwhelm the capacity of the translocation machinery and cause a back-up of ER client proteins in the

cytoplasm. To address this hypothesis, we monitored the abatement of *HAC1*

mRNA splicing and resolution of Ire1 foci after removal of ER stress. Northern

blot analysis revealed that *HAC1* mRNA splicing in WT cells declined within 45

minutes of removing DTT and reset by 90 minutes after DTT removal (Fig. 6A,

top panel). In contrast, *ire1(D797N,K799N)* cells continued to splice *HAC1*

mRNA even 120 minutes after ER stress had been removed (Fig. 6A, bottom

panel), indicating that loss of Ire1 kinase activity profoundly delayed Ire1 shut-off.

The same trend was observed when we measured Ire1 foci formation: the

dissolution of foci in WT cells was noticeable as early as 30 minutes after DTT

washout, whereas Ire1(D797N,K799N) foci were still detectable 120 minutes

after DTT removal (Fig. 6B). These data are consistent with the hypothesis that

the mechanism of deactivation is impaired in Ire1(D797N,K799N).

Hyper-phosphorylation of Ire1 is required for rapid de-oligomerization.

Mass spectrometry data of the purified cytosolic portion of Ire1 suggest

that a 28-amino acid loop (residues 864 - 892) in the C-terminal end of the kinase

domain is highly phosphorylated (AK and PW, unpublished). We propose that

trans-autophosphorylation of this loop by Ire1 (termed HPL for hyper-

phosphorylated loop) might contribute to quenching Ire1 activity. If this were

true, deletion of HPL in WT *IRE1* would mimic the sustained signaling observed

in *ire1(D797N,K799N)* cells, whereas deletion of HPL in Ire1(D797N,K799N)

would have no effect on deactivation phenotype of the mutant protein. To test

this possibility, we created *ire1ΔHPL-GFP* and *ire1(D797N,K799N)ΔHPL-GFP*

cells and monitored attenuation of Ire1 foci after ER stress removal. As shown in

Figure 6B, foci in *ire1ΔHPL-GFP* cells formed readily upon treatment with 5 mM

DTT and were sustained substantially longer than in WT control cells after DTT

was removed. Likewise, the persistence of foci in *ire1(D797N,K799N)ΔHPL-GFP*

cells mirrored that in *ire1(D797N,K799N)-GFP* cells (Fig. 6B, orange and green

lines) indicating that deletion of HPL had no effect on deactivation of Ire1 in the

absence of phosphoryl-transfer. The kinetics of foci disappearance in *ire1ΔHPL*

cells resembled that in *ire1(D797N,K799N)* cells (Fig. 6B), supporting the

hypothesis that the HPL contributes to the regulation of Ire1 shut-off. Notably,

however, the phenotype in *ire1ΔHPL* cells was not as strong as that seen in

ire1(D797N,K799N) cells, indicating that phosphorylation of regions outside the

HPL must also contribute to Ire1 deactivation.

Discussion

Ire1 provides the central gate in the information flow from the ER lumen during UPR induction. In response to sensing excessive concentrations of mis- or unfolded proteins in the ER lumen, Ire1 undergoes oligomerization and activation of its RNase function, which initiates the nonconventional splicing of *HAC1* mRNA. The role of Ire1's kinase domain has remained mysterious. The paradox primarily derives from the observation that phosphate transfer can be entirely bypassed in drug-sensitized Ire1 mutants while still normally activating splicing and the down-stream transcriptional program, yet other mutations in the kinase domain impair the UPR. Here we used a rationally designed mutation in the kinase active site that blocks phosphoryl-transfer activity but preserves nucleotide•Mg^{2+} binding. The mutant retains Ire1's activation potential *in vivo*. Despite activating the canonical set of UPR target genes, however, the mutation prevents cells from restoring homeostasis. We trace this physiological defect to a defect in Ire1 shut-off, revealing a role of Ire1-mediated phosphoryl-transfer in mediating the homeostatic feedback of the UPR that is important for cell survival.

Ire1 mutations allow uncoupling of kinase and RNase activities

Occupancy of the nucleotide-binding pocket in the Ire1 kinase domain renders the cytosolic portion of Ire1 prone to oligomerization by stabilizing the kinase module in the open conformation (Korennykh et al. 2009). Oligomerization in turn causes activation of Ire1's RNAse, as interactions

41

between neighboring Ire1 molecules in the ordered oligomer stabilize essential structural elements in the RNase active site (Korennykh et al. 2009). Conformational control of the Ire1 kinase domain therefore regulates RNase activation.

Using nucleotide analogs, we recently showed that nucleotide binding *per se* is insufficient to activate the RNase; rather, nucleotide and Mg^{2+} must both be properly coordinated to trigger the activating conformational change (Korennykh et al., submitted). Therefore, it comes as no surprise that the D828A mutation, which by analogy to other kinases is predicted to block Mg^{2+} coordination (Huse and Kuriyan 2002), abolishes both phosphate transfer and endoribonucleolytic activity. Consistent with this view, the basal RNase activity of Ire1KR32(D828A) *in vitro* is comparable to that of WT apo-Ire1KR32. Moreover, APY29, a compound that binds to the Ire1 kinase active site without coordinating Mg^{2+}, stimulates the RNase activity of Ire1KR32(D828A) even in the presence of EDTA (Korennykh et al. 2009), indicating that the enzyme is not grossly misfolded and can be activated when a cognate co-factor is provided.

In the ER membrane, oligomerization of Ire1 lumenal domains triggers activation of Ire1's cytosolic kinase/RNase modules by increasing their local concentration. In this manner, Ire1's RNase activity is subservient to events in the ER lumen, and co-factor binding to the kinase domain adjusts the activation threshold. Consistent with this view, Ire1(D828A)-GFP forms foci upon UPR induction as a result of oligomerization of the ER-lumenal domain yet no RNase activation occurs. The data therefore demonstrate that, without binding of

activating cofactor, oligomerization of Ire1's lumenal domains alone (observed microscopically as clustering of Ire1-GFP in foci) is not sufficient to cause the activating oligomerization events on the cytosolic face of the membrane. Thus *in vivo*, Ire1(D828A) clusters but is both kinase- and RNase-inactive. Recent work showed that the nucleotide binding pocket of Ire1 kinase was highly conserved in a sequence comparison of yeast Ire1 species, further supporting the notion that this binding module is an essential component of Ire1 (Poothong et al. 2010).

Despite being kinase-inactive, we found that Ire1(D797N,K799N) preserves activation of the UPR. The RNase activity of Ire1KR32(D797N,K799N) is responsive to the addition of nucleotide *in vitro* and retains ER-stress responsive RNase activity *in vivo*. Taking into account our observation that *ire1(D828A)* cells do not splice *HAC1* mRNA, our data suggest that nucleotide binding is a key step in Ire1 activation *in vivo*.

Sustained production of ER-targeted proteins is detrimental

We found that Ire1(D797N,K799N) activity is sustained well beyond the time when WT Ire1 activity shuts off, illustrating a loss in the quality of the UPR homeostatic feedback regulation. While ER stress properly activates Ire1(D797N,K799N) and induces a canonical transcriptional response, the mutant enzyme continues to signal as though the response were ineffective. Thus, the kinase activity of Ire1 plays a crucial role in completing the negative feedback loop of the UPR.

In WT cells, ero-GFP is localized to the ER and can serve as a reporter of the ER environment. The same is true in *ire1(D828A)* cells, though the over-expressed, ER-targeted reporter itself induces ER stress, which impairs growth of the *ire1(D828A)* cells that cannot mount a corrective UPR. In contrast, despite inducing the canonical UPR transcriptional program, *ire1(D797N,K799N)* cells exclude a portion of ero-GFP from the ER. In this context, a fraction of the reporter is retained in the reducing environment of the cytosol and ero-GFP returns a misleading signal that does not properly report on the condition of the ER lumen. Results obtained with this reporter must therefore be interpreted with caution. We consider it likely that despite the increased baseline r/o ratio measured in *ire1(D797N,K799N)* cells, oxidative folding conditions are restored in the ER lumen. We surmise that the increase in cytosolic signal of ero-GFP is due to impaired ER translocation of the reporter.

The simplest explanation for this translocation block is that an increased load of ER-targeted proteins resulting from sustained activation of the UPR overloads the import machinery. In accordance with this view, long-term, acute ER stress leads to the appearance of pre-Kar2 protein in WT cells as well, where it was previously observed as a higher molecular weight band (e.g., see Figure 5A in reference (Schuck et al. 2009)). Thus, it appears that the capacity of a cell to adapt to the increased ER load on the ER translocation machine may be inherently limited, leading to protein mislocalization—this in turn may result in plethora of pleiotropic defects that could explain the severe growth defects observed in UPR-induced *ire1(D797N,K799N)* cells.

In mammalian cells, activation of the PERK-branch of the UPR serves to down-regulate translation and thereby to reduce the overall load of newly synthesized proteins entering the ER. In *S. cerevisae* no analogous pathway exists. The observed impairment in ER protein translocation might serve a corresponding and thus perhaps physiologically desirable function: to slow the influx of protein into the secretory pathway under conditions of ER stress. While targeted influx of protein into the ER is beneficial early during the UPR, it likely has deleterious effects on the cell when sustained long term.

Phosphorylation of Ire1 is important for deactivation

A compelling finding in this work is that phosphotransfer by Ire1 kinase, while largely dispensable for its activation, plays an important role in Ire1 shut-off. Abatement of *HAC1* mRNA splicing and dispersal of foci are delayed in *ire1(D797N,K799N)* mutant cells, both under mild ER stress where the UPR in WT cells can restore homeostasis and under massive ER stress followed by washout of the inducing agent. Here we propose that phosphorylation of Ire1 contributes significantly to its deactivation. While the molecular mechanism by which phosphorylation promotes Ire1 shut-off is currently not understood, we have shown that a 28-amino acid surface loop (HPL) on the Ire1 kinase domain is important for efficient shut down of Ire1 signaling. Since deletion of the HPL from Ire1 only partially phenocopies the *D797N,K799N* mutation, it is likely that other regions in Ire1 also contribute. The HPL contains 7 serine and 2 threonine residues that could be phosphorylated. Peptides corresponding to this loop are

45

selectively missing from mass spectrometry analyses of recombinant, phosphorylated Ire1KR32 yet can be detected after phosphatase treatment (AK & PW, unpublished observation). Since phosphopeptides are notoriously difficult to detect by mass spectrometry, these data suggest that peptides in this loop may be phosphorylated. Deletion of the HPL from a recombinant Ire1 construct, Ire1KR32Δ28, was necessary in order to yield a high-resolution crystal structure of active oligomeric Ire1 (Korennykh et al. 2009). These observations lead us to speculate that the HPL is highly phosphorylated and destabilizes oligomerization of the cytosolic portion of Ire1 *in vitro,* perhaps by charge repulsion. A similar mechanism might operate *in vivo,* with phosphorylation of the HPL contributing to dissolution of Ire1 oligomers and thereby to Ire1 deactivation. Alternatively, some still unknown UPR-modulating protein might bind the phosphorylated HPL and, akin to arrestin binding to G-protein coupled receptors, coordinate timely shut off of Ire1 signaling. In addition, it remains possible that Ire1 kinase has other, yet unidentified, targets that promote cell survival when phosphorylated.

Demonstrating a role of Ire1 phosphorylation in its shut-off does not contradict the notion that phosphorylation events also play a role in its activation. In particular, we have previously shown that phosphorylated residues in Ire1's activation loop form salt-bridges to adjacent Ire1 subunits in the active oligomer (Korennykh et al. 2009). The hypomorphic effects on *HAC1* mRNA splicing observed in *ire1*(*D797N,K799N)* cells may result from a lack of such positive feedback that enhances oligomer stability initially through phosphorylation.

Destabilization of Ire1 oligomers by phosphorylation of the HPL and other sites may be temporally delayed and serve as a molecular timer that balances oligomer assembly and disassembly. In this scenario, both forward and reverse reactions would remain responsive to changing conditions in the ER lumen and the Ire1 signal transmitted via the oligomerization state of the lumenal domain. Longer Ire1 activity would lead to the accumulation of a greater number of phosphates and an Ire1 oligomer would be increasingly destabilized. In this way, phosphorylation may aid the rapid disassembly even of large oligomers that are held together through multiple, mutually reinforcing intramolecular interactions. The lumenal domain of Ire1 would thus remain empowered as the sole driver of activation and de-activation, thereby rendering Ire1 highly sensitive to changes in the ER lumen.

Materials and Methods

Yeast strains and growth conditions

Cells were grown in 2X SDC supplemented with 100 µg/ml inositol. Over the course of this study, we noticed that Ire1 kinase-inactive cells were sensitive to saturation in culture. Thus, cells grown in culture were kept at sub-saturating conditions for at least 12 hours prior to beginning any experiment.

In vitro assays

Recombinant Ire1 proteins were purified from *E. coli* as described previously (Korennykh et al. 2009).

Kinase assays were performed using 10 µM of purified Ire1 in kinase buffer (20 mM HEPES (pH 7.0 at 30°C), 70 mM NaCl, 2 mM $Mg(OAc)_2$, 5 mM DTT, 5% glycerol) supplemented with 0.033 µM $\gamma^{32}P$-ATP (Perkin Elmer). Reactions were carried out at 30°C. In reactions containing two distinct versions of recombinant Ire1 protein, 5 µM of each was added. Phosphorylated proteins were separated on a 12% denaturing polyacrylamide gel and detected with a phosphorimager screen (Molecular Dynamics).

MALDI mass spectrometry and *in vitro* RNA cleavage assays were carried out as described by Korennykh *et al*. 2009.

Isolation of Total RNA and Northern Blot Analysis

Total RNA was isolated from yeast cells using hot acid phenol chloroform extraction (Ruegsegger et al. 2001). Unless otherwise indicated, the UPR was induced by the addition of 2 mM DTT (Gold Biotechnology) for 40 minutes. Northern blot analysis was carried out using 15 μg of total RNA separated on a 1.5% (w/v) denaturing agarose gel and transferred to a supported nitrocellulose membrane (GE Water & Press Technologies). The *HAC1* mRNA was detected using a radiolabeled 500bp DNA probe directed against the 5'exon of the transcript (Cox and Walter 1996).

Cell Viability Assays

To score the plate phenotype, yeast cells were grown to an OD_{600} of 0.3 or lower and diluted to equal cell numbers. Cell suspensions were serially diluted 1:5 and transferred to plates using a pin tool. UPR-inducing plates contained 0.25 μg/ml tunicamycin (Calbiochem). To analyze cell viability in culture, cells were grown in the presence of 2 mM DTT at 30°C for 26 hours. At each time point, cells were counted, the OD_{600} was measured and 300 cells were plated onto permissive media. Colony forming units (CFUs) were counted from the plates after 3 days at 30°C. Viability was calculated by diving the number of CFUs by the number of cells plated. Cells were kept below an OD_{600} of 0.2 and the DTT was refreshed throughout the course of the experiment.

Isolation of Protein and Western Blot Analysis

Total protein was isolated from cells by vortexing in the presence of glass beads in 8 M urea, 50 mM HEPES pH 7.4, and 1% SDS. Samples were boiled then cleared by centrifugation at 16,000 x g for 10 minutes. 25 µg total protein was separated by SDS-PAGE (NuPAGE, Invitrogen), transferred to nitrocellulose and probed with antibody. For HA-epitope detection, the monoclonal HA.11 (Covance) was used at a dilution of 1:3000. Pgk1 protein was detected using Pgk1-specific antibody at a 1:5000 dilution (Invitrogen). For detection of the Kar2 protein, a Kar2-specific antibody (Walter laboratory, UCSF) was used at a 1:5000 dilution.

Microarray Analysis

Cultures were inoculated to an OD_{600} of 0.05 and grown at 30°C in 2x synthetic media supplemented with 100 µg/ml inositol. Upon reaching an OD_{600} of 0.3, the UPR was induced by the addition of 2 mM DTT. Cells were harvested at 0, 30, 60, and 120 minutes from 500 ml of culture (150 ODs) by filtration onto a nitrocellulose membrane (Millipore). Membranes were frozen in liquid nitrogen and stored at -80°C prior to RNA isolation.

Total RNA was isolated using hot acid phenol choloroform extraction (Sarver and DeRisi 2005). cDNA was reverse transcribed from 15 µg of total RNA using Superscript III (Invitrogen) and a 1:1 mixture of oligo(dT) and random hexamers. Reverse transcription was carried out in the presence of amino-allyl dUTP (aa-dUTP) (Ambion) at a ratio of 2:3 aa-dUTP:dTTP. A fraction of each

cDNA sample was pooled to create a reference sample; the pooled reference was labeled with Cy3 dye (Amersham). The remaining sample cDNA from each time point was labeled with Cy5 dye (Amersham). Each Cy5 labeled sample was mixed with an equal amount of Cy3 labeled pooled reference cDNA and hybridized to oligonucleotide microarrays representing the full yeast genome (DeRisi et al. 1997). Microarray data were extracted and analyzed using the methods described in Sarver & DeRisi (2005). Prior to clustering, data were compressed such that all data corresponding to identical gene products were averaged.

Yeast oligonucleotide arrays were printed using primers for each predicted or known gene supplied by Operon (Alameda, CA). Two primer sets, AROS and YBOX, were combined to create these arrays. Oligonucleotide arrays were printed at the UCSF Center for Advanced Technology.

Measuring Global Translation Rates and ER expansion

Global translation rates were measured by monitoring ^{35}S methionine incorporation during UPR induction. Cells were grown to an OD_{600} of 0.3, harvested by filtration and resuspended in media lacking methionine. Starvation was carried out for 30 minutes at 30°C. The UPR was induced by the addition of 2 mM DTT. At the time of UPR induction, 1 µCi/ml ^{35}S methionine (Perkin Elmer) plus 50 µM cold methionine was added to cells. The OD_{600} was measured and samples were harvested every 15 minutes for 3 hours post UPR induction. Cells were lysed, total protein was isolated by TCA precipitation and scintillation counts

were measured. To graph the results, total scintillation counts were normalized to the OD_{600} and plotted over time.

To quantify ER expansion, WT or mutant *ire1* cells bearing Sec63-GFP on a CEN-ARS plasmid were treated with 2 mM DTT and imaged by confocal microscopy 2 hours after UPR induction. The cortical ER was quantified as described by Schuck *et al*. (Schuck et al. 2009).

Splicing Reporter (SR) Assays

WT or mutant cells bearing SR integrated at the *URA3* locus were induced with DTT as indicated and flow cytometry was carried out as described previously (Pincus 2010).

Measuring the Redox Potential of the ER using the ero-GFP reporter

To measure the ER redox potential the ero-GFP reporter (Merksamer et al. 2008) was integrated into the *TDH3* locus of WT or mutant cells. The UPR was induced with 1 mM or 2 mM DTT. GFP fluorescence at 405 nm and 488 nm was measured by flow cytometry and the ratio of the 405 nm and 488 nm signal (r/o ratio) was plotted as a function of time. Percent ero-GFP re-oxidation was calculated using the equation: *% re-oxidation = 1 – ((F-I) / (M-I)* where
I - initial ero-GFP r/o ratio (at t = 0), *M* - maximum ero-GFP r/o ratio (at t = 30 min), *F* - final ero-GFP r/o ration (at t = 240 min).

Ire1 Foci Formation and Quantitative Fluorescence Microscopy

 IRE1 was tagged with *GFP* as previously described (Aragon et al. 2009) and integrated at the *LEU2* locus to create strains YCR212, YCR213 and YCR214. Cells were grown in an Erlenmeyer flask at 30°C and transferred to a 96-well glass bottom plate coated with Concanavalin A. Ire1-GFP was imaged by spinning disk confocal microscopy and images were processed and quantified as described by Pincus *et al.* (Pincus 2010). In washout experiments, cells were treated with 5 mM DTT for 60 minutes, media was removed and replaced with fresh media lacking DTT. Images were taken prior to washout, after 60 minutes in 5 mM DTT, and at 15, 30, 45, 60, 90, and 120 minutes after washout.

Acknowledgments

References

Aragon, T., E. van Anken, et al. (2009). "Messenger RNA targeting to endoplasmic reticulum stress signalling sites." Nature **457**(7230): 736-740.

Bernales, S., K. L. McDonald, et al. (2006). "Autophagy counterbalances endoplasmic reticulum expansion during the unfolded protein response." PLoS Biol **4**(12): e423.

Bertolotti, A., Y. Zhang, et al. (2000). "Dynamic interaction of BiP and ER stress transducers in the unfolded-protein response." Nat Cell Biol **2**(6): 326-332.

Bossemeyer, D., R. A. Engh, et al. (1993). "Phosphotransferase and substrate binding mechanism of the cAMP-dependent protein kinase catalytic subunit from porcine heart as deduced from the 2.0 A structure of the complex with Mn2+ adenylyl imidodiphosphate and inhibitor peptide PKI(5-24)." EMBO J **12**(3): 849-859.

Cox, J. S., R. E. Chapman, et al. (1997). "The unfolded protein response coordinates the production of endoplasmic reticulum protein and endoplasmic reticulum membrane." Mol Biol Cell **8**(9): 1805-1814.

Cox, J. S., C. E. Shamu, et al. (1993). "Transcriptional induction of genes encoding endoplasmic reticulum resident proteins requires a transmembrane protein kinase." Cell **73**(6): 1197-1206.

Cox, J. S. and P. Walter (1996). "A novel mechanism for regulating activity of a transcription factor that controls the unfolded protein response." Cell **87**(3): 391-404.

Credle, J. J., J. S. Finer-Moore, et al. (2005). "On the mechanism of sensing

    unfolded protein in the endoplasmic reticulum." <u>Proc Natl Acad Sci U S A</u>

    102(52): 18773-18784.

DeRisi, J. L., V. R. Iyer, et al. (1997). "Exploring the metabolic and genetic control

    of gene expression on a genomic scale." <u>Science</u> **278**(5338): 680-686.

Dong, B., M. Niwa, et al. (2001). "Basis for regulated RNA cleavage by functional

    analysis of RNase L and Ire1p." <u>RNA</u> **7**(3): 361-373.

Hanson, G. T., R. Aggeler, et al. (2004). "Investigating mitochondrial redox

    potential with redox-sensitive green fluorescent protein indicators." <u>J Biol</u>

    <u>Chem</u> **279**(13): 13044-13053.

Huse, M. and J. Kuriyan (2002). "The conformational plasticity of protein

    kinases." <u>Cell</u> **109**(3): 275-282.

Kimata, Y., D. Oikawa, et al. (2004). "A role for BiP as an adjustor for the

    endoplasmic reticulum stress-sensing protein Ire1." <u>J Cell Biol</u> **167**(3):

    445-456.

Korennykh, A. V., P. F. Egea, et al. (2009). "The unfolded protein response

    signals through high-order assembly of Ire1." <u>Nature</u> **457**(7230): 687-693.

Lee, K. P., M. Dey, et al. (2008). "Structure of the dual enzyme Ire1 reveals the

    basis for catalysis and regulation in nonconventional RNA splicing." <u>Cell</u>

    132(1): 89-100.

Merksamer, P. I., A. Trusina, et al. (2008). "Real-time redox measurements

    during endoplasmic reticulum stress reveal interlinked protein folding

    functions." <u>Cell</u> **135**(5): 933-947.

Mori, K., T. Kawahara, et al. (1996). "Signalling from endoplasmic reticulum to

    nucleus: transcription factor with a basic-leucine zipper motif is required

    for the unfolded protein-response pathway." <u>Genes Cells</u> **1**(9): 803-817.

Mori, K., W. Ma, et al. (1993). "A transmembrane protein with a cdc2+/CDC28-

    related kinase activity is required for signaling from the ER to the nucleus."

    <u>Cell</u> **74**(4): 743-756.

Okamura, K., Y. Kimata, et al. (2000). "Dissociation of Kar2p/BiP from an ER

    sensory molecule, Ire1p, triggers the unfolded protein response in yeast."

    <u>Biochem Biophys Res Commun</u> **279**(2): 445-450.

Papa, F. R., C. Zhang, et al. (2003). "Bypassing a kinase activity with an ATP-

    competitive drug." <u>Science</u> **302**(5650): 1533-1537.

Pincus, D. (2010). "BiP binding to the ER-stress sensor Ire1 modulates the

    homeostatic regulation of the Unfolded Protein Response." <u>PLoS Biol, in</u>

    <u>press</u>.

Pincus, D., Chevaleir, M., Aragon, T., van Anken, E., Vidal, S., El-Samad, H.,

    Walter, P. (2010). "BiP binding to the ER-stress sensor Ire1 modulates the

    homeostatic regulation of the Unfolded Protein Response." <u>PLoS Biol</u>.

Poothong, J., P. Sopha, et al. (2010). "Domain compatibility in Ire1 kinase is

    critical for the unfolded protein response." <u>FEBS Lett</u>.

Prinz, W. A., L. Grzyb, et al. (2000). "Mutants affecting the structure of the cortical endoplasmic reticulum in Saccharomyces cerevisiae." J Cell Biol **150**(3): 461-474.

Ruegsegger, U., J. H. Leber, et al. (2001). "Block of HAC1 mRNA translation by long-range base pairing is released by cytoplasmic splicing upon induction of the unfolded protein response." Cell **107**(1): 103-114.

Sarver, A. and J. DeRisi (2005). "Fzf1p regulates an inducible response to nitrosative stress in Saccharomyces cerevisiae." Mol Biol Cell **16**(10): 4781-4791.

Schuck, S., W. A. Prinz, et al. (2009). "Membrane expansion alleviates endoplasmic reticulum stress independently of the unfolded protein response." J Cell Biol **187**(4): 525-536.

Shamu, C. E. and P. Walter (1996). "Oligomerization and phosphorylation of the Ire1p kinase during intracellular signaling from the endoplasmic reticulum to the nucleus." EMBO J **15**(12): 3028-3039.

Sidrauski, C. and P. Walter (1997). "The transmembrane kinase Ire1p is a site-specific endonuclease that initiates mRNA splicing in the unfolded protein response." Cell **90**(6): 1031-1039.

Travers, K. J., C. K. Patil, et al. (2000). "Functional and genomic analyses reveal an essential coordination between the unfolded protein response and ER-associated degradation." Cell **101**(3): 249-258.

Tables

Yeast & Plasmid Tables

Table 1	Yeast Strains
Yeast Strain	**Genotype**
YCR200	*ireΔ::TRP1, his3::UPRE-LACZ-HIS3,* W303a derivative
YCR201	as YCR200, except *ura3::IRE1-3xFLAG-URA3*
YCR202	as YCR200, except *ura3::ire1(D797N, K799N)-3xFLAG-URA3*
YCR203	as YCR200, except *ura3::ire1(D828A)-3xFLAG-URA3*
YDP002	*cry1a, ire1::KanMX6* [23]
YCR204	as YDP002, except *ura3::IRE1-3xFLAG*
YCR205	as YDP002, except *ura3::ire1(D797N, K799N)-3xFLAG*
YCR206	as YDP002, except *ura3::IRE1-3xFLAG, his3::HA-HAC1-HIS3*
YCR207	as YDP002, except *ura3::ire1(D797N, K799N)-3xFLAG, his3::HA-HAC1-HIS3*
YCR208	as YDP002, except *IRE1-3xFLAG, leu2::SR-LEU2*
YCR209	as YDP002, except *ire1(D797N, K799N)-3xFLAG, leu2::SR-LEU2*
YCR210	as YCR201, except *TDH3::ero-GFP-kanMX6-4xUPRE-mCherry*
YCR211	as YCR202 except *TDH3::ero-GFP-kanMX6-4xUPRE-mCherry*
YCR212	as YDP002, except *leu2::IRE1-GFP-LEU2*
YCR213	as YDP002, except *leu2::ire1(D797N, K799N)-GFP-LEU2*
YCR214	as YDP002, except *leu2::ire1(D828A)-GFP-LEU2*
YCR215	as YDP002, except *leu2::ire1ΔHPL-GFP-LEU2*
YCR216	as YDP002, except *leu2::ire1(D797N,K799N)ΔHPL-GFP-LEU2*

Table 2	Yeast Plasmids	
Plasmid	**Description**	**Marker**
pCR100	*IRE1-3xFLAG*, pRS306	URA3
pCR101	*ire1(D797N, K799N)-3xFLAG*, pRS306	URA3
pCR102	*ire1(D828A)-3xFLAG*, pRS306	URA3
pCR103	*IRE1-3xFLAG*, pRS303	HIS3
pCR104	*ire1(D797N, K799N)-3xFLAG*, pRS303	HIS3
pPM56	*TDH3-ero-GFP*, 4x*UPRE-mCherry* (Merksamer et al. 2008)	URA3, kanMX6
pJK59	*Sec63-GFP*, CEN (Prinz et al. 2000)	URA3

Figure 1   Mutations in Ire1 kinase abolish phosphate transfer but preserve RNase activity.

A) Two residues in the nucleotide binding pocket of Ire1 kinase are predicted to catalyze phosphotransfer. A schematic representation of Ire1 depicting the location of each functional domain. Residues D797 and K799 in the nucleotide binding pocket of the kinase domain hydrogen bond with the terminal phosphate of ATP to catalyze phosphate transfer to the substrate Serine. Mutation of D797 and K799 to non-catalytic asparagines is predicted to block phosphate transfer but allow for ATP binding. B) Mutations in Ire1 abolish kinase activity. The kinase activity of recombinant Ire1KR32 (WT; lanes 1-3), Ire1KR32(D797N,K799N) (lanes 4 - 6) and Ire1KR32(D828A) (lanes 7 - 9) were measured in an *in vitro* kinase assay. Recombinant Ire1 was mixed with 0.033 μM γ^{32}P-ATP and incubated at 30°C for the time indicated. Reactions were stopped in 1% SDS loading buffer and separated by SDS-PAGE.   A truncated version of WT Ire1, Ire1KR (lanes 10 - 12), was mixed with Ire1KR32(D797N,K799N) (lanes 13 - 15) or Ire1KR32(D828A) (lanes 16 -18). C) Kinase-inactive Ire1 species retain RNase activity *in vitro. In vitro* RNA cleavage assays were performed using purified substrate RNA, HP21, and either WT Ire1KR32, Ire1KR32(D797N,K799N) or Ire1KR32(D828A). Reactions were carried out in the presence and absence of 2 mM ADP or 100 μM APY29, an Ire1-activating drug which does not require Mg^{2+} for binding.

Figure 1

A
Lumenal Domain (1-526)
TM (527-556)
Linker (557-672)
Kinase (673-982)
RNase (983-1115)
cofactor binding pocket

ATP
γP substrate Serine
D797
K799

780   797 799   828   858

Ire1   QIASGVAHLHSLKIIHR**DLK**PQNILVSTSSRFTADQQTGAENLRILIS**D**FGLCKKLDSGQS

Ire1(D797N,K799N) QIASGVAHLHSLKIIHR**NLN**PQNILVSTSSRFTADQQTGAENLRILIS**D**FGLCKKLDSGQS

Ire1(D828A)   QIASGVAHLHSLKIIHRNLNPQNILVSTSSRFTADQQTGAENLRILIS**A**FGLCKKLDSGQS

B

Ire1KR	-	-	-	WT	WT	WT
Ire1KR32	WT	D797N, K799N	D828A	-	D797N, K799N	D828A

time (min): 0.33 3 60 0.33 3 60 0.33 3 60 0.33 3 60 0.33 3 60 0.33 3 60

← Ire1KR32
← Ire1KR

1 2 3 4 5 6 7 8 9 10 11 12 13 14 15 16 17 18   lane

C HP21

k_{obs} (s^{-1})

HP21

APO
2 mM ADP
100 μM APY29

WT   D797N, K799N   D828A   Ire1KR32

D XBP1

k_{obs} (s^{-1})

Xbp1

APO
2 mM ADP
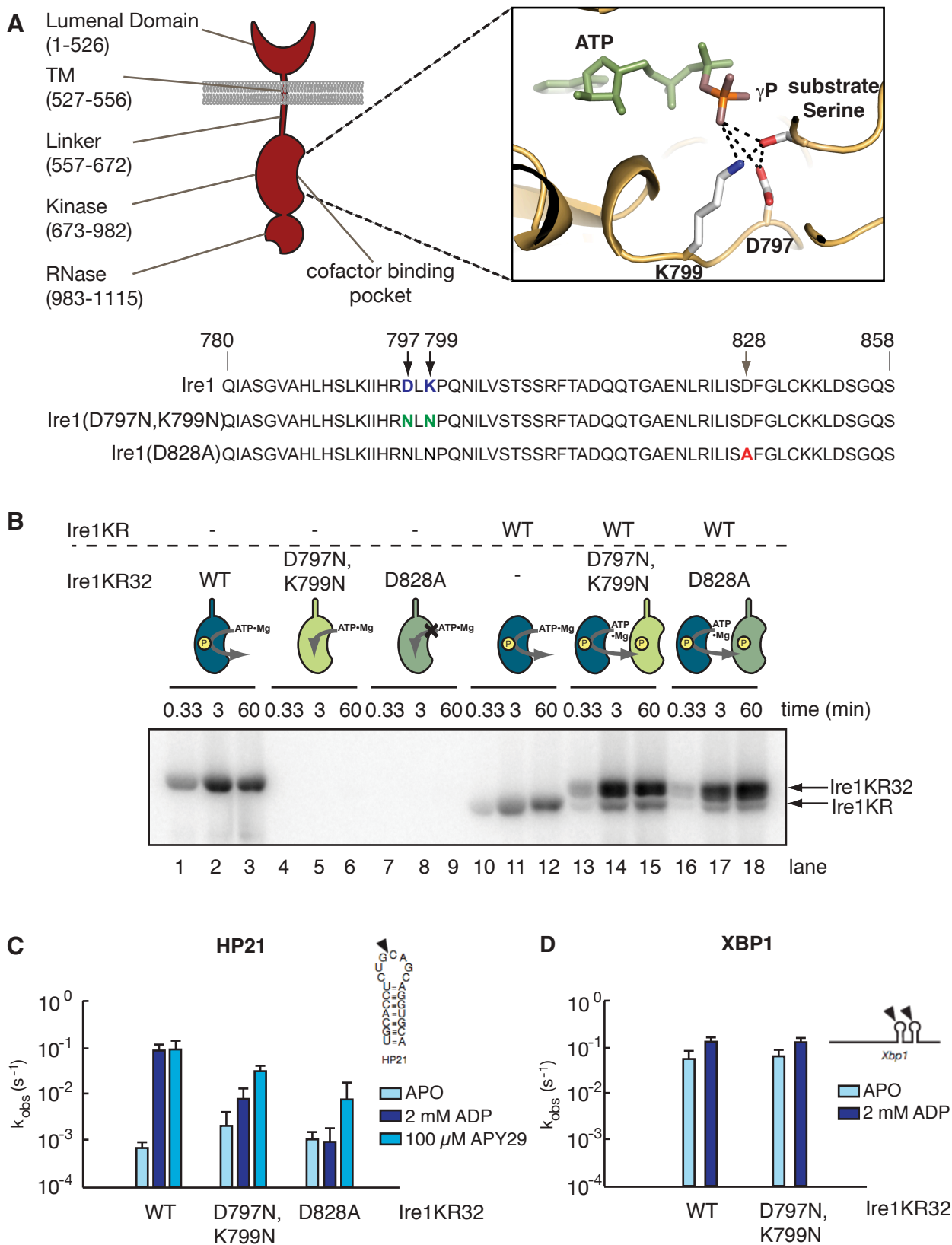
WT   D797N, K799N   Ire1KR32

61

Figure 2   Ire1 kinase activity, uncoupled from *HAC1* mRNA splicing, is important for cell survival during the UPR.

A) *HAC1* mRNA is spliced in *ire1(D797N,K799N)* cells. Cells bearing *WT IRE1* (lanes 1 & 2), a deletion of *ire1* (lanes 3 & 4), *ire1(D828A)* (lanes 5 & 6), or *ire1(D797N,K799N)* (lanes 7 & 8) were left un-induced (-) or induced with 2 mM DTT (+). *HAC1* mRNA splicing was analyzed by Northern blotting. The positions of the unspliced (u) and spliced (s) forms of *HAC1* mRNA are indicated with arrows. B) Growth of Ire1(D797N, K799N)-expressing cells is impaired on UPR-inducing medium. Cells carrying *WT IRE1*, a deletion of *ire1 (lanes 3 & 4),* *ire1(D828A)* (lanes 5 & 6), or *ire1(D797N,K799N)* were grown in culture, diluted to equal cell number, serially diluted 1:5 and plated onto permissive medium (-Tm) or medium containing 0.25 *μ*g/ml tunicamycin (+Tm). C) *Ire1(D797N, K799N)* cells lose viability under sustained, low-level ER stress. *WT IRE1* or *ire1(D797N,K799N)* cells were grown in culture to OD600 0.2, the UPR was induced by the addition of 2 mM DTT. The percent viable cells was determined by measuring the number of colony forming units over time (see Methods). DTT was refreshed and cells were kept at an optical density at or below 0.2 throughout the duration of the experiment. D-E) Hac1 protein is produced in *ire1(D797N,K799N)* cells. WT or mutant ire1 cells carrying HA-tagged Hac1 were left un-induced or induced with 2mM DTT and total protein was isolated. Samples were separated by SDS-PAGE and subjected to Western blotting using an anti-HA antibody or an anti-PGK1 antibody. Hac1 levels were

quantified using Image J software, normalized to Pgk1 levels and plotted in panel
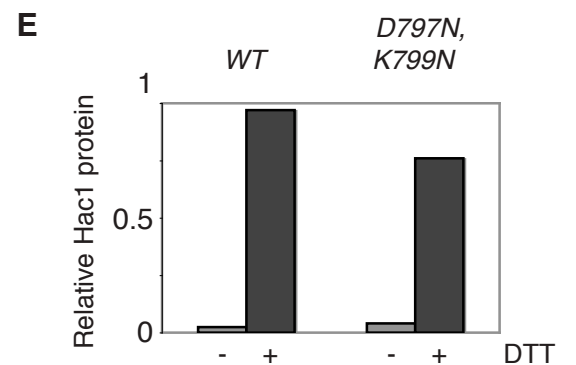
E.

Figure 2-2

A

	IRE1		ire1Δ		ire1(D828A)		ire1 (D797N,K799N)		
2 mM DTT	−	+	−	+	−	+	−	+	
	u →								HAC1 mRNA
	s →								
% spliced	4.9	65.5	1.6	0.8	2.4	1.9	3.7	31.8	
lane	1	2	3	4	5	6	7	8	

B

- Tm   + Tm

IRE1
ire1Δ
ire1(D828A)
ire1(D797N,K799N)

C

IRE1
ire1(D797N,K799N)

% viable cells

Time (hours)

D

WT   D797N, K799N   IRE1

DTT   − +   − +

HA-Hac1p

Pgk1p

E

WT   D797N, K799N

Relative Hac1 protein
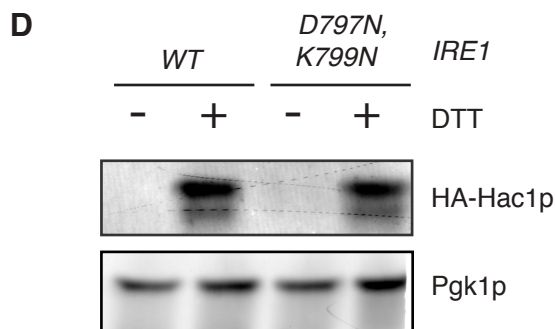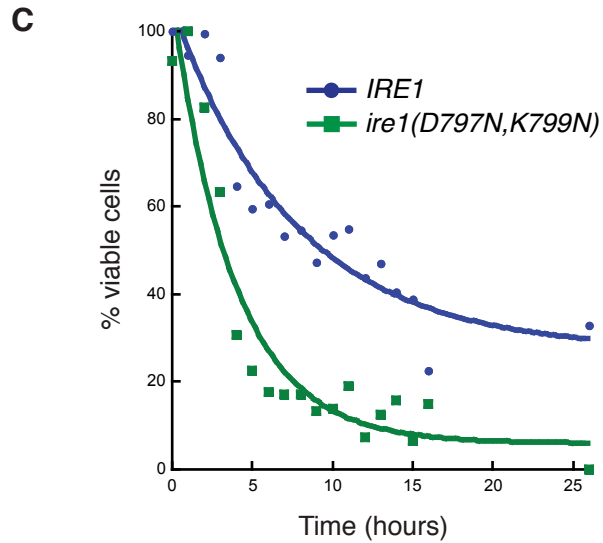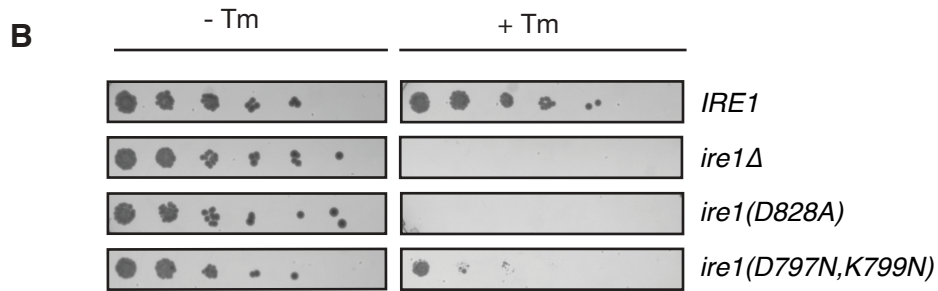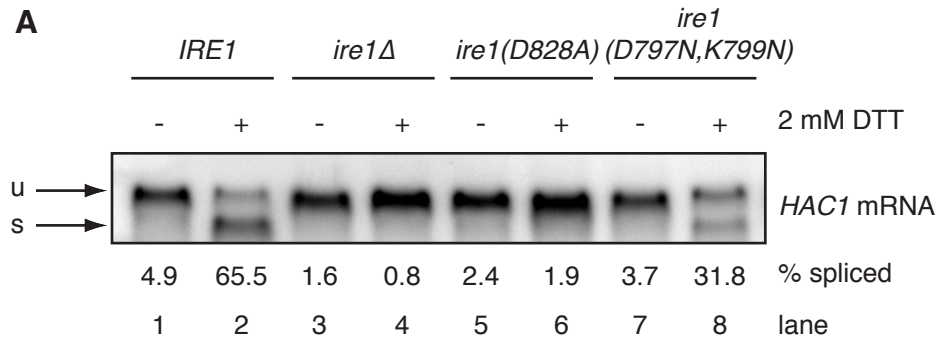
− +   − +   DTT

64

Figure 3   Downstream events in UPR activation are normal in

ire1(D797N,K799N) cells.

A) Canonical UPR target genes are upregulated in *ire1(D797N,K799N)* cells.

Microarray analysis was carried out to assess the total mRNA expression profiles

of *WT IRE1* or *ire1(D797N,K799N)* cells over time after induction with 2 mM DTT.

Cells were sampled at time 0, 30, 60 and 120 minutes. Canonical target genes,

KAR2, ERO1, *DER1*, *PDI1*, & *LHS1* were upregulated and *YDJ1* was

downregulated equally upon UPR induction in both strains. B) Kar2 protein is

induced in *ire1(D797N,K799N)* cells and mirrors mRNA induction. Total protein

was isolated from cells bearing *WT IRE1* or *ire1(D797N,K799N)* after 0, 30 or 60

minutes in 2 mM DTT and analyzed by Western blot for Kar2 protein.

Characteristic increase in Kar2 protein upon UPR induction was observed in both

strains. C-D) ER expansion occurs normally in *ire1(D797N,K799N)* cells. The

UPR was induced in WT or mutant *ire1(D797N,K799N)* cells bearing GFP-tagged

version of Sec63 as an ER marker. Images were taken prior to and after 2 hours

after UPR induction, cortical ER expansion was quantified as described in [2] and

expressed as the ER expansion index (IE). Scale bar in panel C is 2 μm in

length.

Figure 2-3

A

WT   D797N,K799N   *IRE1*

KAR2

ERO1

DER1

PDI1

LHS1

YDJ1

0   30   60   120   0   30   60   120   time (min)

scale

- 3   - 2   - 1   0   + 1   + 2   + 3

B

WT   D797N,K799N   *IRE1*

0   30   60   0   30   60   time (min)

Kar2 protein

C

Sec63-GFP

IRE1

ire1 (D797N, K799N)

untreated   2 mM DTT

D

ER expansion (IE)

untreated

2 mM DTT
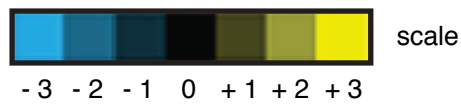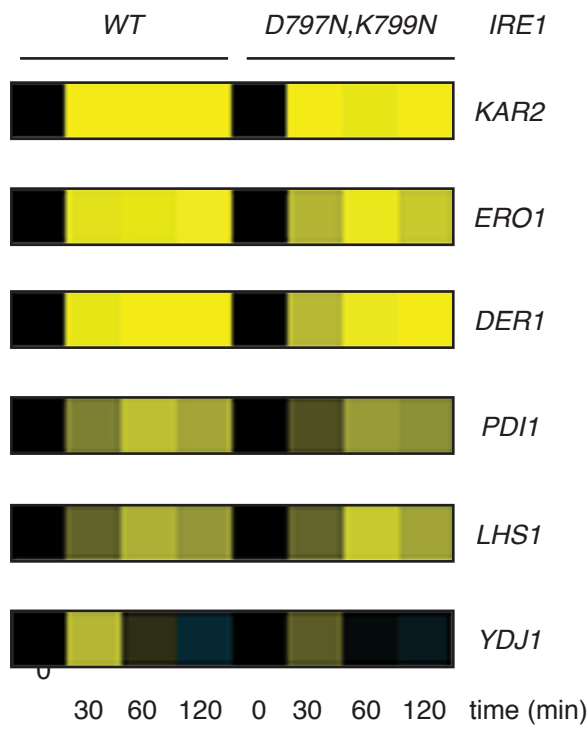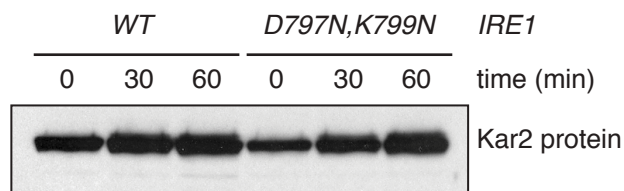
IRE1   *ire1(D797N,K799N)*

Figure 4   Activation of Ire1(D797N,K799N) continues after WT activity

has plateaued.

A) A schematic of the fluorescent splicing reporter (SR) for Ire1 activation. The

HAC1 ORF was replaced with GFP such that Ire1-mediated splicing of this

reporter produces fluorescent GFP. B-C) Splicing of SR in response to

increasing amounts of DTT. A dilution series of DTT, from 0 to 3.3 mM, was

added to cells in culture. B) WT or C) *ire1(D797N,K799N)* cells were grown at

30°C and sampled at 30-minute intervals over a 4-hour time course. GFP signal

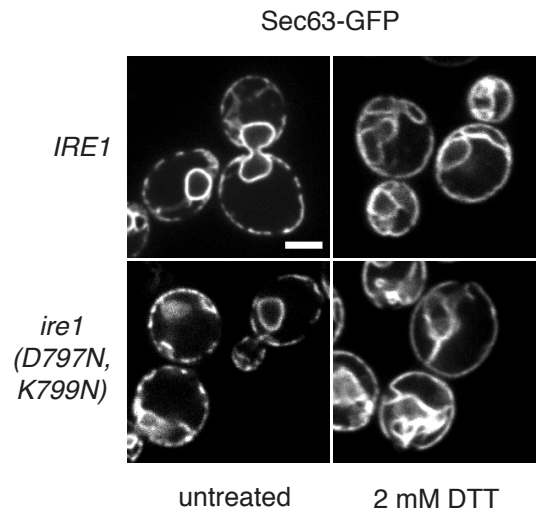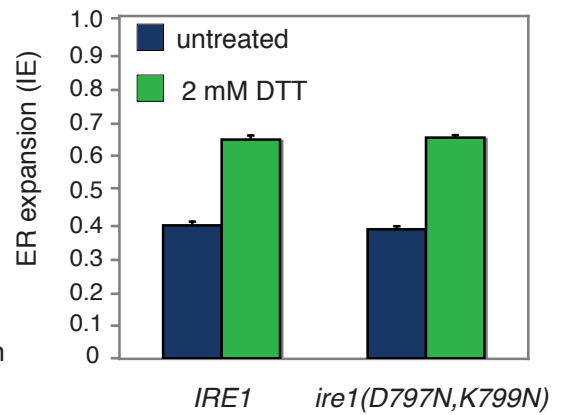was measured by flow cytometry, normalized to baseline and plotted over time.

D) The dose-response of WT and *ire1(D797N,K799N)* cells during the activation

phase of the UPR are identical. SR fluorescence was plotted as a function of

increasing [DTT] in WT and *ire1(D797N,K799N)* cells at 60 minutes after DTT

addition. E) The dose-response of WT and *ire1(D797N,K799N)* cells in the

adaptation phase of the UPR differ significantly. SR fluorescence plotted as a

function of [DTT] at 240 minutes after induction reveals that Ire1(D797N,K799N)

was significantly more active than WT at all concentrations of DTT. The dotted

line indicates the concentration of DTT at which the two curves most deviated.

F-G) Ire1(D797N,K799N)-GFP forms foci in 1 mM DTT. F) WT or

ire1(D797N,K799N) cells bearing GFP-tagged Ire1 were treated with 1 mM DTT

and formation of Ire1 foci was imaged by confocal microscopy over time. G) Foci

formation measured in 4F was quantified as % Ire1 in foci and plotted over time.

Figure 4
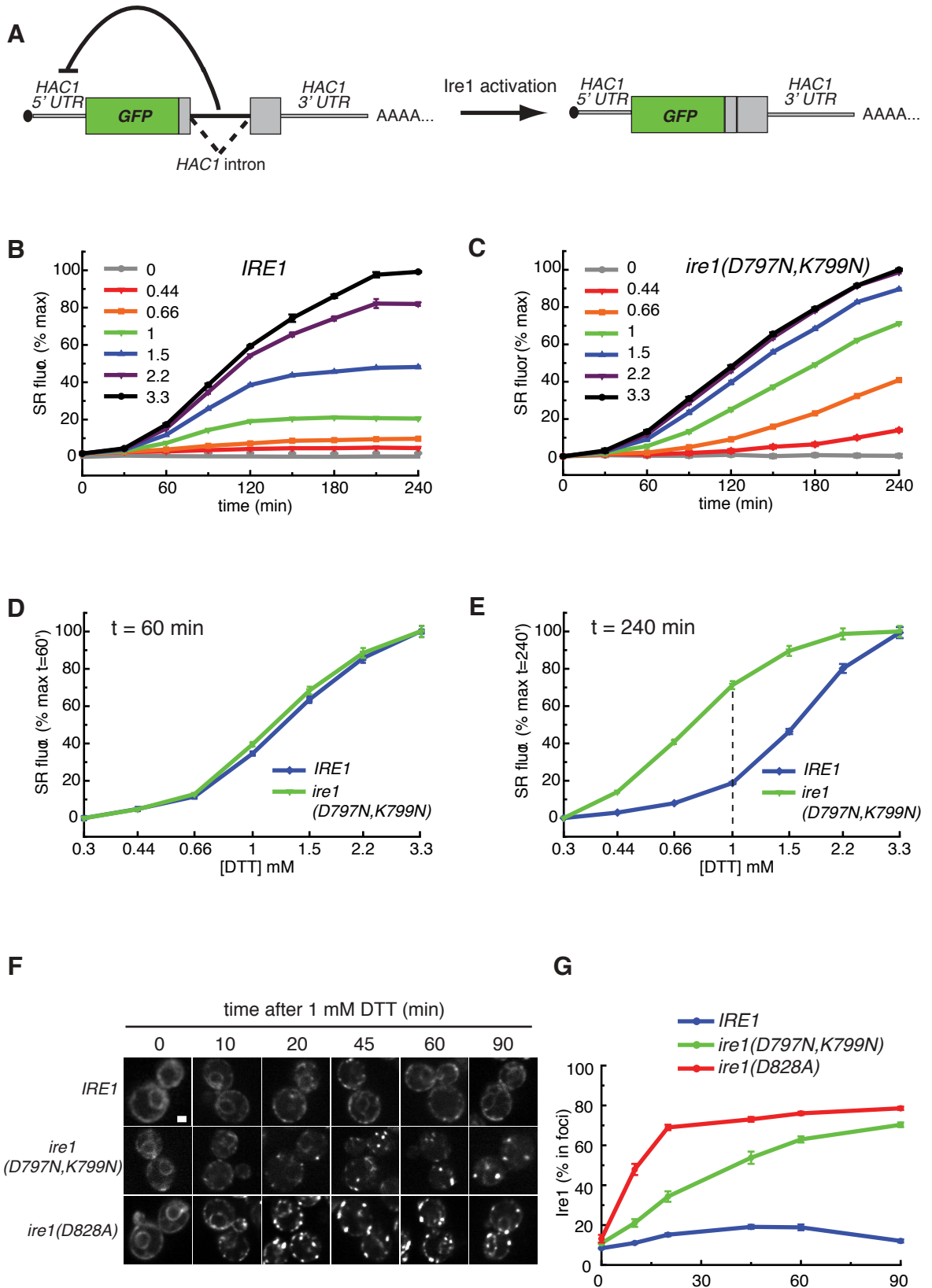
Figure 5   The oxidation potential of the ER is restored in

***ire1(D797N,K799N)* cells.**

A-D) Re-oxidation of the ero-GFP reporter occurs in the absence of kinase

activity. A) WT, B) *ire1(D797N,K799N)* and C) *ire1(D828A)* cells bearing the ER-

targeted redox reporter, ero-GFP, were treated with 0, 1 mM or 2 mM DTT.   The

ratio of reduced to oxidized signal (r/o ratio) was measured by flow cytometry and

plotted over time. D) Percent re-oxidation of ero-GFP was calculated for WT,

ire1(D797N,K799N) and *ire1(D828A)* cells in 0, 1 and 2 mM DTT (see Methods).

E) The ero-GFP reporter is partially localized to the cytoplasm in

ire1(D797N,K799N) cells. Cells expressing ero-GFP were analyzed by spinning

disk confocal microscopy.

Figure 5
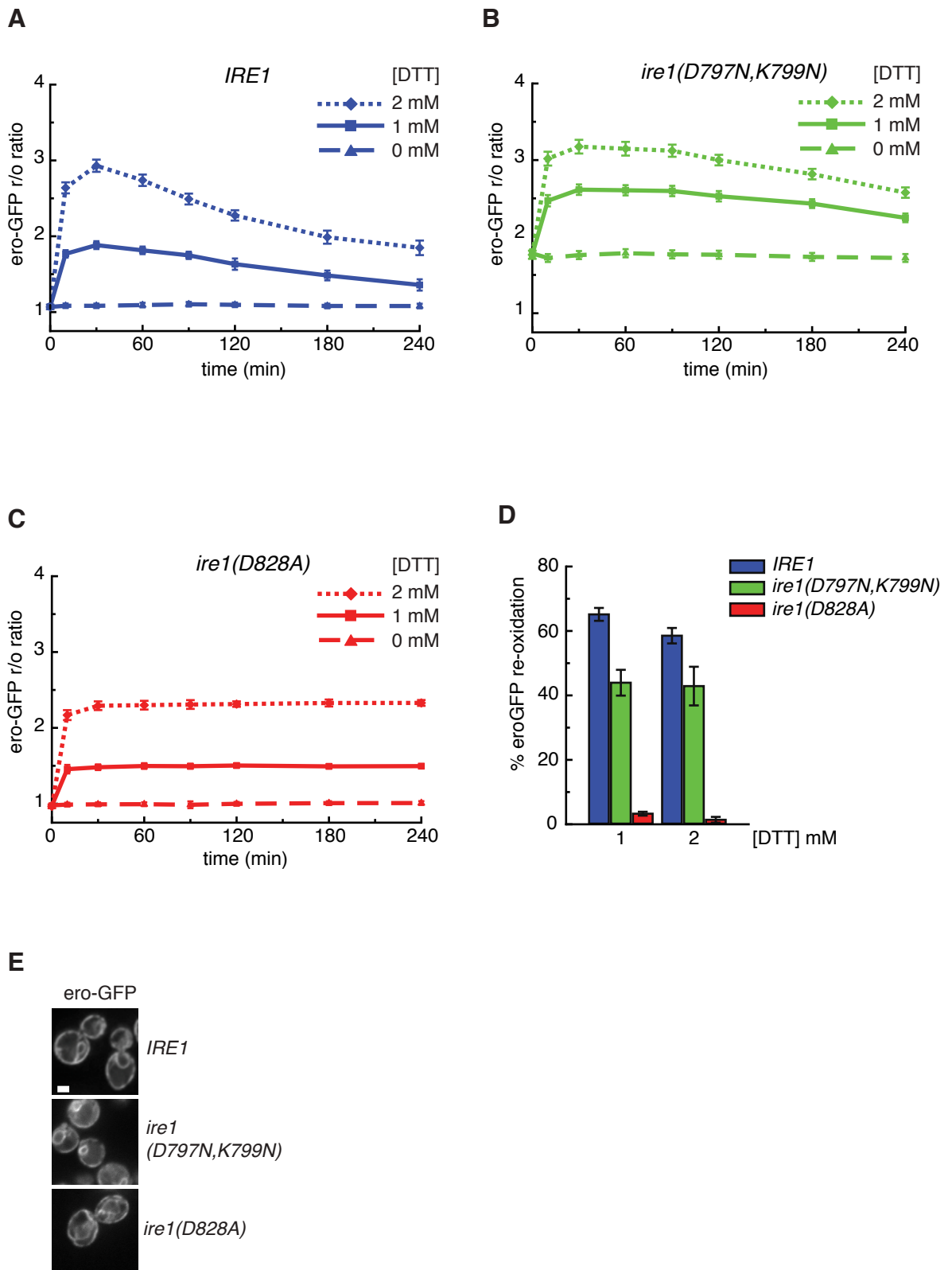
Figure 6   Shut-off of Ire1(D797N,K799N) is delayed after removal of ER stress.

A) In *ire1(D797N,K799N)* cells *HAC1* mRNA splicing continues after removal of ER stress. WT or *ire1(D797N, K799N)* cells were treated with 5 mM DTT for 60 minutes prior to DTT washout. Cell samples were taken after DTT washout and total RNA was analyzed by Northern blot for *HAC1* mRNA. B) Phosphorylation of Ire1 contributes to dissolution of oligomers after DTT washout. GFP-tagged variants of Ire1 were visualized after washout of 5 mM DTT by fluorescence microscopy. Quantitation of Ire1 foci is displayed in the lower panel.

Figure 6

A

time after DTT washout (min)

	0	15	30	45	60	75	90	105	120

IRE1 → u, s

% spliced: 62 50 44 29 18 13 8 5 3

HAC1 mRNA

ire1 (D797N,K799N) → u, s

% spliced: 70 65 61 60 43 38 25 23 20

B

time after DTT washout (min)

0   15   30   60   90   120

IRE1

ire1(D797N,K799N)

ire1(D828A)

ire1ΔHPL

ire1(D797N,K799N) ΔHPL

- *IRE1*
- *ire1(D797N,K799N)*
- *ire1(D828A)*
- *ire1ΔHPL*
- *ire1(D797N,K799N)ΔHPL*
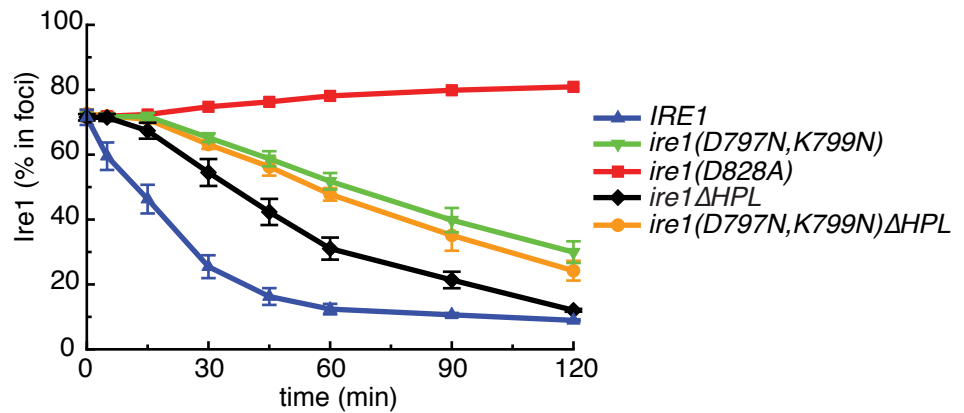
Ire1 (% in foci) vs time (min)
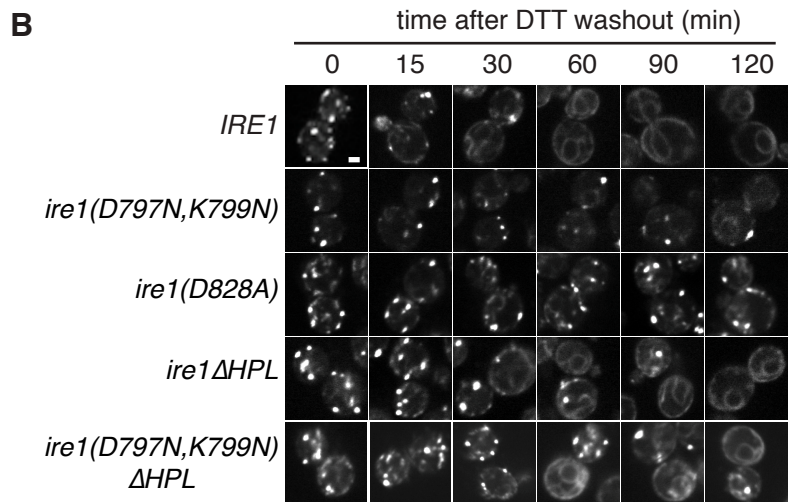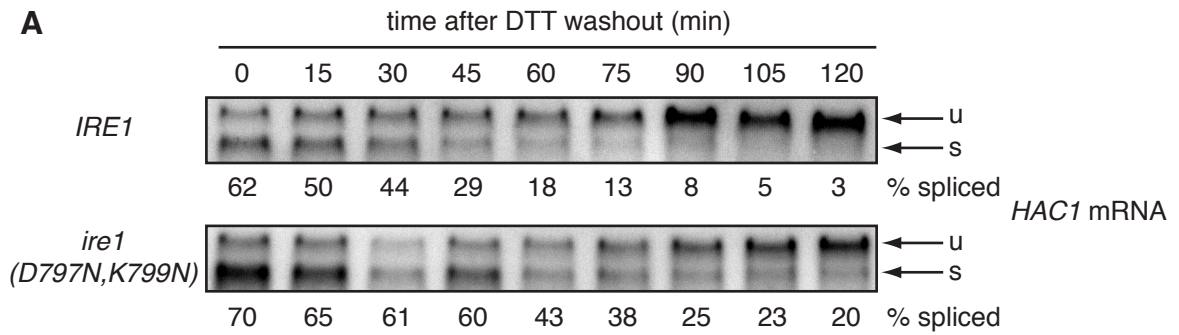
Figure S1: Mutations in Ire1 kinase abolish phosphoryl-transfer.

A) The role of D797 and K799 in phosphate transfer. Schematic diagram

depicting predicted hydrogen bonding and proton transfer between key residues

in the nucleotide-binding pocket of Ire1 kinase. B) Recombinant

Ire1(D797N,K799N) is unphosphorylated. MALDI mass spectrometry of purfied

recombinant Ire1KR32 reveals that the mass to charge ratio of WT Ire1KR32 is

1.3 kD higher than expected from its amino acid composition. A 1.3 kD shift in

molecular weight corresponds to approximately 17 phosphates. C) Phosphatase

treatment of Ire1KR32 reduces its M/z value.Phosphatase treatment of

recombinant Ire1KR32 reduces its M/z value to its true molecular weight + 0.2

kD. This reduction in molecular weight is consistent with the removal of

approximately 12 phosphates.

Figure S1

A

WT   D797N,K799N

B

C

74
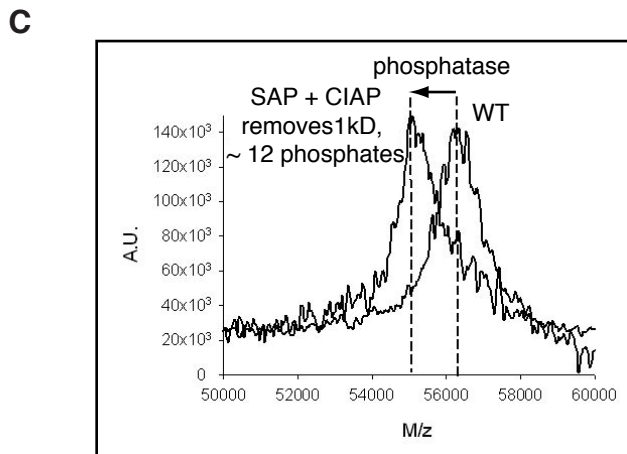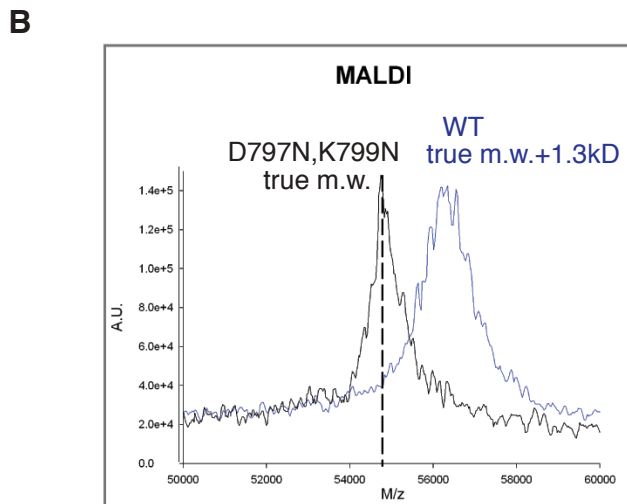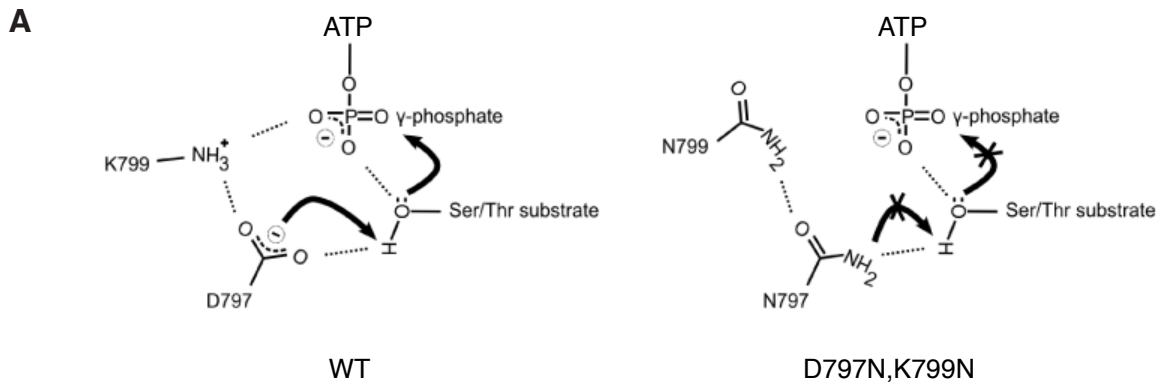
Figure S2   The transcriptional response and global translation rates are

normal in *ire1(D797N,K799N)* cells.

A) Microarray analysis of genome-wide mRNA abundance. Total mRNA

expression profiles of WT and *ire1(D797N,K799N)* cells were determined over a

2-hour time course of UPR induction. B) Global translation rates during UPR

induction are comparable in WT and *ire1(D797N,K799N)* cells. Global translation

rates were measured by [35S] -methionine incorporation over a 3-hour time

course of UPR induction. [35S] scintillation counts were normalized to cell

number and plotted over time (p = 0.12).

Figure S2

A

IRE1 | *ire1*
        | *(D797N,K799N)*

0 30 60 120   0 30 60 120   time (min)

B

76
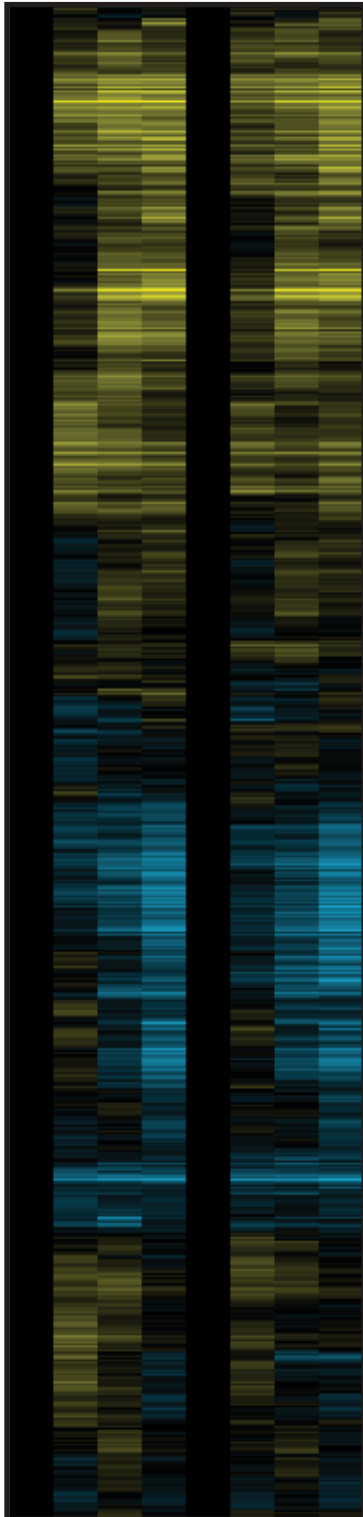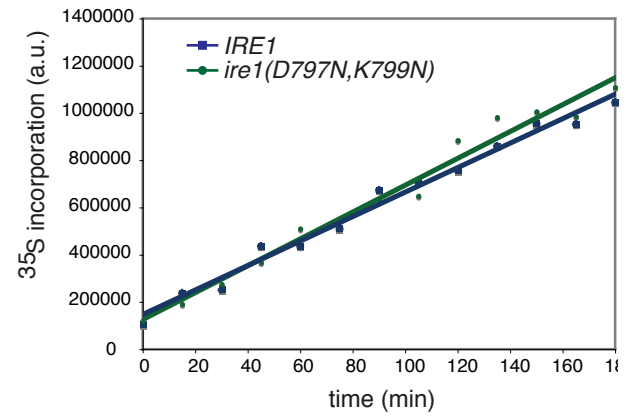
Figure S3   The fold change of SR splicing in WT and *ire1(D797N,K799N)* cells are comparable.

Minimum and maximum values were taken from SR splicing assays using 5 mM DTT at times 0 and 240 minutes, respectively.

Figure S3
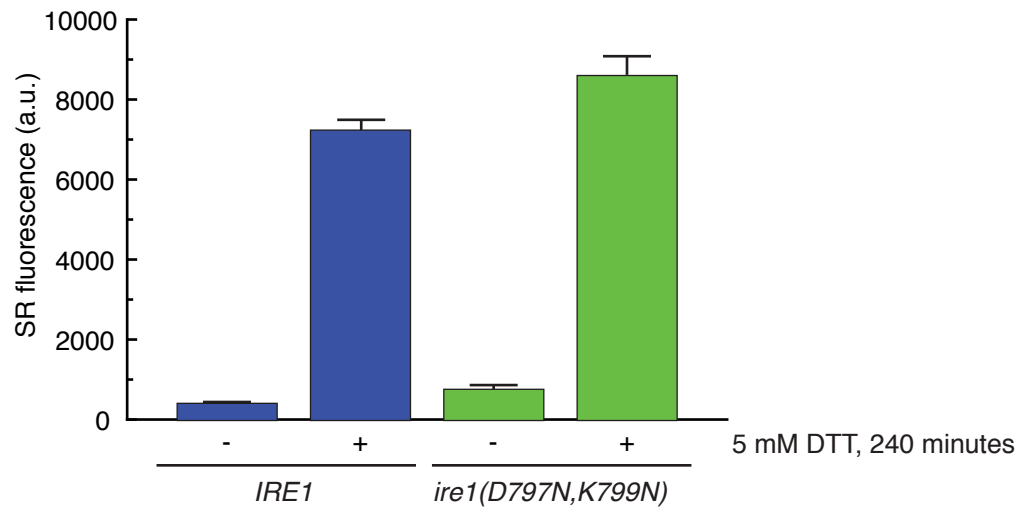
Chapter 3

Exploring the UPR-specificity of tRNA ligase

Introduction

Our understanding of the mechanism by which tRNA ligase (Trl1) acts in the Unfolded Protein Response (UPR) is limited. The role of Trl1 in *HAC1* mRNA splicing was discovered in a genetic screen for essential components of the UPR (Sidrauski et al. 1996). In this screen, a mutation in tRNA ligase, *trl1-100*, prevented growth on UPR-inducing medium and abolished ligation of the *HAC1* mRNA exons produced by Ire1 cleavage. In *trl1-100* strains, the unligated exons are rapidly degraded and cells are unable to produce the Hac1 transcription factor. Ligation of tRNA halves is intact in *trl1-100* strains, however (Sidrauski et al. 1996), thus the role of Trl1 in the UPR is separable from its role in tRNA splicing. Moreover, the mutant enzyme retains normal *HAC1* mRNA ligation activity *in vitro* (Gonzalez, T.N. 2003), suggesting that the basis for the *HAC1* mRNA splicing defect in mutant strains is not due to a loss in enzymatic function. Notably, over-expression of *trl1-100* rescues *HAC1* mRNA splicing suggesting that the basis for its defect lies in its affinity for UPR-specific partners. Limiting quantities of Trl1-100 protein or sequestering of the mutant protein away from the UPR could result in its observed defect. The mutation does not alter overall Trl1-100 protein levels (Gonzalez 2003). Since the discovery that Trl1 plays an essential role in the UPR, little has been learned about how the enzyme achieves specificity for *HAC1* mRNA splicing. In Chapter 3 of this thesis, we explore the

notion that Trl1 functions in the UPR through an exclusive mechanism that is separate from its essential role in tRNA processing.

We hypothesized that Trl1 must have unique, pathway-specific associations with one or more UPR component(s) and that the UPR-specific *trl1-100* defect would impair such an interaction. The link could exist between Trl1 and known components of the *HAC1* mRNA splicing reaction, namely Ire1 or *HAC1* mRNA itself, or on another yet to be identified player in *HAC1* mRNA splicing. Based on this conjecture, we set out to identify specific association of Trl1 with UPR partners. We hypothesized that these interactions would be absent in *trl1-100* strains if the basis for the defect were due to impairment of an association with one or more UPR components. Three lines of experimentation were carried out to address this idea: 1) Localization studies to measure proximity to known UPR factors, 2) Immunoprecipitation followed by mass spectrometry to identify binding partners *in vivo* and 3) *In vitro* measurements of Trl1 binding to substrate RNAs.

Materials and Methods

Yeast strain construction

Yeast strains used in this study are listed in Table 3-1. *TRL1-GFP* and *trl1-100-GFP* were tagged using the Pringle method for C-terminal epitope tagging. The GFP cassette from Pringle vector pFA6a-GFP_kanMX6 (Longtine et al. 1998) was PCR amplified using the forward oligonucleotide primer oCR88 5'-GTGGTGAAATTGGACAACTCGAAGGAATTTGTTGGCAGTGTATATTTAAATTT Tcggatccccgggttaattaa-3' and the reverse primer oCR89 5'-CCAAGCAAATAAAG CACTTGGTTAAACGAAATTAACGTTTTTAAGACAGCCAGACCGCGGTgaattcg agctcgtttaaac-3' (the capitalized sequence in these primers is homologous to the *TRL1* gene). The product of this PCR was transformed into PWY1050 (*TRL1*) and PWY612 (*trl1-100*) cells and transformants were selected on medium containing neomycin to select for cells carrying the *KAN^R* gene linked to GFP.

Measuring plate phenotype

Cells were grown at 30°C overnight in YPD, diluted to OD_{600} 0.1 and grown to OD_{600} 0.3. Cultures were aliquoted, diluted to equal cell number and serially diluted 1:5 five times. 3 μl of each diluted sample was pipetted with a multi-channel pipetman onto permissive YPD plates or onto YPD plates containing 0.25 μg/ml tunicamycin. Plates were incubated for 2-3 days at 30°C and photographed using the GelDoc system.

Microscopy

Cells were grown in 2X synthetic complete medium and kept at an OD_{600} between 0.1 and 0.2 prior to the start of any experiment. To prepare the cells for imaging, 1 ml of culture was pelleted and resuspended in 100 μl of 2X minimal medium (note: yeast cells in synthetic complete liquid medium do not pellet efficiently, to increase the efficiency of pelleting, 20 μl of 1X liquid YPD was added to each 1 ml of cells. It is unclear why this promotes cell pelleting but it works like a charm). Glass bottom Petri dishes were coated with Concavillin A (5 μg / ml) washed 3 times with 1X PBS and 100 μl of cells were applied to the dishes and allowed to settle before imaging.

Cells were visualized using an inverted microscope (Nikon TE2000) and a spinning disk confocal microscope (Yokogawa CSU22). A Cascade II:512 camera (Photometrics) was used to acquire images and was controlled by MicroManager software (Stuurman 2007). GFP was excited at 488 nm using an argon laser and imaged using a 525/50 emission filter; mCherry was excited at 568 nm using an argon krypton laser and imaged using a 615/55 emission filter. Resulting images were cropped and the brightness was adjusted using Photoshop (Adobe).

Immunoprecipitation and mass spectrometry

IgG-coated magnetic beads were prepared by incubating M270 Epoxy-activated Dynabeads (Dynal) with rabbit IgG (Sigma) at a ratio of 5 μg antibody

per 1 mg Dynabeads. Dry Dynabeads were weighed and aliquoted accordingly,

washed 4 times in 1X PBS and resuspended in 1X PBS containing 1M

ammonium sulfate and 15 mg IgG per 1 x 10^9 Dynabeads. Beads were rotated

at 30°C for 24 hours to couple the IgG, then and 10 times with 1 ml of 1X PBS to

removed remaining free IgG. IgG-coated Dynabeads were equilibrated in Trl1 IP

buffer (see below for buffer composition) prior to use.

The C-terminal TAP-tagged *TRL1* strain was obtained from the epitope-

tagged collection made by Howson *et al.* (Howson et al. 2005). One to two liter

YPD cultures were inoculated to OD_{600} 0.1 from overnight, saturated cultures and

grown at 30°C to OD_{600} 0.4 - 0.5. Where relevant, the UPR was induced for 45

minutes by the addition of 5 mM DTT. Cells were harvested by centrifugation,

frozen in liquid nitrogen and stored at -80°C. Cells pellets were thawed, and

resuspended in Trl1 IP buffer (20 mM HEPES, pH 8, 150 mM KCl, 2 mM $MgCl_2$,

1 mM phenylmethylsufonyl fluoride (PMSF), complete EDTA-free protease

inhibitors (Roche)). The resulting cell slurry was dripped into liquid nitrogen for

cryogenic breaking in a bead mill (Retsch). Cells were broken by shaking 5 times

at a frequency of 15 Hz/sec for 3 minutes. The bead mill was dipped in liquid

nitrogen between each round of shaking to preserve cryogenic freezing. Broken

cell matter was stored at -80°C. Once thawed, the membranes were solubilized

by adding Triton X-100 or NP-40 to a final concentration of 1% and rotated at 4°C

for one hour. Cell lysates were cleared by ultracentrifugation at 2500 rcf.

Cleared supernatants were incubated with IgG-coated Dynabeads for 1-2 hours

84

at 4°C. Beads were washed 5-10 times with an equal volume of Trl1 IP buffer containing 1% Triton X-100. Trl1 was removed from the beads by cleaving with Ac-TEV protease (Invitrogen) for 2 hours at 16°C. Ac-TEV was removed from the sample by incubation with TALON Dynabeads (Invitrogen) for 15 minutes at 4°C. Samples were heated in denaturing SDS-PAGE sample buffer at 70°C prior to loading on a 10% SDS-PAGE gel (Invitrogen). The resulting gel was stained overnight at room temperature using mass spectrometry-compatible colloidal coomassie (GelCode Blue Stain Reagent, Thermo Scientific).

Mass spectrometry

SDS-PAGE separated proteins were cut from the gel in a dust-free hood and samples were prepared for mass spectrometry following the protocol for In-gel digestion available on the Laboratory for Biological Mass Spectrometry website (http://cms.biomslab.org). Matrix-assisted laser desorption ionization (MALDI) mass spectrometry was carried out using a vMALDI-Ion trap mass spectrometer (Thermo Finnigan).   The resulting spectra were analyzed as described by Deng *et al.* (Deng et al. 2009).

Recombinant Trl1 purification

Trl1 was expressed and purified from *E. coli* cells. A vector carrying GST-fused Trl1 (pSD103) was transformed into chemically competent BL21*-DE3 (Stratagene) and cells were plated for single colonies on LB containing Ampicillin

(100 mg/ml). Single colonies were used to inoculate 5 ml LB + Ampicillin and grown at 37°C for ~4 hours. The 5 ml culture was transferred to a 3-liter Erlenmeyer flask containing 1 liter LB + Ampicillin and grown at 37°C to OD_{600} 0.5 (about 3 hours). Trl1-GST expression was induced by the addition of 0.1 mM IPTG and cultures were shifted to 22°C for 16 hours. Cells were harvested by centrifugation, the pellet was washed with 250 ml dH_2O and resuspended in 40 ml Trl1 Extract Buffer (20 mM HEPES, pH 8, 2 mM EDTA, 200 mM NaCl, 1 mM DTT, 10 % glycerol, 1 mM PMSF, protease inhibitors (Roche)). Cells were lysed by passing the suspension 3 times through a microfluidizer. Triton X-100 was added to the lysate to a final concentration of 1% and rotated at 4°C for 10 minutes. Cell debris was pelleted by ultracentrifugation at 30,000g, 1 hour at 4°C. Polyethylinimine (Sigma) was added to the cleared supernatant to a final concentration of 0.15% and the sample was rotated at 4°C for 30 minutes.   The samples was cleared by ultracentrifugation at 30,000g for 30 minutes and 3 ml bed volume of glutathione S-transferase (GST)-coated Sepharose beads (GE Healthcare; pre-equilibrated in Trl1 Extract buffer) was added to the cleared supernatant. Trl1 was captured by rotating 12-16 hours at 4°C. The GST resin was pelleted (1000 rpm, 5 min at 4°C) and washed 4 times in 50 ml Trl1 Extract buffer. Resin was resuspended in 3 ml Trl1 Elution buffer (20 mM HEPES pH 8, 2 mM EDTA, 200 mM NaCl, 20 mM Glutathione pH 8, 1% Triton X-100) and eluted for 30 minutes rotating at 4°C. Eluate was exchanged back into Trl1 Extract buffer on a desalting column. Eluted protein was run over a Mono Q

column to remove any remaining nucleic acid and passed over a Superdex 200

gel filtration column to remove truncated forms of Trl1 generated during the

purification. Purified Trl1 was exchanged into a low salt storage buffer (20 mM

HEPES pH 8, 100 mM NaCl, 1 mM DTT, 10 % glycerol) and stored in 50 μl

aliquots at -80°C.

Mobility Shift assays

Mobility shift assays were carried out as described previously (Apostol and

Greer 1991). Radiolabeled substrate RNAs were *in vitro* transcribed from

linearized plasmid DNA (See Table 3-2) as previously described (Gonzalez and

Walter 2001). 6 fmol of substrate RNA was mixed with recombinant Trl1 in Trl1

Binding buffer (20 mM HEPES pH7.5, 50 mM KOAc, 2.5 mM Mg(OAc)$_2$, 0.5 mM

DTT) and incubated for 10 minutes on ice. Samples were mixed 1:1 with native

gel loading buffer (1X TBE, 5 mM Mg(OAc)$_2$, 10% glycerol, 0.5% bromphenol

blue, 0.5% xylene cyanol) and loaded on non-denaturing polyacrylamide gels

(4% polyacrylamide (29:1 acrylamide:bisacrylamide), 2.5 mM Mg(OAc)$_2$, and

0.5X TBE). All gels were pre-run at 100 volts for one hour at 4°C prior to loading

the samples. Gels were dried and exposed to a phosphorimager screen

(Molecular Dynamics).

Results

Localization studies

GFP-tagged Ire1 was recently shown to form foci upon UPR induction in living cells (Kimata et al. 2007; Aragon et al. 2009). The unspliced form of *HAC1* mRNA is recruited to these foci and its recruitment is dependent on three factors: 1) a bipartite element in the *HAC1* 3'UTR, termed *3'BE*, 2) translational repression mediated by the *HAC1* mRNA intron and 3) Ire1 (Aragon et al. 2009). Ire1 foci thus act as *HAC1* mRNA splicing centers during the UPR. Since *HAC1* mRNA splicing requires the ligation activity of Trl1, we surmised that Trl1 would also localize to these splicing centers. To determine the intracellular localization of Trl1, we created a variant of Trl1 carrying a C-terminal GFP tag, Trl1-GFP, at the genomic locus. This GFP-tagged Trl1 retained function since strains carrying Trl1-GFP as the sole copy of the tRNA ligase were viable on permissive plates and able to survive on UPR-inducing medium. Similarly, strains carrying GFP-tagged *trl1-100* that were otherwise isogenic were viable under permissive conditions but, as expected, were unable to survive on UPR-inducing medium (Fig. 3-1). Notably, cells expressing *TRL1* with 3 tandem GFP tags at its C-terminus were not viable (data not shown). Trl1-GFP localization was visualized by spinning disk confocal microscopy before and after UPR induction. In untreated cells, Trl1-GFP localized to the cytoplasm and treatment with DTT did not significantly alter its localization (Fig. 3-2). In a few cells, a single focus was

visible after UPR induction, however, these foci were invariably associated with the vacuole and were therefore suspected to be protein aggregates bound for degradation (Fig. 3-2A, right panel). To determine whether Trl1 would co-localize with Ire1 foci, a fluorescently tagged variant of Ire1 carrying the fluorescent mCherry tag within its cytoplasmic domain was expressed on a plasmid in Trl1-GFP cells. Ire1-mCherry produces a lower signal than GFP and localizes partially to the vacuole (Fig. 3-2B; E. van Anken, personal communication). Upon treatment with 5 mM DTT, Ire1-mCherry quickly formed foci while both Trl1-GFP and trl1-100-GFP remained diffusely localized in the cytosol (Fig. 3-2B). In some cells, a single Trl1-GFP focus colocalized with an Ire1-mCherry focus (Fig. 3-2B, arrows). These foci were consistently adjacent to the vacuole, suggesting that these were also aggregates bound for degradation and were likely non-functional for *HAC1* mRNA splicing which occurs adjacent to the ER.

We considered it possible that functional Trl1-GFP/Ire1-mCherry foci were not observed because interactions might be transient and therefore difficult to capture. Similarly, transient association of these two proteins might occur below the limits of detection and therefore were not detected by microscopy. In order to increase the likelihood of detecting such interactions, we over-expressed known UPR components that we expected to interact with Trl1. Ire1-mCherry was over-expressed on a 2-micron yeast plasmid in *TRL1-GFP* strains. Cells were treated with 5 mM DTT and visualized by spinning disk confocal microscopy. Ire1-mCherry formed foci as expected upon UPR induction while Trl1-GFP foci were

not observed in these cells (Fig. 3-3A). Over-expression of wild-type *HAC1*

mRNA likewise did not cause Trl1-GFP to form foci (data not shown). In an

attempt to trap Trl1-GFP in foci with *HAC1* mRNA, we expressed a form of *HAC1*

with mutations in both 3' and 5' splice sites that abolish cleavage by Ire1

(Gonzalez et al. 1999). This form of *HAC1* mRNA is efficiently localized to Ire1

foci and remains associated in splicing centers for a prolonged period (T. Aragon,

personal communication). We expected that any association of Trl1-GFP with

these foci would also be prolonged and might therefore be more readily

detectable if short-lived interactions had made Trl1-GFP undetectable in UPR

splicing centers. When Trl1-GFP was visualized in cells expressing this

unspliceable form of *HAC1* mRNA, we observed a slight increase in the number

of foci in these cells. Foci were visible both before and after UPR induction in

TRL1-GFP cells and in *trl1-100-GFP* cells. Notably, fewer foci were observed in

mutant *trl1-100* cells (Fig. 3-3B) and foci were not visible in the absence of UPR

induction (Fig. 3-3B, lower left panel). Since foci seen in these cells were most

often associated with the vacuole and were also visible, albeit to a lesser extent,

in *trl1-100* cells, we were unconvinced that these were representative of

functionally relevant interactions between Trl1 and *HAC1* mRNA. Likewise, the

vast majority of Ire1-mCherry observed as ER-associated foci in living cells did

not co-localize with Trl1-GFP. Several possible explanations for the lack of

detectable co-localization remain: 1) interactions between Trl1 and Ire1 are

transient and therefore rarely detected by microscopy, 2) detectable, stable

complexes of Ire1 and Trl1 are sent to the vacuole for degradation; these could be late-stage splicing complexes that are no longer functional, or 3) since Trl1 signal is high throughout the cytoplasm, small, functional Trl1-GFP foci may not be detectable above the background fluorescence in these cells.

Searching for interactions *in vivo*

We were interested in taking an unbiased approach to identify interactions between Trl1 and other partner proteins within the cell under both normal growth conditions and UPR inducing conditions. To this end, we used a variant of Trl1 carrying a C-terminal TAP tag (Howson et al. 2005) and immunoprecipitated Trl1 from cells that were left untreated or treated with 5 mM DTT for 30 minutes. Immunoprecipitated material was separated by SDS-PAGE and the resulting gel was stained for protein using mass-spectrometry-compatible Coomassie blue (see Methods). Trl1 was detectable as a prominent 95 kD band in the immunoprecipitated (IP) samples from Trl1-TAP-expressing cells both before and after UPR induction. This band was not present in the IP sample obtained from cells carrying untagged Trl1 (Fig. 3-4A). Notably, all other bands present in IP samples from *TRL1-TAP* cells were also present in the untagged control sample and none were present in significant quanities. Thus, no evidence of physical interaction between Trl1 and any other proteins was evident in these experiments.

To further evaluate whether any proteins were specifically present in Trl1-TAP IP samples, mass spectrometry analysis of IP material from both TAP-tagged and untagged control strains was carried out. Analysis by mass spectrometry confirmed that the protein composition of TAP-tagged IP samples was not different from the control sample (data not shown). IP experiments were repeated a number of times with varying salt and detergent concentration and variable wash conditions (see Methods). No specific interacting partners were discovered in any IP-mass spectrometry experiments.

To evaluate the nucleic acid composition of Trl1-TAP IP samples, RNA was isolated from IP material and analyzed by denaturing RNA gel electrophoresis and Northern blotting for *HAC1* mRNA. By ethidium bromide staining, only contaminating ribosomal RNA (rRNA) was visible in IP samples from *TRL1-TAP* strains (Fig. 3-4B, lanes 4 & 5). Northern blotting for *HAC1* mRNA showed no detectable *HAC1* species in IP samples (Fig. 3-4C, lanes 4 & 5), though *HAC1* mRNA was visible in total RNA controls (Fig. 3-4C, lanes 1 & 2). A non-specific, small molecular weight band was visible in the IP samples (Fig. 3-4C, lanes 4 & 5) and was enriched compared to the untagged control (Fig. 3-4C, lane 3). We speculate that these are tRNAs, though we were unable to confirm this by Northern blotting for tRNA^{phe}. Taken together, these data suggest that Trl1 does not form a stable interaction with its RNA substrates *in vivo*.

In vitro analyses of Trl1-RNA interactions

We reasoned that one possible explanation for the *trl1-100* defect could be an altered affinity for its substrates, thus, we set out to measure the affinity of Trl1 for *HAC1* mRNA *in vitro*. The UPR-specific defect could be due to a loss in affinity of Trl1-100 for *HAC1* mRNA or, alternatively, an increase in its affinity for tRNA substrates could sequester Trl1-100 away from its UPR substrate. To carry out *in vitro* binding assays, we expressed and purified recombinant Trl1 (See Methods). Trl1 purification yielded a single, 95 kD band after final purification by gel filtration (Fig. 3-5A, fractions 2 & 3). During the purification, we noticed that Trl1 purified from *E. coli* contained a significant amount of small molecular weight nucleic acid, which we suspected was RNA (Fig. 3-5B). To confirm our suspicion we treated a portion of the purified Trl1 sample with either RNase or DNase. Ethidium bromide staining of material separated by agarose gel electophoresis revealed that the contaminating nucleic acid was digested by RNase but not by DNase (Fig. 3-5C). To remove this RNA from Trl1 during the purification, we added a polyethylinimine treatment step in the protocol (see Methods), which was previously used to remove RNA from Trl1 during purification (Xu et al. 1990). This RNA-free Trl1 was used for *in vitro* studies described below.

Two methods were used to measure Trl1-RNA interactions: filter binding assays and mobility shift assays. By filter binding, we were unable to detect specific binding of Trl1 to either tRNA or *HAC1* mRNA (data not shown), thus we

93

chose to abandon this assay and turned to mobility shifts. Mobility shift assays

were modeled after those undertaken by Apostol & Greer (Apostol and Greer

1991). The RNA substrates used in these experiments - pre-tRNA^{phe}, a 600-

nucleotide *HAC1* mRNA substrate *HAC600* (Sidrauski et al. 1996), and a 500-

nucleotide form of the mRNA encoding actin, *ACT500* – were *in vitro* transcribed

in the presence of ^{32}P-UTP as previously described (Gonzalez and Walter 2001).

Radiolabeled RNA was mixed on ice with increasing concentrations of Trl1,

incubated for 10 minutes and analyzed by native gel electrophoresis. *ACT500*

and pre-tRNA^{phe} were used in these experiments as negative and positive

controls, respectively. No increase in the mobility of *HAC600* was observed at

the highest concentration of Trl1 used, 625 nM (Fig. 3-6A, lane 10). Likewise,

neither pre-tRNA^{phe} (Fig. 3-6A, lanes 1-2) nor *ACT500* (Fig. 3-6A, lane 3) was

shifted at the concentrations of Trl1 used with these substrates (5 nM). To

determine whether a mobility shift could be measured with these substrates, we

incubated pre-tRNA^{phe} or *ACT500* with higher concentrations of Trl1. In a second

experiment, we increased the concentration of Trl1 up to 5000 nM. At the

highest concentration of Trl1 used, 5000nM, we were able to detect a shift in the

mobility of *HAC600* (Fig 3-6B, lanes 3 and 10, respectively). Previous reports

indicated that the affinity of Trl1 for pre-tRNA substrates was ~ 1 nM (Apostol and

Greer 1991). However, no shift in mobility of pre-tRNA^{phe} was observed at 50 nM

Trl1. To test whether a shift pre-tRNA mobility would occur at higher

concentrations of Trl1, we increased the amount of Trl1 up to the concentration at

which the *HAC600* shift was observed (5000 nM). In this experiment, a shift was

observed for both the negative control, *ACT500* (Fig.3-6C, lane 3), and for pre-

tRNA^{phe} at 5000 nM Trl1 (Fig.3-6C, lane 10). Based on these data, we conclude

that the observed shifts in the mobility of *HAC600* and pre-tRNA^{phe} were non-

specific.

Discussion

Trl1 localization is does not account for UPR specificity

The data presented here show that Trl1 localizes diffusely to the cytoplasm and does not form detectable, functionally relevant associations with UPR components. Occasionally, a single, large Trl1-GFP focus was observed within a cell. Curiously, these foci co-localized with Ire1-mCherry yet were invariably associated with the vacuole, indicating that these were complexes bound for vacuolar degradation. The association of Ire1-mCherry with these Trl1 foci is intriguing, yet it remains to be shown that Trl1 is able to interact with Ire1 in functional, ER-associated *HAC1* mRNA splicing centers within the cell. Similarly, foci observed in cells overexpressing unspliceable *HAC1* mRNA appeared to be vacuole-associated. Co-localization studies of these foci with Ire1-mCherry were not carried out but might clarify the functional relevance of the observed foci.

One possible explanation for the difficulty in detecting functional association of Trl1-GFP with sites of UPR signaling is that the fluorescent signal produced by short-lived interaction of Trl1 with Ire1 foci would be obscured by the high cytoplasmic Trl1-GFP signal. Experiments using photo-activatable fluorophores or FRET-based assays could be done to measure transient interactions and may yield more fruitful results that those described here. Likewise, specific tethering of Trl1 to the sites of *HAC1* mRNA splicing or,

alternatively, away from Ire1 foci might highlight the importance of Trl1's proximity to *HAC1* splicing centers.

Trl1 alone does not interact with substrate RNA

Early measurements of Trl1 binding to pre-tRNA substrates were made using a cellular fraction containing ~ 25% tRNA ligase. The association of various pre-tRNA species with protein in this fraction was shown to be Trl1-specific. However, binding measurements could not be made from a further-purified Trl1-containing fraction (Apostol and Greer 1991). In keeping with these observations, we were unable to measure binding of purified Trl1 to pre-tRNA or *HAC1* mRNA. Taken together, these data strongly indicate that tRNA ligase requires a partner molecule in order to bind its substrate RNA.

Cooperation with an adaptor protein or RNA likely contributes to Trl1's function in living cells. However, our *in vivo* search for protein or nucleic acid partners of Trl1 were unfruitful. The simplest explanation for the difficulty in measuring interactions between Trl1 and other proteins is that any such association is transient or very low affinity.   In the future, cross-linking studies might prove useful to identify low affinity interactions *in vivo*, however they are messy and often difficult to interpret. Cellular fractionation experiments are more appealing since binding of substrate RNA can be measured using a Trl1-containing fraction (Apostol and Greer 1991). An unbiased approach to identify all the components in a substrate-binding, Trl1-containing fraction could pinpoint

candidate adapter molecules. Such studies could be done by quantitative mass

spectrometry using a Trl1-containing fraction that has lost the ability to bind

substrate RNA as a control.

References

Apostol, B. L. and C. L. Greer (1991). "Preferential binding of yeast tRNA ligase to pre-tRNA substrates." <u>Nucleic Acids Res</u> **19**(8): 1853-1860.

Aragon, T., E. van Anken, et al. (2009). "Messenger RNA targeting to endoplasmic reticulum stress signalling sites." <u>Nature</u> **457**(7230): 736-740.

Deng, C., X. Xiong, et al. (2009). "Unifying fluorescence microscopy and mass spectrometry for studying protein complexes in cells." <u>Mol Cell Proteomics</u> **8**(6): 1413-1423.

Gonzalez, T. N. (2003). "Unconventional Splicing of the HAC1 mRNA During the Unfolded Protein Response." <u>Thesis</u>.

Gonzalez, T. N., C. Sidrauski, et al. (1999). "Mechanism of non-spliceosomal mRNA splicing in the unfolded protein response pathway." <u>EMBO J</u> **18**(11): 3119-3132.

Gonzalez, T. N. and P. Walter (2001). "Ire1p: a kinase and site-specific endoribonuclease." <u>Methods Mol Biol</u> **160**: 25-36.

Howson, R., W. K. Huh, et al. (2005). "Construction, verification and experimental use of two epitope-tagged collections of budding yeast strains." <u>Comp Funct Genomics</u> **6**(1-2): 2-16.

Kimata, Y., Y. Ishiwata-Kimata, et al. (2007). "Two regulatory steps of ER-stress sensor Ire1 involving its cluster formation and interaction with unfolded proteins." <u>J Cell Biol</u> **179**(1): 75-86.

Longtine, M. S., A. McKenzie, 3rd, et al. (1998). "Additional modules for versatile and economical PCR-based gene deletion and modification in Saccharomyces cerevisiae." <u>Yeast</u> **14**(10): 953-961.

Sidrauski, C., J. S. Cox, et al. (1996). "tRNA ligase is required for regulated mRNA splicing in the unfolded protein response." <u>Cell</u> **87**(3): 405-413.

Stuurman, N., N. Abodaj, R.D. Vale (2007). "Micro-Manager: Open Source software for light microscope imaging." <u>Microscopy Today</u> **15**: 42-43.

Xu, Q., E. M. Phizicky, et al. (1990). "Purification of yeast transfer RNA ligase." <u>Methods Enzymol</u> **181**: 463-471.

Table 3-1	Yeast strains
Strain Name	**Genotype**
PWY1050	*W303, MATa cry1 ade2-1 trp1-1 can1-100 leu2-3,112 his3-11,15 ura3 psi+*
PWY612	*W303, MATalpha ade2-1 trp1-1 can1-100 leu2-3,112 his3-11,15 ura3 psi+ trl1-100*
YCR16	*W303, MATa cry1 ade2-1 trp1-1 can1-100 leu2-3,112 his3-11,15 ura3 psi+ TRL1-GFP::kanMX6*
YCR17	*W303, MATalpha ade2-1 trp1-1 can1-100 leu2-3,112 his3-11,15 ura3 psi+ trl1-100-GFP::kanMX6*
YCR35	*S288C, MATa his3Δ1 leu2Δ0 met15Δ0 ura3Δ0 TRL1-TAP*

Table 3-2: Plasmids

Plasmid Name	Important Gene	Vector Backbone	Source	Reference
pEvA97	*IRE1-mCherry (in linker)*	pRS315	E. van Anken	This study
pEvA123	*IRE1-mCherry (in linker)*	pRS425	E. van Anken	Aragon *et al.* 2009
pCR62	*hac1(3'5'ss mut)*	pRS426	T. Aragon	This study
pSD103	*TRL1-GST*	pGEX6	S. Dorfler	Gonzalez *et al.* 1999
pCF150	*T7-HAC600*	pBluescript IISK(-)	C. Sidrauski	Sidrauski *et al.* 2000
pUC12T7	*T7-pre-tRNA^{phe}*	pUC12	C. Greer	Gonzalez *et al.* 1999
pPW411	*T7-ACT500*	pBR322	C. Guthrie	N/A

Figure 3-1   GFP-tagged *TRL1* strains are viable

Strains carrying *TRL1-GFP* or *trl1-100-GFP* as the sole copy of tRNA ligase were

plated onto YPD (control) or YPD containing 0.25 μg/ml Tunicamycin. Cultures

containing equal cell numbers were serially diluted 1:5 and spotted onto plates.

Isogenic, untagged *TRL1* and *trl1-100* strains were plated as controls.

Figure 3-1

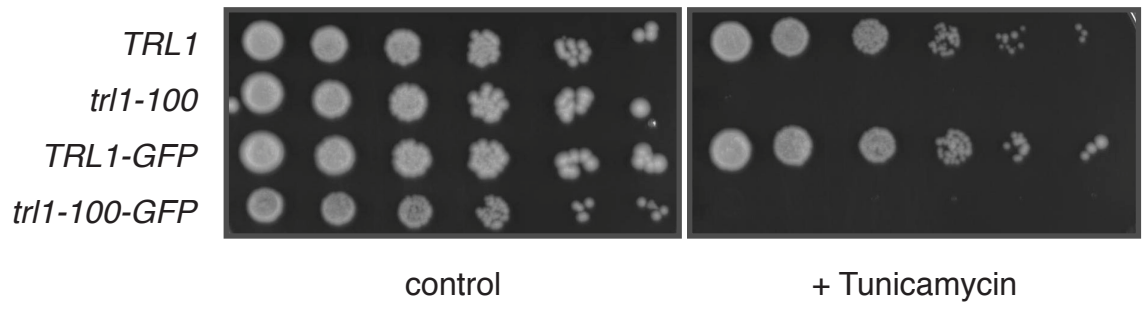|	control	+ Tunicamycin
TRL1		
trl1-100		
TRL1-GFP		
trl1-100-GFP		

Figure 1-2 Trl1-GFP localizes to the cytoplasm

Trl1-GFP was visualized by spinning disk confocal microscopy. A) *TRL1-GFP* cells were left untreated or treated with 5 mM DTT for 20 minutes prior to visualization. Upon DTT treatment a single, rare Trl1-GFP focus was occasionally seen in association with the vacuole (third panel, arrow). B) *TRL1-GFP* cells carrying Ire1-mCherry on a cen/ars plasmid were visualized after the addition of 5 mM DTT. The rare Trl1-GFP foci were seen to co-localize with Ire1-mCherry foci (indicated by arrows in the third set of panels) but were associated with the vacuole rather than the ER.

Figure 3-2

A

	- DTT	+ DTT

Trl1-GFP

B

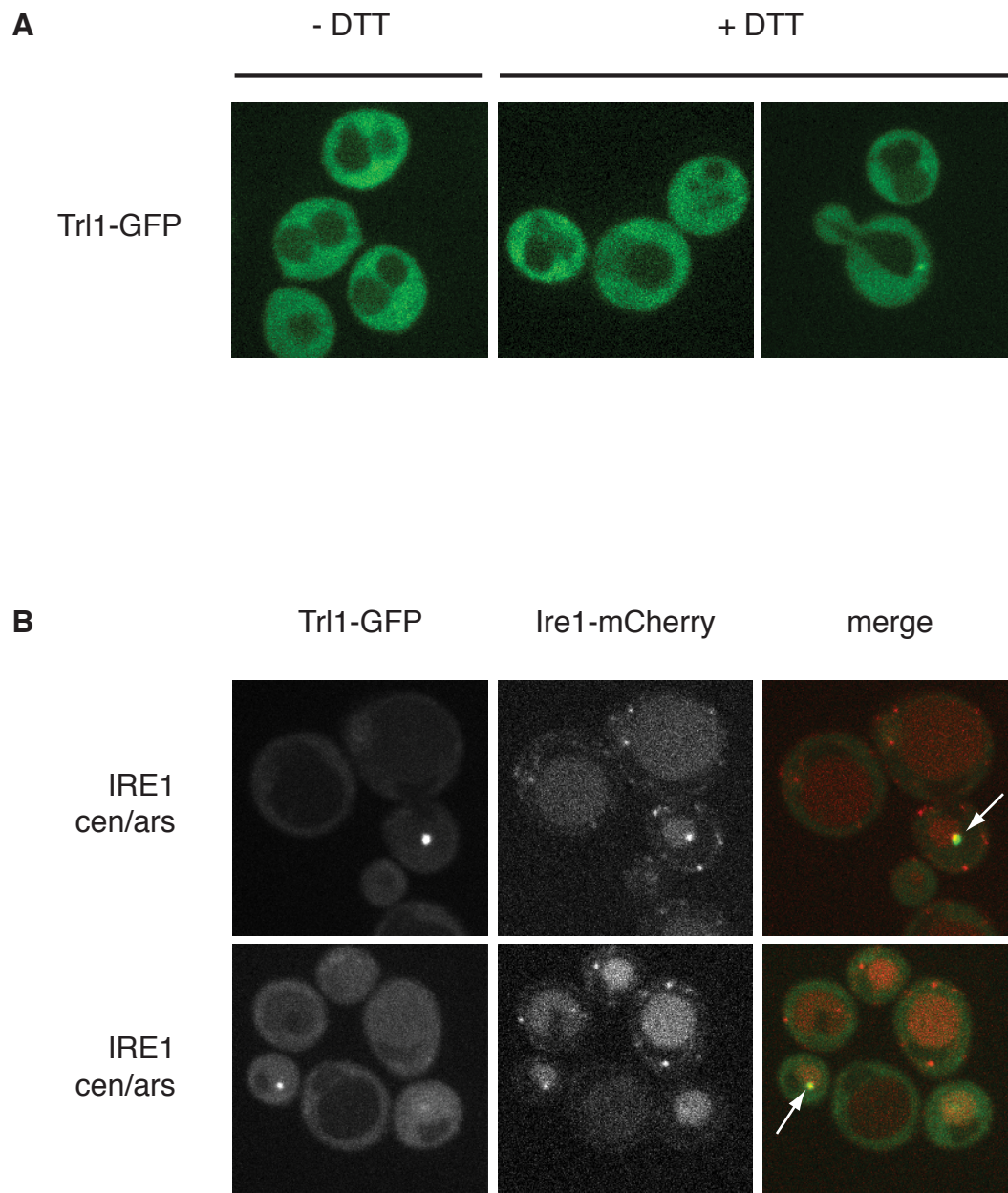|	Trl1-GFP	Ire1-mCherry	merge

IRE1
cen/ars

IRE1
cen/ars

**Figure 3-3   Localization of Trl1-GFP with over-expressed UPR partners**

A) TRL1-GFP cells carrying Ire1-mCherry on a 2-micron over-expression plasmid were visualized by spinning disk confocal microscopy after treatment with 5 mM DTT. Trl1-GFP was not seen to form foci and did not co-localize with Ire1-mCherry. B) *TRL1-GFP* or *trl1-100-GFP* cells carrying an unspliceable form of *HAC1* mRNA on a 2-micron over-expression plasmid were visualized before and after UPR induction.   Trl1-GFP foci (indicated by arrows) were seen associated with the vacuole both before and after DTT treatment.

Figure 3-3

A

	TRL1-GFP	IRE1-mCherry	merge
IRE1 2μ			
IRE1 2μ			

B

HAC1 3' 5' ss mut

TRL1-GFP

trl1-100-GFP

- DTT   + DTT

**Figure 3-4   Immunoprecipitation of Trl1-TAP**

Trl1 carrying a C-terminal TAP tag was immunoprecipitated from cells before and after UPR induction. A) Immunoprecipitated material from untagged *TRL1* cells (lane 1), *TRL1-TAP* cells (lane 2) and *TRL1-TAP* cells treated with 5 mM DTT (lane 3) was separated by SDS-PAGE and stained with colloidal coomassie. B-C) RNA was extracted from immunoprecipitated material (IP), analyzed by denaturing agarose gel electrophoresis (B) and subjected to Northern blotting (C). Total RNA was included as a control for *HAC1* mRNA detection from untreated (-) (lane1) or cells treated with 5 mM DTT (+) (lane 2). IP material from untagged cells (lane 3), *TRL1-TAP* cells (lane 4) or *TRL1-TAP* cells treated with 5 mM DTT (lane 5) was analyzed by ethidium bromide staining (B) and by Northern blotting for *HAC1* mRNA (C). Northern blotting included a probe for *SCR1* RNA as a loading control (visible in lanes 1-2). The lower band in panel C, lanes 3-5 (*) is likely non-specific signal from Trl1-associated tRNA.

Figure 3-4
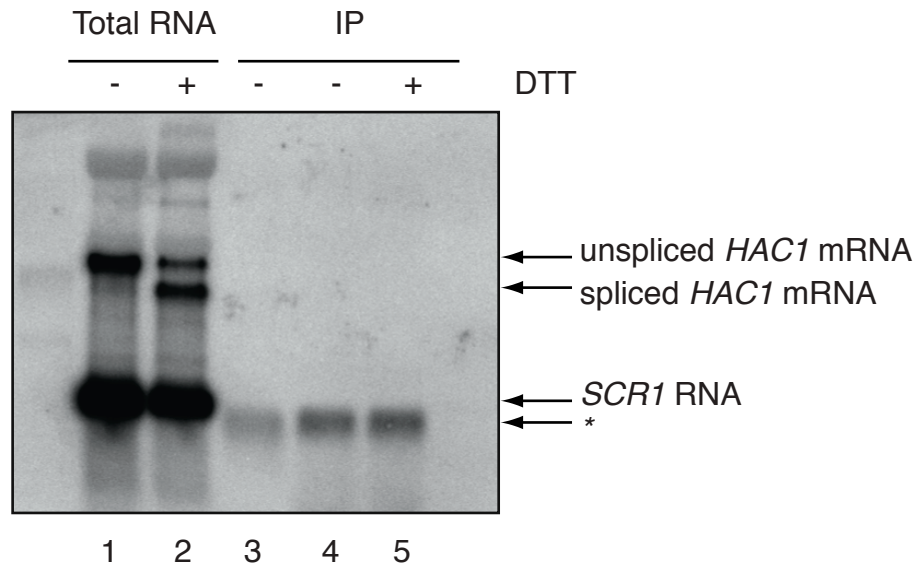
A

B

C

110
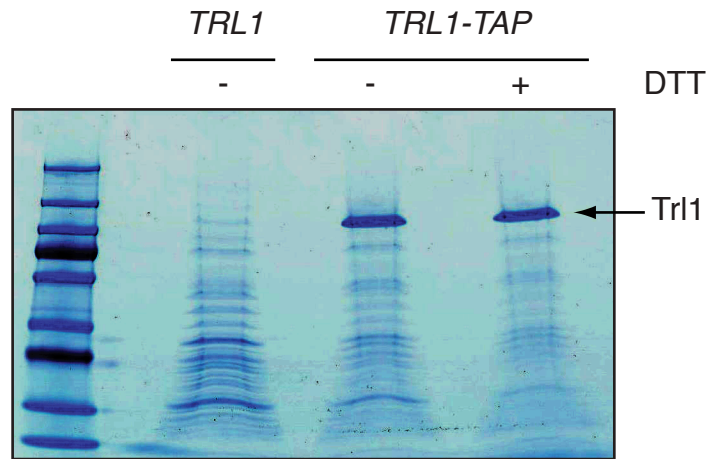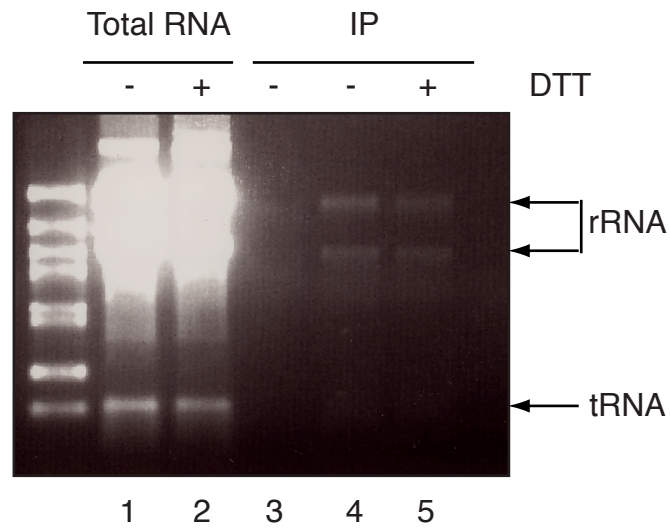
Figure 3-5   Recombinant Trl1 associates with RNA

Trl1 was recombinantly expressed and purified from *E. coli*. A) Purified Trl1 was

run over a Superdex 200 column, protein-containing fractions were separated by

SDS-PAGE and stained with coomassie. B) Nucleic acid from Trl1 containing

fractions (2, 3 and 4) was isolated and analyzed by agarose gel electrophoresis

in the presence of ethidium bromide. C) Nucleic acid from fraction 3 was left

untreated (lane 1), treated with RNase (lane 2) or treated with DNase (lane 3)

and analyzed by agarose gel electrophoresis in the presence of ethiduim

bromide.

Figure 3-5

A

1   2   3   4   fraction

← Trl1

B

3   2   4   fraction

C

no nuclease

+ RNase
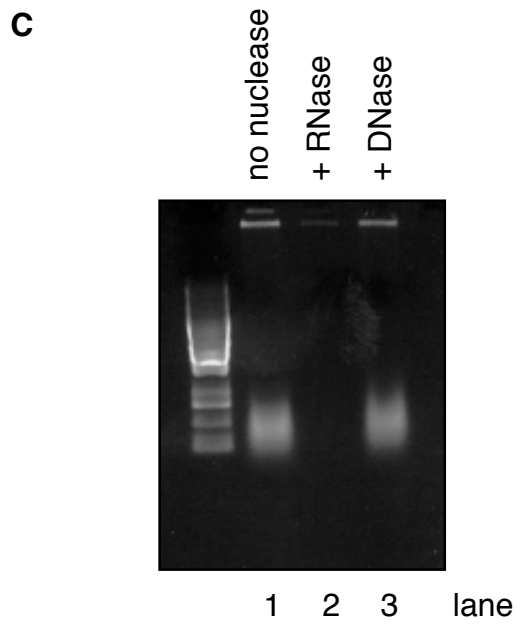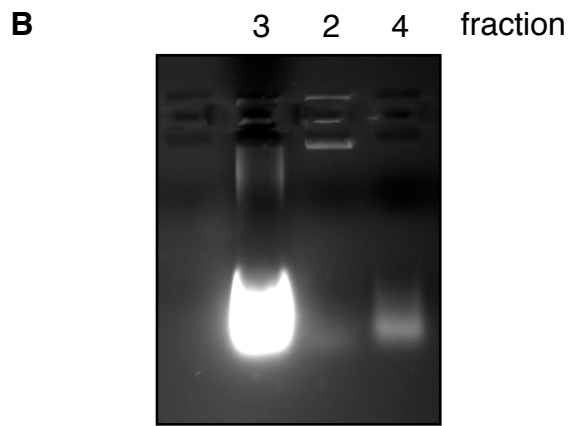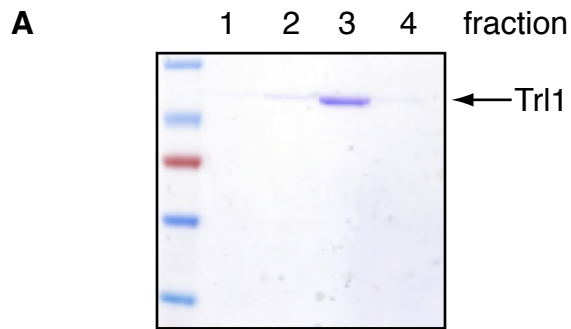
+ DNase

1   2   3   lane

112

Figure 3-6   Trl1 binds non-specifically to RNA at high concentrations

Mobility shift assays using radiolabeled substrate RNA. A) A shift in mobility was not observed for the positive control RNA, pre-tRNA^{phe} (lanes 1 & 2), the negative control RNA, *ACT500* (lane 3), or for *HAC600* RNA (lanes 4-10) at concentrations of Trl1 ranging from 0 to 625 nM . B) A 10-fold increase in Trl1 concentration did not produce a shift of positive control pre-tRNA^{phe} (lanes 1 & 2) or negative control *ACT500* (lanes 3 & 4). A shift in mobility of *HAC600* (lanes 5-10) was observed at 5000 nM Trl1 (lane 10, indicated by an arrow), the highest concentration tested. C) Both *ACT500* (lanes 1-3) and pre-tRNA^{phe} (lanes 4-10) shifted at 5000 nM Trl1 (lanes 5 and 10, respectively, indicated by an arrow.)

Figure 3-6

A

B

C

114
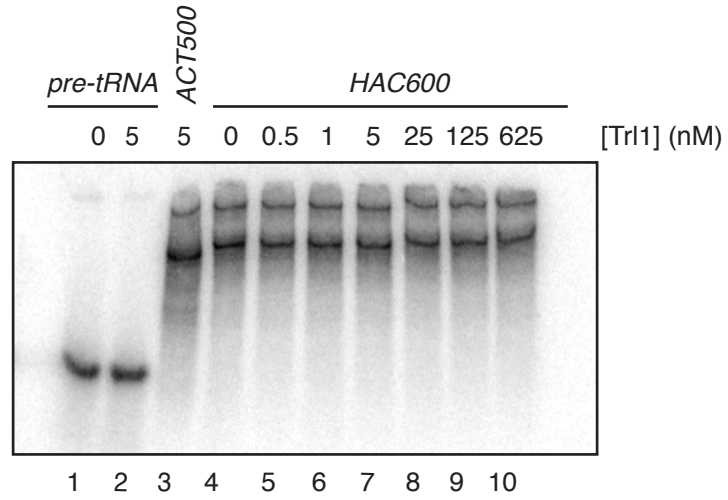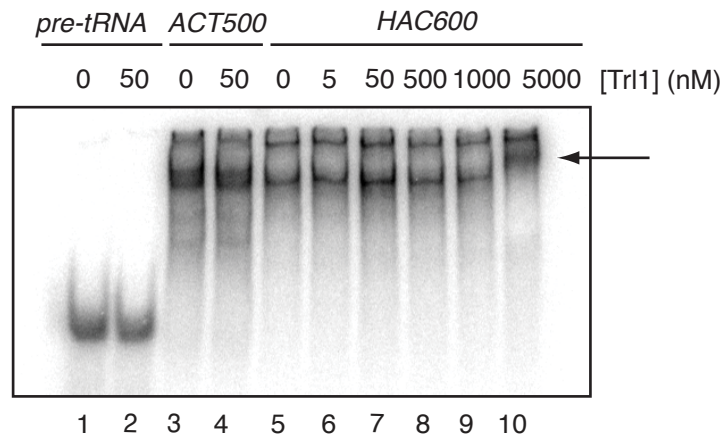
Chapter 4

The SOR mutants: mapping suppressors of *trl1-100*

Introduction

Trl1 is a multidomain protein with three catalytic activities. Each of it's

activities is required for ligating the products of tRNA endoclease-mediated and

Ire1-mediated RNA cleavage (see mechanism in Figure 1-3 of this thesis) and is
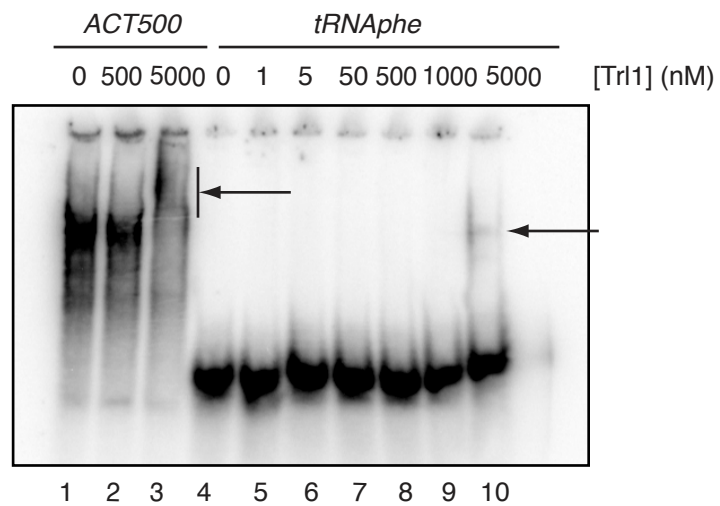
essential for cell survival due to the vital role of Trl1 in tRNA processing. The

three activities of Trl1 are each encoded in a separate domain and can be

expressed as separate polypeptides (Sawaya et al. 2003). The first is an

adenylylate transferase domain (amino acids 1-388) that shares homology with a

superfamily of covalent nucleotide transferases (CNTs) through 3 conserved

motifs. Motif I (consensus KX(D/N)G; amino acids 114-117) contains the site of

covalent AMP attachment, Lys^{114}, required for adenyl-transfer (Xu et al. 1990)

and defines the CNT superfamily. Motif IV (EGFVI; amino acids 266-270) and

motif V (FFKYK; amino acids 282-286) contact AMP during adenyl-transfer

(Sriskanda and Shuman 2002). The second domain is a kinase (amino acids

389-561) that bears resemblance to the kinase of T4 PNK. This domain contains

the canonical Walker A-box (GXGKT; amino acids 390-395) and Walker B-box

(RXXXR; amino acids 507-511) motifs (Sawaya et al. 2003) that are conserved

among kinases. The last domain is a cyclic phosphodiesterase (CPD) (amino

acids 562-827) and belongs to the 2H-superfamily of phosphoesterases. This

superfamily is defined by the presence of two histidine-containing motifs: HϕTϕ

(where ϕ indicates a hydrophobic residue) at amino acids 674 and 777 (Sawaya et al. 2003).

The role of tRNA ligase in the UPR was first discovered when a UPR-defective allele, *trl1-100*, was isolated in a genetic screen for essential UPR components (Sidrauski et al. 1996). Since then, several screens for UPR components have been carried out in our laboratory and *TRL1* has yet to be identified a second time. The *trl1-100* mutation (H148Y) renders the enzyme defective for *HAC1* ligation *in vivo* but the enzyme retains its ability to act in tRNA splicing (Sidrauski et al. 1996). Additionally, the mutant protein is fully capable of ligating *HAC1* mRNA *in vitro* (Gonzalez 2003). The mutation maps to a conserved histindine residue within the adenylyltransferase domain that is distant from the canonical CNT motifs. Thus, the fact *trl1-100* does not alter the catalytic activity of the ligase comes as no surprise. Structure-function analysis of Trl1 revealed that mutation of H148 to alanine, asparagine, or glutamine was lethal and therefore must have abolished Trl1 function in tRNA splicing (Wang and Shuman 2005). These data highlight the importance of this residue in Trl1 function but do not provide evidence for how it may contribute to ligation. In addition, the neighboring residue A149 is likewise conserved among yeast tRNA ligases and may therefore contribute to Trl1 function in conjunction with H148. Mutation H148Y results in the UPR-specific abrogation of *HAC1* mRNA ligation. In *trl1-100* cells, the *HAC1* mRNA fragments produced by Ire activation are

117

degraded and cells are unable to survive UPR insult. To date, the manner in which the *trl1-100* mutation impairs ligation of *HAC1* mRNA remains mysterious.

In our endeavor to learn more about how Trl1 functions in the UPR a forward genetic screen for suppressors of *trl1-100* was carried out (Gonzalez 2003). This screen yielded a large set of suppressor mutants, called SOR mutants for <u>S</u>uppressor <u>o</u>f <u>R</u>lg1 (note: Rlg1 was the original name for tRNA ligase; the name has since been changed in the Saccharomyces Genome Database to Trl1. Thus, tRNA ligase is referred to as Trl1 throughout this thesis). The SOR mutants were isolated as individual colonies that were able to grow on YPD plates containing tunicamycin, a drug that induces the UPR by blocking glycosylation inside the ER. Each SOR mutant was subsequently analyzed by Northern blotting for *HAC1* mRNA splicing. Based on the *HAC1* mRNA splicing phenotype, the SOR mutants were separated into three classes. The first class, SOR1, was composed of ten mutants in which ligation of *HAC1* mRNA fragments was restored. The second class, SOR2, was made up of nine mutants in which the fragments of *HAC1* mRNA produced upon cleavage by Ire1 were stabilized rather than being degraded. In this SOR2 class, a truncated Hac1 protein was produced, corresponding to that encoded by the 5' exon of *HAC1* (Gonzalez 2003). Presumably, this Hac1 protein product is sufficient to act as a transcription factor and upregulate UPR target genes to restore cell survival. The third class of suppressors, SOR3, was the largest collection of mutants. In this class, the *trl1-100 HAC1* mRNA splicing phenotype was unchanged. We

118

speculate that mutations falling into this class effect UPR efficacy downstream of Hac1 protein production. This could occur by increasing Hac1-independent production of ER chaperones, by increasing ER-associated degradation (ERAD) or by slowing translocation of proteins into the ER. Since this class of mutants did not alter the *HAC1* splicing, they were not pursued beyond this initial characterization.

In this chapter, we describe the methods used to identify mutated residues in SOR1 and SOR2 mutants.   We show that intragenic SOR1 mutations cluster in a region of Trl1 with an undefined function. We speculate what role this domain might play in Trl1's function in the UPR. Next, we identify candidate extragenic SOR2 mutations. In order to identify these mutations we undertook a novel whole genome sequencing approach that yielded the complete genomic sequence of two candidate SOR2 strains.

Materials and Methods

Sequencing *TRL1*

      Genomic DNA was isolated from the eight *SOR1* strains. Cells were

pelleted from 10 ml of overnight culture, washed in 1 ml water and resuspended

in 200 μl breaking buffer (1% SDS, 100 mM NaCl, 10 mM Tris pH 8, 1 mM EDTA

pH 8). 200μl of glass beads and 200 μl phenol:chloroform:isoamyl alcohol (pH

7.4) was added and cells were broken by vortexing 5 minutes at 4°C. The

supernatant was isolated by centrifugation into a new tube and cell debris was

pelleted. DNA was ethanol precipitated from the resulting supernatant. 10 ng of

genomic DNA was sequenced using 3.2 pmol of each primer (see Table 4-1),

following the Big Dye sequencing protocol (ABI). Sequences obtained were

aligned using Sequencher DNA alignment software (Gene Codes Corporation).

Solexa Whole Genome Sequencing

      SOR2+ or *trl1-100* segregants (see Fig. 4-2) were grown overnight in 5 ml

YPD. Cultures were pooled and cells were pelleted and washed with an equal

volume of water. Genomic DNA was isolated by resuspending cells in

spheroplast buffer (10 mM Tris pH 7.9, 1 M Sorbitol, 0.1 M EDTA, 1 mM DTT),

adding lyticase (1 μl per OD of cells) and incubating at 37°C for 20 minutes.

Spheroplasted cells were harvested by centrifugation and resuspended in lysis

buffer (50 mM Tris pH 8, 1 mM EDTA) and moved to SS34 centrifuge tubes.

SDS was added to a final concentration of 1% and tubes were incubated at 65°C

for 30 minutes, mixing occasionally. Cell debris was pelleted at 11,000 rpm in

the GSA rotor and the supernatant was collected and ethanol precipitated to

isolate nucleic acid. The resulting DNA was treated with RNase A and purifed

using a Qiagen tip (250). The eluate from the Qiagen tip was ethanol

precipitated, resuspended in TE (10 mM Tris pH 8, 0.1 mM EDTA) and stored at -

30°C. Genomic DNA was prepared for sequencing according to the methods

outlined in the manual, Sample Preparation for Genomic DNA (Illumina). 5 μg of

genomic DNA was nebulized in 750 μl of 1X TE buffer + 10% glycerol.

Nebulizers were obtained from Invitrogen (K7025-05). Nebulization was carried

out at 35 psi (using compressed argon as the source) for 6 minutes on ice.

Nebulized DNA was separated on a 0.8% agarose gel and the fraction between

500 and 800 base pairs was isolated by gel purification (Qiagen). The ends were

repaired using T4 DNA polymerase, Klenow DNA polymerase and T4 DNA PNK

(New Enlgand Biolabs). To prepare the DNA for adapter ligation a single

adenine base was added to the 3' end of the DNA fragments using Klenow (3', 5'

exo minus) (New England Biolabs). DNA fragments with 3'-'A'-base overhangs

were ligated into BsaBI-linearized vector BHM1447 (a generous gift from Hiten

Madhani's lab). This vector contains the BsaBI site flanked by Illumina adaptor

sequences such that ligation of DNA fragments by A/T cloning into the BsaBI site

yields adaptor-ligated DNA that can be amplified for Solexa sequencing. The

BsaBI-linearized vector was treated with Taq in the presence of 100 mM dTTP to

produce a 5'-T overhang for A/T cloning. The subcloned, adapter-ligated

genomic DNA fragments were PCR amplified with ExTaq (Takara) using Solexa

primers PCR1b and PCRb2 (Illumina). PCR cycles were as follows: 93°C, 1

min. 30 sec.; 18 cycles of 93°C, 15 sec., 55°C, 15 sec., 72°C, 45 sec.; 72°C, 5

min. PCR products ranging in size from 33 to 500 bp were gel purified (Qiagen)

followed by a second round of PCR purification (Qiagen) to remove the remnants

of the QG buffer. The resulting material was quantified on an agarose gel using

Image J software.

Solexa sequencing was carried out precisely according to the protocols for

Cluster Generation Kit G-A11 (Illumina GD-203-1001) and the 36-cycle SBS

Sequencing Kit v2 (Illumina FC-204-2036) in the UCSF Center for Advanced

Technology (CAT).

Results

SOR1: Intragenic suppressors of _trl1-100_

In the _SOR1_ class of suppressors of _trl1-100_, _HAC1_ mRNA ligation was restored. Genetic analysis showed that these mutations were linked to the _trl1-100_ gene, suggesting that the mutated residues were within the _trl1_ gene itself. Additionally, sequencing of the _trl1-100_ mutation showed that reversion of the original mutation back to wild-type was not responsible for restoring ligation (Gonzalez 2003). To determine the location of these mutations the entire _trl1_ gene from each suppressor strain was sequenced. Oligonucleotide probes were tiled across the gene starting 550 nucleotides upstream of the translation start site and ending 37 nucleotides upstream of the termination codon. Probes were spaced 300 nucleotides apart to guarantee that high fidelity sequencing data would be obtained for the entire open reading frame (ORF), including the 5' and 3' untranslated regions (UTRs). The _TRL1_ gene of the original parent strain from which the suppressor mutants were generated was sequenced as well as the eight suppressor mutants that were linked to _trl1-100_. The resulting sequences were aligned to the _TRL1_ sequence archived in the Saccharomyces Genome Database (SGD) (www.yeastgenome.org) using Sequencher alignment software. Non-silent, single nucleotide mutations were identified within the _trl1_ gene in each of the eight _SOR1_ strains (Fig.4-1). The mutation G363R was present in 3 independent isolates (_SOR1- 5.1_, _- 62.1_, and _- 96.1_), thus six SOR1 residues

were identified. Notably, all mutations clustered in a portion of the gene located at the C-terminal end of the adenylyltransferase domain (between amino acids 289 and 370). This region of the protein bears no homology to the nucleotidyl transferase superfamily and has not been assigned a functional relevance to tRNA ligase. We term this region of Trl1 the SOR1 domain (Fig. 4-1B & C).

SOR2: Extragenic suppressors of trl1-100

Nine suppressor mutants were isolated that rescued the growth of *trl1-100* cells on UPR-inducing medium without restoring *HAC1* mRNA splicing. In these mutant cells the *HAC1* mRNA fragments produced by Ire1 cleavage were stabilized and a truncated Hac1 protein was produced from the *HAC1* 5' exon. In this class of suppressors, termed SOR2, mutations were unlinked to the *trl1* gene and were therefore extragenic mutations. Six of the eight of the SOR2 mutants were dominant when expressed in *trl1-100/trl1-100, SOR2* diploid strains (Gonzalez 2003). Previous attempts to identify the recessive mutations by complementation with a wild-type library were unsuccessful (Gonzalez 2003). Here, efforts were undertaken to identify the genes harboring the dominant SOR2 mutations by constructing libraries from the genomic DNA of dominant *SOR2* strains. Dominant *SOR2* libraries were transformed into *trl1-100* strains and plated onto tunicamycin-containing plates. Colonies that grew on these plates were restreaked to confirm the growth phenotype and analyzed for *HAC1* mRNA splicing by Northern blotting. In parallel, plasmids that suppressed the *trl1-100*

growth defect on UPR-inducing medium were rescued, from yeast colonies, amplified in *E. coli* and sequenced to determine the nature of the genomic fragment which conferred suppression. Among the colonies analyzed in this manner, none of the isolates showed stabilization of *HAC1* mRNA splicing intermediates by Northern blotting. Thus, we were unable to identify Dominant *SOR2* genes by this method. However, two genes, *HAC1* and *SUP53*, were present seven and five times, respectively, within genomic fragments that rescued *trl1-100*. The complete lengths of both genes were sequenced and found to contain no mutations. Thus, neither of these genes harbored the *SOR2* mutations that we were in search of. Rather, extra-chromosomal copies of the wild-type *HAC1* or *SUP53* gene were able to suppress the *trl1-100* growth defect for some other unexplained reason.

Since efforts to identify the genes carrying the causative *SOR2* mutations by standard genetic techniques were unsuccessful, we devised a whole-genome sequencing strategy to search for these mutations. To this end we took advantage of Solexa whole genome sequencing technology available at the UCSF Center for Advanced Technology (CAT). In order to control for normally occurring single nucleotide polymorphisms (SNPs) in these yeast strains two of the dominant *SOR2* strains (PWY707 and PWY712) were crossed to a *trl1-100* strain (PWY610 or PWY612). Segregants from this cross were isolated by tetrad dissection, analyzed for growth on UPR-inducing medium and separated into groups based on this phenotype: the *trl1-100* group (control), the PWY707

125

SOR2 group or the PWY712 *SOR2* group (Fig.4-2). Thirteen to twenty

segregants from each group were collected, grown individually overnight in 5 ml

of YPD and cultures belonging to the same group were pooled into a single

sample. The pooled cultures were pelleted and genomic DNA was isolated from

each pellet to be used for sequencing analysis. Solexa sequencing of three

samples - the *trl1-100* control, the PWY707 *SOR2* sample, and the PWY712

SOR2 sample - yielded a large set of overlapping 36 base pair reads. The reads

were aligned to a W303a reference genome obtained from the Saccharomyces

Genome Database (www.yeastgenome.org) using MAQ alignment software (Li et

al. 2008). Sequence alignments gave 5 to 10-fold coverage of the genome in

each Solexa-sequenced sample. In all three alignments, the *trl1-100* mutation

(C442T in the *TRL1* ORF) was evident as a single mismatch present in all

overlapping reads in the assembled genomic sequence. Likewise, SNPs were

easily recognizable in each assembled genome since overlapping reads

displayed variable single nucleotide mismatches at identical locations in the

reference genome. This provided proof that our strategy to distinguish SNPs

from single nucleotide mutations by analyzing multiple isogenic segregants from

a single cross was successful. In the sequence alignment derived from PWY707

SOR2 we discovered three single nucleotide mismatches that were not present in

either the *trl1-100* control or the PWY712 *SOR2* sequences. One of these

mutations was a non-silent G to A mutation in a region of the genome annotated

as a putative cDNA (chromosome IV, 1514885-1514274). The other two

mutations were both present within the *SKI2* gene, one silent mutation (G1317A) that was linked to a second non-silent mutation (G1360A) that caused the amino acid substitution R454H.

Discussion

The SOR1 domain of Trl1 is annotated as part of the adenylyltransferase domain. However, by biochemical analysis, the C-terminal portion of this domain was partially dispensable for adenyl-transfer activity *in vitro*. In addition, deletion of amino acids 363-388 yielded an adenylyltransferase domain that was able to compliment a *trl1* deletion when co-expressed with a Trl1(kinase-CPD) fusion protein (Sawaya et al. 2003). These findings suggest that the C-terminal portion of the adenylyltransferase domain is not required for adenyl-transfer or for ligation of tRNA halves. Moreover, the canonical motifs that define to nucleotidyl transferases (ref) and are required for catalysis are distant from this region. However, the amino acid sequence of the SOR1 domain is conserved among yeast tRNA ligases (Gonzalez 2003) and, by NCBI BLAST analysis, contains an annotated uncharacterized conserved domain in the COG database (COG5324), lending further support to the notion that this region contributes an important, albeit unknown function to Trl1. The fact that the *SOR1* mutations cluster in this portion of Trl1 suggests that the region specifically contributes to *HAC1* mRNA ligation, at least in the context of the *trl1-100* mutation, since the defect in *HAC1* mRNA ligation in *trl1-100* cells is rescued in *SOR1* strains. In six of the eight *SOR1* mutants, the causative mutation alters the amino acid sequence such that negatively charged glutamic acid or neutral glycine residues are changed to positively charged lysine or arginine residues, respectively. Since our

128

understanding for the basis of the *trl1-100* defect is extremely limited, we can

only speculate about the functional contribution that this region might confer to

Trl1-100 to overcome its *HAC1* mRNA splicing defect. One possibility is that a

SOR1 mutation increases the affinity of Trl1-100 for its UPR-specific partners. In

support of this notion, overexpression of mutant *trl1-100 in vivo* is able to rescue

growth on UPR-inducing medium and restore *HAC1* mRNA splicing (Gonzalez

2003). However, we were unable to measure an affinity of purified Trl1 for *HAC1*

mRNA or for a pre-tRNA substrate (See Chapter 3 of this thesis). In fact, the

only successful measurements of Trl1's affinity for its pre-tRNA substrates were

made using a Trl1-enriched cellular fraction containing 25% Trl1 and further

purification of Trl1 from this fraction abolished binding (Apostol and Greer 1991).

Taken together, these data suggest that Trl1 alone does not bind to its substrate

RNAs. Rather, some other, yet unidentified cellular component may be required

to bridge the interaction of Trl1 with its substrates. In this scenario, Trl1 might

transiently interact with different adapter proteins or RNAs that confer specificity

for ligating either *HAC1* mRNA or tRNA. The *trl1-100* mutation could decrease its

affinity for UPR-specific adapters thereby abolishing *HAC1* mRNA ligation while a

SOR1 mutation might serve to restore this affinity and thereby its function the

UPR. Alternatively, the *trl1-100* mutation could increase the affinity of the ligase

for it's tRNA substrates and therefore sequester Trl1-100 away from its UPR

substrates. In either case, both *trl1-100* and *SOR1* mutations alter the ability of

Trl1 to act in *HAC1* mRNA-specific ligation. More research is required to

determine the mechanism by which pathway specificity is achieved in Trl1. This collection of mutants promises to be a great tool for discovery in such investigations.

At the time this thesis was written, attempts to clone *SKI2* had been unsuccessful. We therefore have yet to determine whether mutation R454H is the causative mutation for the PWY707 *SOR2* phenotype. Ski2 is a DEVH-box RNA helicase and a component of the Ski2/3/8 complex involved in 3'-5' cytoplasmic mRNA decay in yeast (Anderson and Parker 1998; Wang et al. 2005). Several lines of evidence lead us to believe that *ski2(R454H)* is likely to be a *SOR2* gene. First, defects in the *SKI* genes are known to increase translation of poly(A)-minus mRNAs (Widner and Wickner 1993; Benard et al. 1998; Benard et al. 1999; Brown and Johnson 2001). Second, protein homology searches using the amino acid sequence of Trl1 find that Ski2 shares sequence homology with portions of the kinase and cyclic phosphodiesterase domains of Trl1 (Gonzalez 2003). Third, the R454H mutation (G1360A) identified by Solexa sequencing was invariably linked to a second, silent mutation (G1317A). Thus, both mutations were inherited by all *SOR2+* segregants that were used for sequencing. Similarly, the fact that *SKI2* has proven challenging to clone from genomic DNA may explain why we were unable to identify this mutant by standard library construction methods. Efforts to clone *SKI2* are ongoing and will ultimately allow us to determine whether R454H produces the *SOR2* phenotype.

References

Anderson, J. S. and R. P. Parker (1998). "The 3' to 5' degradation of yeast
  mRNAs is a general mechanism for mRNA turnover that requires the SKI2
  DEVH box protein and 3' to 5' exonucleases of the exosome complex."
  EMBO J **17**(5): 1497-1506.

Apostol, B. L. and C. L. Greer (1991). "Preferential binding of yeast tRNA ligase
  to pre-tRNA substrates." Nucleic Acids Res **19**(8): 1853-1860.

Benard, L., K. Carroll, et al. (1999). "The ski7 antiviral protein is an EF1-alpha
  homolog that blocks expression of non-Poly(A) mRNA in Saccharomyces
  cerevisiae." J Virol **73**(4): 2893-2900.

Benard, L., K. Carroll, et al. (1998). "Ski6p is a homolog of RNA-processing
  enzymes that affects translation of non-poly(A) mRNAs and 60S ribosomal
  subunit biogenesis." Mol Cell Biol **18**(5): 2688-2696.

Brown, J. T. and A. W. Johnson (2001). "A cis-acting element known to block 3'
  mRNA degradation enhances expression of polyA-minus mRNA in wild-
  type yeast cells and phenocopies a ski mutant." RNA **7**(11): 1566-1577.

Gonzalez, T. N. (2003). "Unconventional Splicing of the HAC1 mRNA During the
  Unfolded Protein Response." Thesis.

Li, H., J. Ruan, et al. (2008). "Mapping short DNA sequencing reads and calling
  variants using mapping quality scores." Genome Res **18**(11): 1851-1858.

131

Sawaya, R., B. Schwer, et al. (2003). "Genetic and biochemical analysis of the

    functional domains of yeast tRNA ligase." <u>J Biol Chem</u> **278**(45): 43928-

    43938.

Sidrauski, C., J. S. Cox, et al. (1996). "tRNA ligase is required for regulated

    mRNA splicing in the unfolded protein response." <u>Cell</u> **87**(3): 405-413.

Sriskanda, V. and S. Shuman (2002). "Role of nucleotidyltransferase motifs I, III

    and IV in the catalysis of phosphodiester bond formation by Chlorella virus

    DNA ligase." <u>Nucleic Acids Res</u> **30**(4): 903-911.

Wang, L., M. S. Lewis, et al. (2005). "Domain interactions within the Ski2/3/8

    complex and between the Ski complex and Ski7p." <u>RNA</u> **11**(8): 1291-1302.

Wang, L. K. and S. Shuman (2005). "Structure-function analysis of yeast tRNA

    ligase." <u>RNA</u> **11**(6): 966-975.

Widner, W. R. and R. B. Wickner (1993). "Evidence that the SKI antiviral system

    of Saccharomyces cerevisiae acts by blocking expression of viral mRNA."

    <u>Mol Cell Biol</u> **13**(7): 4331-4341.

Xu, Q., D. Teplow, et al. (1990). "Domain structure in yeast tRNA ligase."

    <u>Biochemistry</u> **29**(26): 6132-6138.

Table 4-2: *TRL1* sequencing primers		
Primer Name	Location in ORF	Sequence
PCR-mF1	- 576	**TATCATACTTGGAAGCTTCGT**
SP1	- 532	**GAATTCAATGTACTTTCA**
SP2	- 330	**TCAAATACGTTTAAGCAC**
SP3	+ 67	**GTTAGAAAAGGCAGAAAA**
SP3.5	+ 201	**TTGCCATGTAATGCAAGAGGC**
SP4	+ 382	**TATCTGGTTTAGAGATG**
SP5	+ 667	**AACTTGGGATATGAAAGA**
SP6	+ 975	**TAACCAACAAGTATCTTG**
SP7	+ 1266	**CAGCTGGGGTCATATTC**
SP8	+ 1569	**TTAAATGGGACGAATTAG**
SP9	+ 1867	**TAATCAACAAAAAACGCC**
SP10	+ 2168	**AATAACCAAAATACGCAG**
SP11	+ 2446	**GTGAAATTGGACAACTC**

Table 4-1: SOR1 yeast strains	
SOR1 Name	**Mutation**
5.1	G363R
8.1	E365K
61.1	G360N
62.2	G363R
63.1	P290S
72.1	E289K
96.1	G363R
302D1.1	E370K

Table 4-3: SOR2 yeast strains

Strain Name	Genotype
PWY610	*W303, MATalpha ade2-1 trp1-1 can1-100 leu2-3,112 his3-11,15 ura3 psi+ trl1-100*
PWY612	*W303, MATa ade2-1 trp1-1 can1-100 leu2-3,112 his3-11,15 ura3 psi+ trl1-100*
PWY707	*W303, MATa ade2-1 trp1-1 can1-100 leu2-3,112 his3-11,15 ura3 psi+ trl1-100 UPRE-lacZ::HIS3+ SOR2-11.1*
PWY712	*W303, MATalpha ade2-1 trp1-1 can1-100 leu2-3,112 his3-11,15 ura3 psi+ trl1-100 UPRE-lacZ::HIS3+ SOR2-65.1*

Figure 4-1   Domain organization of tRNA ligase and the location of UPR-related mutations

A) The Trl1 protein has three domains: an adenylyltransferase (1-388), a kinase (389-561) and a cyclic phosphodiesterase (562-827). B) The adenylyltransferase domain is defined by the presence of three canonical motifs (I, IV and V) that define a superfamily of covalent nucleotide transferases and contribute to the catalysis of AMP transfer. Mutation *trl1-100* sits between motif I and motif IV, and is distant from both. The *SOR1* mutations cluster near the C-terminal end of this domain.
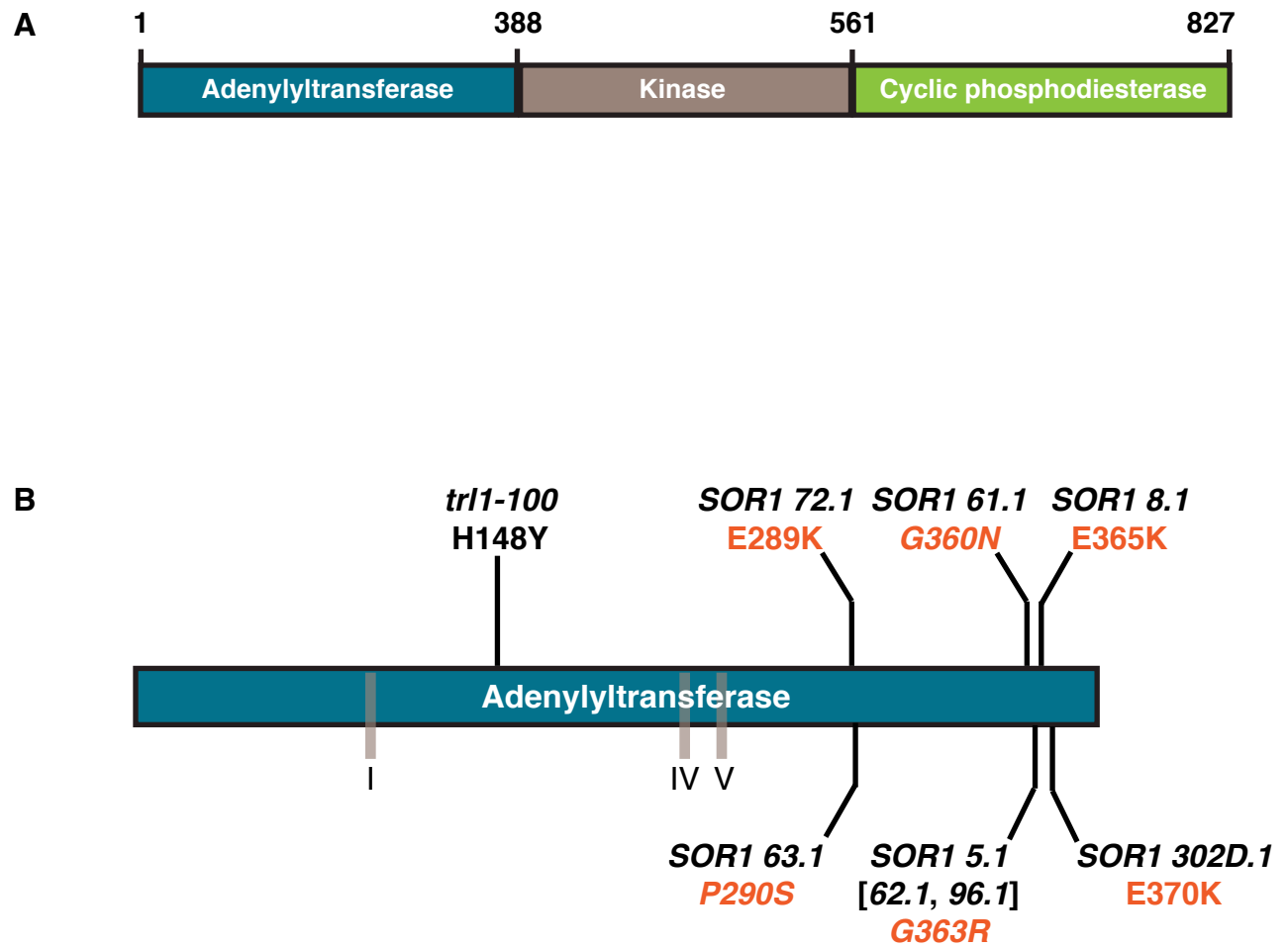
Figure 4-1

Figure 4-1

C) The *SOR1* sub-domain of tRNA ligase lies at the C-terminal end of the

adenylyltransferase domain; its limits are defined by the location of *SOR1*

mutations: E289K, P290S, G360N, G363R, E365K, E370K (the location of each

is indicated by an arrow).

Figure 4-1

C

Figure 4-2   Strategy for identification of *SOR2* mutations by Solexa sequencing.

1. *SOR2+* strains (PWY707 or PWY712) were crossed to *trl1-100* strains (PWY610 or PWY712, respectively).

2. Diploid cells were selected on minimal medium.

3. Diploids were sporulated and tetrad spores were dissected by microscopy.

4. Segregants were tested for their *SOR2* phenotype by growth on UPR-inducing plates; those that tested *SOR2+* were pooled in the *SOR2* pool while those that tested *trl1-100* positive were included in the Control pool.

5. Pooled genomic DNA was used for Solexa whole genome sequencing.

Figure 4-2
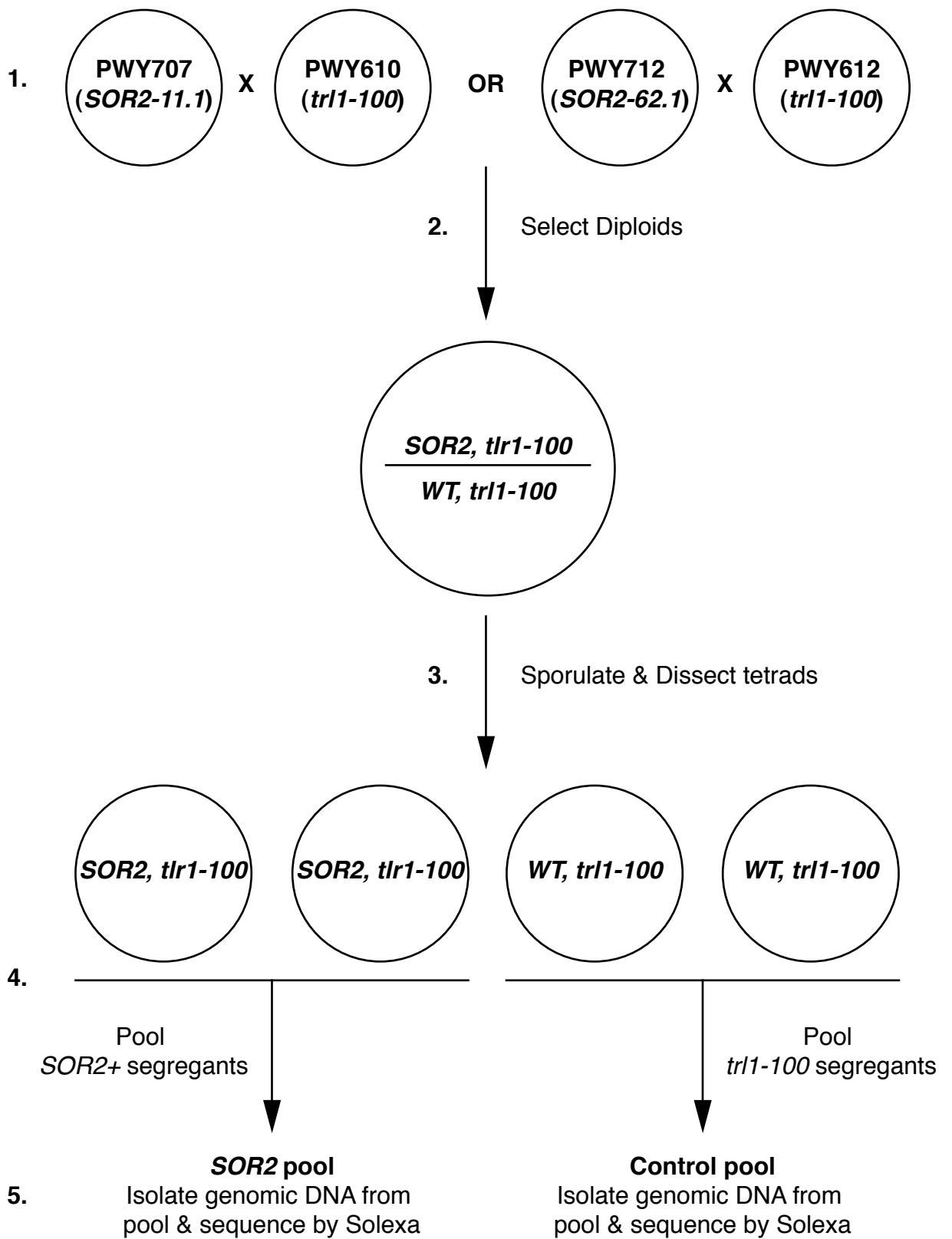
UCSF Library Release Form

It is the policy of the University to encourage the distribution of all theses,

dissertations, and manuscripts. Copies of all UCSF theses, dissertations, and

manuscripts will be routed to the library via the Graduate Division. The library will

make all theses, dissertations, and manuscripts accessible to the public and will

preserve these to the best of their abilities, in perpetuity.

Please sign the following statement:

I hereby grant permission to the Graduate Division of the University of California,

San Francisco to release copies of my thesis, dissertation, or manuscript to the

Campus Library to provide access and preservation, in whole or in part, in

perpetuity.

_____   9/8/2010
Author Signature   Date